

2022-01

Impact of Delays on Antenna-Array Noise

Ali, Roshaan

Ali, R. (2022). Impact of delays on antenna-array noise (Master's thesis, University of Calgary, Calgary, Canada). Retrieved from <https://prism.ucalgary.ca>.

<http://hdl.handle.net/1880/114340>

Downloaded from PRISM Repository, University of Calgary

UNIVERSITY OF CALGARY

Impact of Delays on Antenna-Array Noise

by

Roshaan Ali

A THESIS

SUBMITTED TO THE FACULTY OF GRADUATE STUDIES
IN PARTIAL FULFILLMENT OF THE REQUIREMENTS FOR THE
DEGREE OF MASTER OF SCIENCE

GRADUATE PROGRAM IN ELECTRICAL ENGINEERING

CALGARY, ALBERTA

JANUARY, 2022

© Roshaan Ali 2022

Abstract

Antenna arrays are increasingly being used in radio telescopes that operate with large bandwidth and demand very-low-noise performance. Designing the receivers for these telescopes involves the use of equations that were developed for narrowband receivers. One of the impeding factors in receiver design is array mutual coupling that degrades system noise performance. The effects of mutual coupling can be mitigated completely, provided the receiver is designed to noise match the active array for a single scan direction. This type of matching was developed for narrow band receivers where signal delays between antennas can be safely ignored.

This work develops equations and techniques for matching wideband active arrays to the receiver while taking into consideration the propagation delays in the array that become relevant with large bandwidth. Matching the receiver to the active array requires matching the individual LNA separately to the active array, which is not ideal. For this reason, matching the active array to identical LNAs while minimizing receiver noise is also explored. The equations developed are verified using simulation of antenna arrays designed for radio astronomy use. Finally, minimizing array noise for multiple scan directions while using identical LNA in the receiver is discussed.

Acknowledgements

I would like to express my sincerest gratitude to Dr. Belostotski for providing invaluable guidance and mentorship in my graduate studies and thesis work. Dr. Belostotski has been incredibly understanding and patient with me in regards to my thesis work and only through his help have I been able to complete this thesis.

I would like to thank Alexander Sheldon of MiNT lab for providing the LNA noise simulation code that greatly accelerated the development of simulation code used in this thesis.

Finally, I would like to thank Kaj Hedin for providing the necessary encouragement for me to undertake graduate studies and for making it all possible.

Dedicated to my wife and parents

Table of Contents

Abstract	ii
Acknowledgments	iii
Dedication	iv
Table of Contents	vii
List of Figures	ix
Glossary	x
1 Introduction	1
1.1 Background and Motivation	1
1.2 Contribution	3
1.3 Thesis Organization	3
2 Electronic Noise	5
2.1 Introduction	5
2.2 Historical Perspective	6
2.2.1 Maximum Thermal Noise Power of a Resistor	8
2.3 Other Sources of Electronic Noise	9
2.3.1 Shot Noise	9
2.3.2 Flicker Noise (1/f)	9
2.4 Noise in Antennas	10
2.5 Mathematical Modeling of Noise	11
2.5.1 Noise in Frequency Domain	12
2.6 Signal-to-Noise Ratio	12
2.7 Noise Temperature	13
2.8 Friis's Formula	14
2.8.1 Noise Factor	14
2.8.2 Noise Figure	14
2.8.3 Friis's Formula	14
2.8.4 Friis's Formula for Noise Temperature	15
2.9 Power Spectral Density and Einstein-Wiener-Khinchin Theorem	15
2.10 Multi-port Noise and Bosma's Theorem	16

2.11	Noise Waves	18
2.12	Noise Waves and LNAs	19
2.13	Noise Parameters	20
2.13.1	The Lange Invariant Noise Parameter	21
2.14	Input and Output Referred Noise	23
2.14.1	Input Referred Noise Temperature	26
2.15	Traveling Noise Wave Delays in Transmission Lines	26
2.16	Conclusion	27
3	Antenna Array	29
3.1	Modeling Antennas as Circuit Elements	29
3.1.1	Antenna Losses, Matching, and Radiation Efficiency	30
3.2	Antenna Array	31
3.2.1	Active Antenna Arrays	35
3.2.2	Beam Steering	37
3.2.3	Noise in Antenna Arrays	38
3.3	Array Factor	39
3.4	Antenna S-parameters	40
3.5	Antenna-Array Mutual Impedance and Mutual Coupling	41
3.6	Effects of Mutual Coupling on Array Noise	44
3.6.1	Mutual Coupling and Antenna Separation Distance	45
3.7	Active Array Impedance	46
3.7.1	Active Reflection Coefficient Matching	47
3.8	Conclusion	49
4	Propagation Delays in Antenna Array	50
4.1	Modeling Propagation Delays in Antenna Array	50
4.2	Effects of Delays on Noise Output of Beamforming Arrays	57
4.2.1	Noise Due to LNAs	58
4.2.2	Total Noise Power of Receiver with Delays	63
4.2.3	Total Noise Power of Array with Delays	64
4.2.4	Receiver Noise Temperature with Delays	65
4.2.5	Verification Using Simulation	66
4.3	Γ_{act} with Delays and Γ_{act} Matching	69
4.4	Impact of Noise Bandwidth on Antenna Array Matching	73
4.4.1	Simulation of 71 Element Array with Optimal Γ_{act}	80
4.5	Optimizing For Multiple Scan Directions	85

4.6	Weighted Average Multi-beam Optimization	87
4.7	Conclusion	88
5	Discussion	89
6	Conclusion	92
	Bibliography	93
A	19 element array simulation code	100
B	Γ_{act} search simulation code	111
C	Optimal Γ_{act} derivation	123
D	71 element Vivaldi array simulation code	133
E	Multi-beam average optimal Γ_{act} derivation	143

List of Figures

2.1	Noisy-resistor power-transfer circuit.	6
2.2	Noisy-resistor power-transfer circuit with transmission line.	7
2.3	Antenna modeled as a circuit.	10
2.4	Multi-port noise representation.	16
2.5	LNA noise waves.	19
2.6	LNA with lossless transforming network at the input.	21
2.7	Input-referred noise in multi-component system.	23
2.8	Input referred noise in 2-port network.	23
2.9	Antenna with LNA and matched load	24
3.1	Circuit model of receiving and transmitting antennas with $Z_{ant} = Z_{self} + R_{rad}$	30
3.2	Simple antenna array	31
3.3	Plot of normalized E-field for $3/2\lambda$ dipole	34
3.4	Simple receiving phased array	35
3.5	Receiving array with incident wave at an angle of θ	37
3.6	Plot of array factor pattern with array operating at 45°	38
3.7	Antenna modeled with free space port.	40
3.8	N-element array modeled as 2M-port network.	42
3.9	2-element array model with free-space mutual-coupling matrix.	43
3.10	Array with LNA noise waves	44
3.11	2-element array with identical LNAs having $s_{11} = s_{22} = 0$	47
4.1	Antenna array with transmission line, antenna feed, and inter antenna delay.	51
4.2	Simplified diagram of thick dipole antenna with long feed line.	52
4.3	CAD model of $1/2\lambda$ dipole 1-GHz antenna array in CST.	53
4.4	CST simulation results for 0.9λ separation of 2-element dipole array showing phase of s_{21} of the array as a function of frequency.	54
4.5	Dipole array delay simulation.	56
4.6	Simplified model of receiving array with band-pass filter at the output.	57
4.7	Antenna displacement pattern of the 19 element array.	67
4.8	Wideband 19-element array simulation	68
4.9	Results of 2-element dipole array simulations with varied bandwidth	72
4.10	Smith chart of optimal Γ_{act}	82
4.11	Plot of $ \Gamma_{act} $ vs bandwidth for various transmission line lengths.	83

4.12 Plot of T_{rec} vs bandwidth for various transmission line lengths. 84

Chapter 1

Introduction

1.1 Background and Motivation

Antenna arrays see ever-expanding application in communications (e.g., emerging 5G and 6G systems, massive and holographic MIMO systems), radar, radio astronomy, magnetic resonance imaging, remote sensing, signal intelligence, and spectrum sensing [1–11]. In commercial applications, antenna arrays are used in MIMO (multiple-input-multiple-output) systems used in cellular communication (5G cellular network), while in military applications, antenna arrays are used in AESA (active electronically scanned array) radars, communication systems, synthetic aperture synthesis, etc. In most applications, there is a need to improve the SNR (signal-to-noise ratio) of arrays. For AESA radars, improved SNR means increased detection range. In commercial communication systems, increased SNR means faster link speeds for wireless devices. And in radio astronomy, improving the SNR of a telescope receiver reduces observation times or improves observation quality. In radio astronomy, wider band arrays and receivers are required for the SKA (Square Kilometer Array) [12]. However, contemporary noise analyses of antenna arrays are not accurate for wideband systems. Therefore, designing these receivers involves use of techniques developed for narrowband arrays and receivers. Wideband analysis of arrays with frequency varying antenna and low-noise amplifiers (LNA) S-parameters had not been discussed in literature. This work aims to generalize the narrowband equations and techniques for antenna arrays to the wideband case. In a recent article, it was shown that noise delays and bandwidth have an effect on the LNA noise output [13], and in this work, special emphasis is placed on studying the effects of noise delays and bandwidth on antenna array noise equations and discover their impact on antenna array matching.

Past research showed that minimizing the noise of a receiving antenna array requires the optimum reflection coefficient for minimum noise, $\Gamma_{\text{opt}} \in \mathbb{C}$, of the receiver front-end

LNA to equal the “active” reflection coefficient, $\Gamma_{\text{act}} \in \mathbb{C}$, of the antenna array [14–17]. The determination of Γ_{act} requires the knowledge of beamforming coefficients and the electrical parameters, e.g., S-parameters, of the antenna array. However, typically focusing on narrow-band applications, prior analyses did not consider the effects of noise bandwidth on Γ_{act} . As such, a typical noise analysis was performed at a single frequency for a 1-Hz bandwidth and simply extended to wideband by multiplying the noise by the desired bandwidth.

For each frequency of array operation, the conventional noise analysis proceeds as follows: a) S-parameters of an antenna array and the LNA are simulated or measured in a 1-Hz bandwidth, f_{B0} ; b) noise parameters (NPs) of the LNA are simulated in a 1-Hz bandwidth or measured over a ~ 1 -MHz bandwidth, $f_{B,np}$, and the NPs are assumed to be invariant of $f_{B,np}$; c) noise power at the array output, beam-equivalent receiver noise temperature, T_{rec} , and Γ_{act} are calculated in a 1-Hz bandwidth based on the results in a) and b) and the knowledge of the beamformer coefficients [14–17]; and, if needed, d) T_{rec} and Γ_{act} are assumed unchanged over operating noise bandwidth f_B , and the output noise power for f_B is calculated by multiplying the result in c) by f_B .

Three observations are made: a) measured S-parameters manifest any propagation delays through the array as phases at each frequency; b) while wide $f_{B,np}$ increases the LNA output noise power and accelerates measurements, the assumption of LNA NP invariance on $f_{B,np}$ is not accurate as it ignores bandwidth-dependent decorrelation of LNA noise sources [13]; and c) the linear scaling of the output noise power by f_B may also be inaccurate due to noise decorrelation problem akin discussions in [13]. This last observation has not been investigated in the past for compact arrays, while for physically large antenna arrays, such as single-pixel aperture-synthesis radio telescopes, it is well-known that even bandwidths of a few kHz result in noise decorrelation [18]. Therefore, this thesis investigates f_B impact of noise decorrelation on T_{rec} and Γ_{act} of wideband compact arrays, with the particular focus on ultra-sensitive system, such as those for radio astronomy, where

even small increases in T_{rec} are considered as highly undesirable. Note that as f_{B} is the noise bandwidth, it may be much narrower than the RF system bandwidth; therefore, in this thesis “wideband” refers to wide noise bandwidths.

1.2 Contribution

The main contributions of this work are as follows:

1. Presentation of frequency varying equation for determining antenna array noise
2. Development of a new optimal matching scheme for wideband arrays with noise delays taken into consideration
3. Development of multi-beam optimal noise matching scheme for wideband arrays with noise delays taken into consideration
4. Development of a method for allocating importance to particular scan directions when minimizing array noise for multiple scan directions

The first and second contributions in the list above have resulted in the following publication:

- Ali, Roshaan et al., “Impact of bandwidth on antenna array noise matching,” *Electronics Letters*, vol. 57, 4, pp. 158-160, Feb. 2021,
url: <https://onlinelibrary.wiley.com/doi/10.1049/ell2.12018>

1.3 Thesis Organization

The thesis is comprised of the following chapters:

1. Introduction
2. Electronic Noise

3. Antenna Arrays
4. Noise Delays in Antenna Arrays
5. Discussion
6. Conclusion

Introduction presents the background and motivation for this thesis. The second chapter explores electronic noise in detail, and discusses the concept of noise waves as function of time and frequency. The third chapter details prerequisite concepts in antenna array theory. In particular, the chapter discusses modern methods of calculating array receiver noise. In the fourth chapter, noise delays in antenna arrays and their impact on array noise matching is discussed. This is accomplished by developing array equations that include bandwidth and delay effects including verification of these equations via numerical simulations. The final two chapters are dedicated to discussion and conclusion of findings of this work.

Chapter 2

Electronic Noise

2.1 Introduction

Noise is one of most important performance constraint of electronic circuits design. It sets the boundaries for what can and cannot be achieved with devices available to a designer. A common design goal encountered in electronics and system design is to obtain the best noise performance possible. Signal-to-noise ratio (SNR) and many of its derivatives, such as noise temperature, noise figure, etc., are simply different ways of expressing the noise performance of a circuit. In order to understand SNR, two fundamental quantities must be defined and characterized: signal and noise. An electrical signal can be described as desirable information encoded in the electromagnetic field. Electrical noise can be described as the undesired disturbance of the electromagnetic field and this disturbance obscures the signal of interest. In some applications, the signal can be buried in noise, for example in GPS (global positioning system), but can be recovered because part of the signal is known and can be correlated out of the noise. In all applications, improving the SNR is desirable. In radio astronomy, it is important to maximize the SNR in order to speed up the acquisition of signal and distinguish it from system noise. Consider the radiometer equation, as applied to a radio telescope,

$$\frac{S}{N} = \frac{T_{src}}{T_{sys}} \sqrt{\tau \cdot B}, \quad (2.1)$$

where $\frac{S}{N}$ is the SNR, T_{src} is the noise temperature of the signal source, T_{sys} is the system (telescope) noise temperature, τ is the observation time, and B is the bandwidth of observation. It is clear from Equation 2.1 that in order to improve the SNR for a given T_{src} , τ , and B , the system temperature must go down. Herein lies the need to understand and minimize electronic noise in radio astronomy.

2.2 Historical Perspective

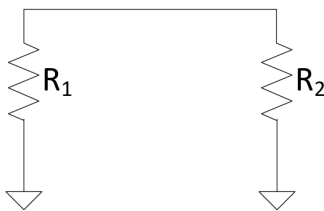


Figure 2.1: Noisy-resistor power-transfer circuit.

Electronic noise was first reported by Dr. Johnson of Bell labs in 1928 as spontaneous voltage fluctuations present in conductors. Johnson found that the mean squared value of the voltage fluctuation, $\overline{V_n^2}$, was in proportion to the resistance of the conductor and its absolute temperature [19]. Johnson shared his measurement results with Nyquist at Bell labs who mathematically quantified it using thermodynamics and statistical mechanics [20]. Nyquist's argument, which is now well known and illustrated in many classical textbooks in electronics, is as follows: consider two resistors R_1 and R_2 with resistance R at temperature T connected in series in absence of any sources (Figure 2.1). At temperature T , there is an electromotive force due to the thermal agitation of electrons in resistor R_1 that causes a current in this circuit of total resistance $2 \cdot R$. This current, I , causes the thermal heating of R_2 , and is found by dividing the electromotive force V by $2R$, $V/(2R) = I$. Similarly, the thermal agitation of electrons in R_2 causes a current I , which is absorbed by R_1 . Because both resistors are at temperature T , the net power flow should equal zero in accordance with the second law of thermodynamics. Since $P = I^2R$, the noise power from R_1 is

$$P_n = R \cdot (V/2R)^2 = \frac{V^2}{4R}, \quad (2.2)$$

where P_n is the noise power.

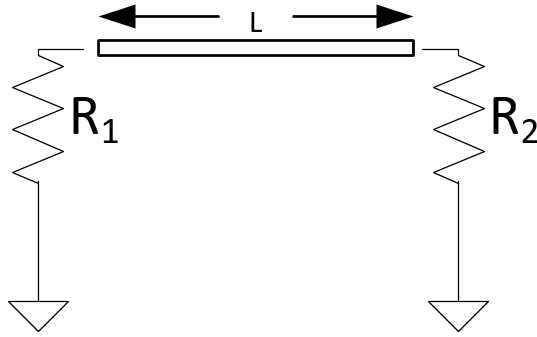


Figure 2.2: Noisy-resistor power-transfer circuit with transmission line.

Nyquist related the thermal noise power with Boltzmann's constant and temperature by thinking of a circuit in Figure 2.2 with two resistors separated by a lossless transmission line of length L with propagation velocity of v and a characteristic impedance of R . He then imagined short circuiting both of the resistors once thermal equilibrium was reached. In this scenario, assuming no radiative losses, noise voltage generated by two resistors would be trapped and reflect back and forth within the transmission line. This allowed Nyquist to show that the energy transferred from the resistors to the transmission line is related to Boltzmann's constant and temperature through the equipartition law. Equipartition law states that, on average, the energy in an oscillator, such as the voltage oscillation in the transmission line, is $k_b T$ per degree of freedom, where k_b is the Boltzmann's constant and T is temperature. In the case of the transmission line, the degree of freedoms correspond to the modes of vibration with wavelength $0.5\lambda, 1\lambda, 1.5\lambda, 2\lambda \dots$ corresponding to frequencies of $0.5f_0, 1f_0, 1.5f_0 \dots$. In a sufficiently large transmission line, the number of modes of vibration that can exist in a frequency bandwidth of B starting at frequency f_0 is $2B/f_0 = 2B(L/v)$. The average energy in the transmission line can then be derived using Equipartition law as $E = 2(L/v) \cdot Bk_b T$, because each mode of vibration corresponds to one degree of freedom. Finally, the average power delivered to the transmission line by *each* resistor is arrived at by assuming a time interval of L/v in which the energy is transferred

as

$$P = Bk_bT. \quad (2.3)$$

Combining 2.2 and 2.3 yields

$$\overline{V^2} = 4k_bTBR, \quad (2.4)$$

which is a well-known equation for finding average noise voltage in a resistor within a frequency band.

One important point to note from Nyquist's paper is that the reactive parts of the circuit do not contribute to this type of noise, and neither do they distort it in any way. Therefore, an inductor with series resistance of R_s will generate a mean squared voltage of $4k_bTBR_s$. The noise voltage of R_s is thought to be in parallel with the series resistor R_s .

2.2.1 Maximum Thermal Noise Power of a Resistor

Maximum noise power that can be delivered by a resistor occurs when it is connected to a matched load. Consider the circuit in Figure 2.1 with $R_1 = R_2$. Noise from R_1 travels through the transmission line to R_2 where all of the noise power is absorbed. Starting with $\overline{V^2} = 4k_bTBR_1$, the current through the circuit is restricted by both resistors, $I = \frac{V}{(2 \cdot R_1)}$. The total power delivered by R_1 is $P = I^2 \cdot R_2$. Combining the 3 equations yields

$$I^2 \cdot 4 \cdot R_2^2 = 4k_bTBR_1. \quad (2.5)$$

Since $R_1 = R_2$ and $I^2 R_2 = k_bTB$,

$$P = k_bTB. \quad (2.6)$$

In other words, the maximum noise power available from the resistor is independent of its resistance and is only a function of bandwidth and temperature. In a sense, this is a favorable outcome because if it were that the available noise power from a resistor was

dependent on its resistance, then achieving lowest noise for a given circuit would involve tweaking each resistor to produce least amount of noise while preserving the performance of the circuit.

2.3 Other Sources of Electronic Noise

According to Nyquist's Equation 2.4, there should be an infinite noise voltage in any resistor because there are infinite frequencies in the frequency domain. This indeed is not true because infinite noise bandwidth would mean infinite noise power. Thermal noise power spectrum must therefore disappear at very high frequencies. There are however other sources of noise at very high frequencies such as shot noise. On the other hand, flicker noise dominates the low end of the noise spectrum and this becomes important when designing very low frequency (VLF) systems.

2.3.1 Shot Noise

Shot noise is result of random fluctuations of charge carriers within a device. It was first described by Walter H. Schottky and has mean squared value of $\overline{i^2} = 2IqB$ [21]. This type of noise is related to bandwidth B , DC current I , and the charge of an electron q . It is evident from the I in the expression that this type of noise relies heavily of the number of charges flowing through a device, and it is not perturbed by the temperature of the device.

2.3.2 Flicker Noise (1/f)

Flicker noise or (1/f) noise appears in frequencies near DC. It appears in all circuits and device types. There is a general consensus in literature that this noise is due to some fundamental physical effects [22–24]. Flicker noise has a power spectral density of the form:

$$S(f) = 1/f^\alpha,$$

where $0 < \alpha < 2$ and α is usually close to 1. $\alpha = 1$ is called pink noise. Pink noise power spectral density (PSD) is negligible beyond a few kHz range for bipolar circuits and MHz for FET based circuits.

In this work, circuits with frequency of operation in the excess of 10 MHz and up to tens of GHz are considered. Therefore, flicker noise is not important and is not considered any further.

2.4 Noise in Antennas

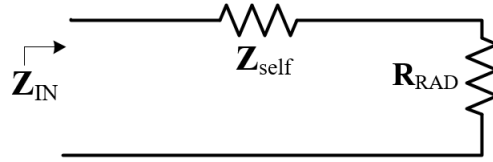


Figure 2.3: Antenna modeled as a circuit.

The main source of noise from antenna elements in a circuit, excluding the noise from outside the circuit that the antenna tunes into, is thermal noise. Generally, antennas can be modeled as a series circuit with self-impedance $Z_{self} = R_{self} + jX_{self}$ and a radiation resistance R_{rad} at each frequency as shown in Figure 2.3 [25]. The radiation resistance is the loss in the antenna attributed to the radiating nature of the antenna, and the self-impedance is the impedance of the antenna that contributes to the thermal noise. Note that only the self-impedance of the antenna contributes noise to the circuit it is driven by because the radiation resistance is not related to a physical resistor in the antenna. The thermal noise voltage of the antenna depends on the temperature, bandwidth, Boltzmann's constant, and the real part of antennas self-impedance as follows [25]

$$\overline{V_{ant}^2} = 4k_bTB \cdot \Re(Z_{self}) = 4k_bTB \cdot R_{self} \quad (2.7)$$

2.5 Mathematical Modeling of Noise

Thermal noise is *mostly* white because at very high frequencies the PSD of thermal noise diminishes completely due to quantum effects [20]. For the frequency ranges considered in this work, thermal noise will be considered white. This means that it has a constant PSD. Mathematically speaking, white noise is a zero mean wide-sense-stationary continuous-time random process with Gaussian distribution.

Thermal noise is a continuous-time random process X_t with the following properties:

- Zero mean: implies that the noise does not have a DC offset
- Gaussian distribution: $X_t \sim N(\mu, \sigma)$, where N is the normal function. At any point in time t , the sample $X_t = x(t)$ can be thought of as a random variable with zero mean, $\mu = 0$, and a constant standard deviation, $\sigma(t) = \sigma, \sigma > 0$
- Wide Sense Stationary (WSS): means that it has a constant mean and the auto-correlation (or auto co-variance) depends only on the different in time, $AutoCorr(N_t) \sim F(t_1 - t_2)$

The WSS property of thermal noise will prove useful later when auto-correlation of noise in antenna arrays is considered. Electronic noise signal can be written as

$$x(t) = X_t, \quad (2.8)$$

$$X_t \sim N(\mu, \sigma) \quad (2.9)$$

with

$$AutoCorr(X_t) \sim f(t_1 - t_2). \quad (2.10)$$

Noise signals that are uncorrelated always mix in terms of power in an additive manner. For example, when noise signals $x_1(t)$ and $x_2(t)$ are combined, the power of each signal is simply added as $\overline{(x_1(f) + x_2(f))^2} = \overline{x_1^2(f)} + \overline{x_2^2(f)}$.

2.5.1 Noise in Frequency Domain

Noise signals can be transferred to the frequency domain via the Fourier transform. The resultant expression is a function of frequency and has two components, the amplitude A and phase ϕ in the polar coordinate system

$$n(t) \xrightarrow{\mathcal{F}} n(f) = A(f) \cdot e^{j\phi(f)}, \quad (2.11)$$

or the real and imaginary component in the rectangular coordinate system,

$$n(f) = B(f) + jC(f). \quad (2.12)$$

In the polar coordinate system, the amplitude and phase are both random variables with the expected value of amplitude being $\sigma^2 = \text{Var}[n_t]$, while the expected value of the phase is zero. In the rectangular coordinate system, the expected value of both the real and imaginary component is $\sqrt{2} \cdot \sigma^2$, where again, σ^2 is the variance of the noise signal in time domain.

2.6 Signal-to-Noise Ratio

An important performance metric for electronic devices and circuits is the signal to noise ratio. It comes in many flavors but the fundamental concept remains the same. It is a way of quantifying noise performance of a circuit. Traditionally, it is defined as

$$SNR = \frac{P_s}{P_n}, \quad (2.13)$$

where P_s is the average signal power and P_n is the average noise power.

2.7 Noise Temperature

An equivalent formulation of noise power can be derived using noise temperature. The available noise power for a component is described as

$$P_n = k_b T B. \quad (2.14)$$

This equation can be rearranged to find the equivalent noise temperature of a component, given the available noise power, as

$$\frac{P_n}{k_b B} = T_{eq}. \quad (2.15)$$

Noise temperature is a useful means of comparing different arrays and receiver chains particularly in radio astronomy where the signal source (matter in outer space) emits black body radiation. This radiation has a brightness temperature, which in some conditions is equivalent to the actual temperature of the radiating body [26]. The radiation power that arrives at the radio telescope from the source has a spectral flux density measured in jansky (Jy). A telescope with an effective collecting area of A_e detects this radiation power as having an equivalent noise temperature of

$$T_{src} = \frac{S_{src} \cdot A_e}{k_b}, \quad (2.16)$$

where S_{src} is the power spectral flux density of the source in $\text{W}/\text{m}^2/\text{Hz}$, and assuming that radio telescope has no losses. T_{src} and the telescope system temperature can then be used to calculate how long an astronomical observation has to last to produce a signal with a particular SNR using the radiometer Equation 2.1.

Generally speaking, radio telescopes with lower system noise temperatures are able to make faster observations. Or, given an observation time frame, a radio telescope with lower system temperature can produce an observation with a better SNR.

2.8 Friis's Formula

2.8.1 Noise Factor

Noise Factor (F) is a measure of deterioration of SNR as signal and noise go into a circuit block and emerge at its output

$$F = \frac{SNR_o}{SNR_i}, \quad (2.17)$$

where SNR_i is the input SNR, and SNR_o is the output SNR. Noise Factor must be greater than 1 for any realizable circuit because noise factor less than 1 means that noise was removed from the signal rather than added to it. For that to occur, the circuit must have prior knowledge of the noise in the input signal, which is not physically possible.

2.8.2 Noise Figure

Noise Factor is commonly expressed as Noise Figure (NF) in dB

$$NF = 10 \log(F). \quad (2.18)$$

2.8.3 Friis's Formula

Electronic systems are often configured as a cascaded blocks of circuits that signals flow through. If the circuits in the system are linear and time independent, then each of the blocks can be thought of as a gain stage, which has its own noise performance. Friis's formula is a way to express the overall noise performance of the circuit provided that the noise and gain performance of each block is known. Noise factor is used in one of the more common definition of Friis's formula

$$F_{total} = F_1 + \frac{F_2 - 1}{G_1} + \frac{F_3 - 1}{G_1 G_2} + \frac{F_4 - 1}{G_1 G_2 G_3} + \cdots + \frac{F_n - 1}{G_1 G_2 \cdots G_{n-1}} \quad (2.19)$$

Looking at this formula, the noise of the overall system is largely determined by 2 vari-

ables: the noise factor of the first component in the chain (F_1), and the gain of the first component (G_1). In wireless receiver architectures, the first stage is usually the LNA. The main objective of an LNA in a receiver chain is to provide maximum gain with minimum added noise. With these two conditions, the noise and the gain of the subsequent stages have negligible effect provided those stages do not have extremely poor noise or gain performance.

2.8.4 Friis's Formula for Noise Temperature

Friis formula can be expressed in terms of noise temperature. It is a way to describe how each component adds to the overall noise temperature of a system

$$T_{eq} = T_1 + \frac{T_2 - 1}{G_1} + \frac{T_3 - 1}{G_1 G_2} + \frac{T_4 - 1}{G_1 G_2 G_3} + \dots + \frac{T_n - 1}{G_1 G_2 \dots G_{n-1}}. \quad (2.20)$$

Again, the noise temperature of the system is determined mainly by the first component in the system.

2.9 Power Spectral Density and Einstein-Wiener-Khinchin Theorem

Power spectral density is defined as the power per unit frequency over the entire frequency domain. In terms of noise power of a resistor, PSD is $4k_bTR$. The PSD of a resistor is constant over frequency and depends only on temperature and the resistor.

The PSD of a signal can be found using Einstein-Wiener-Khinchin theorem, which states that the PSD of a signal is the Fourier transform of the auto-correlation of the signal:

$$S = \mathcal{F}(f \times f) = \mathbf{F}^* \cdot \mathbf{F} = |\mathbf{F}|^2, \quad (2.21)$$

where \mathbf{F} is the Fourier transform of the function f . The total power of a signal can be obtained by integrating the PSD over the frequency domain

$$P = \int_{-\infty}^{\infty} S \cdot df. \quad (2.22)$$

In the case of a resistor, this is simply $P = 4k_bTR(f_2 - f_1) = 4k_bTRB$, where $B = (f_2 - f_1)$ is the bandwidth of the circuit.

2.10 Multi-port Noise and Bosma's Theorem

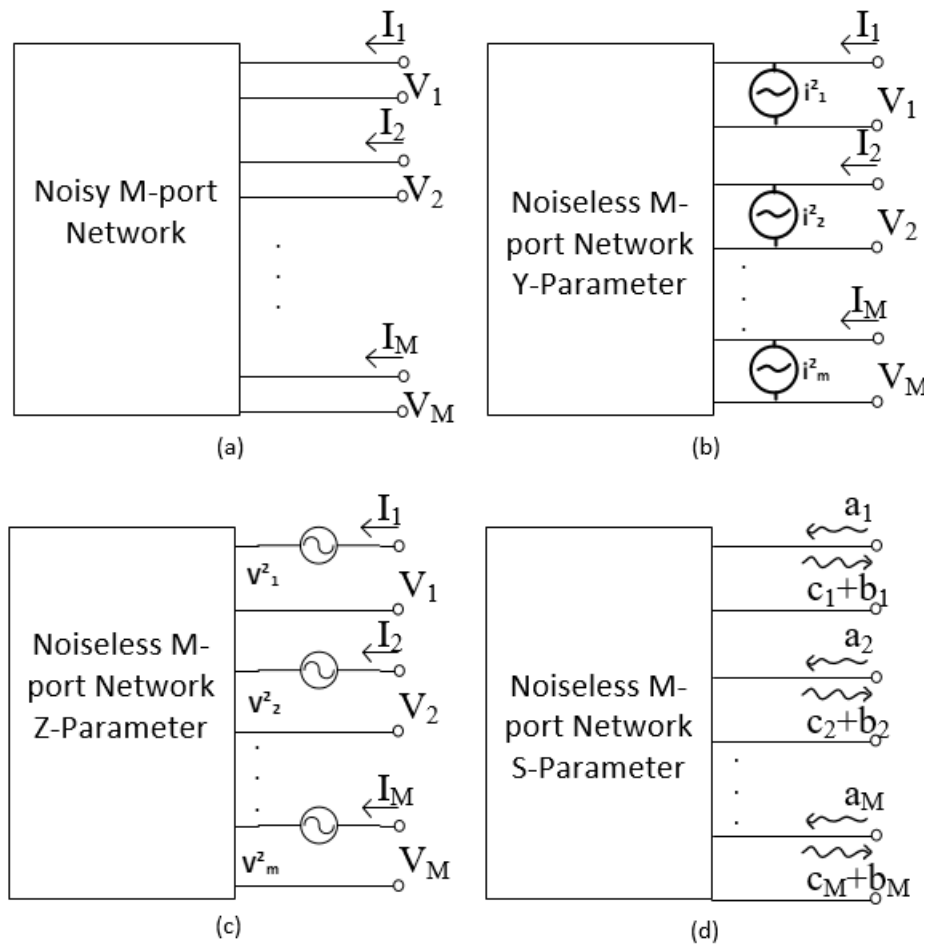


Figure 2.4: Multi-port noise representation.

Figure 2.4 describes a noisy M-port circuit. Much like noisy single ports, such as resistors, multi-port noisy components are described as having a noiseless multi-port network and noise sources in parallel or series of each of the port of the network. For a network with

Z-parameters, the noise sources are voltage source at each port (Figure 2.4c), and the noisy multi-port can be described as

$$\mathbf{V} = \overrightarrow{\mathbf{I}}\mathbf{Z} + \overrightarrow{\mathbf{V}}_n, \quad (2.23)$$

where $\overrightarrow{\mathbf{V}}_n$ is the vector of noise voltage sources in parallel with each port, $\overrightarrow{\mathbf{V}}$ is a vector of voltages at each port, $\overrightarrow{\mathbf{I}}$ is a vector of currents going into the ports, and \mathbf{Z} is the Z-parameter matrix. The noise voltages are added to the regular Ohm's law, $\overrightarrow{\mathbf{V}} = \overrightarrow{\mathbf{I}}\mathbf{Z}$, in matrix form, which captures the noise as an additive quantity as a natural consequence of representing noise sources separate from the noiseless network.

These noise voltage sources, $v_1, v_2, v_3, v_4, \dots, v_n \in \overrightarrow{\mathbf{V}}_n$, can be correlated with a noise correlation matrix:

$$\mathbf{C}_Z = \overline{\mathbf{V}_n \mathbf{V}_n^*}. \quad (2.24)$$

For a 2-port network the expanded equation is

$$\mathbf{C}_Z = \begin{bmatrix} \overline{|v_1|^2} & \overline{v_1 v_2^*} \\ \overline{v_2 v_1^*} & \overline{|v_2|^2} \end{bmatrix}. \quad (2.25)$$

Bosma showed that the noise emanating from multi-port network is correlated and this correlation can be derived from the network S-parameters [27]. While Bosma used thermodynamic equilibrium and net zero power flow as main arguments for his derivations, Wedge and Rutledge used directional couplers to derive the same results [28]. The following equation for the noise correlation of a passive multi-port is now known as Bosma's theorem:

$$\mathbf{C}_s = k_b T (\mathbf{I} - \mathbf{S}\mathbf{S}^H), \quad (2.26)$$

where H denotes Hermitian conjugate and \mathbf{S} is a *passive* multi-port-network S-parameter matrix.

2.11 Noise Waves

Scattering parameters are the most popular method for describing a multi-port network at RF frequencies. This is because it is easier to measure S-parameters at RF frequencies than Z or Y parameters. S-parameters inherently capture reflection, transmission, and cross coupling of signals incident to the multi-port network, and so provide a straight forward way to model signal propagation in antenna arrays. However, S-parameters necessitate the conversion of voltage and current signals to traveling power waves using the systems characteristic impedance Z_0 . The equivalent formulation for noise that works with S-parameters are the traveling noise waves [29]. These traveling noise waves are identical to the traveling waves used in S-parameter formulation; however, they are generated by the multi-port noisy components and are distinguished from the reflected wave \mathbf{b} as an additive quantity (Figure 2.4d)

$$\mathbf{b} = \mathbf{S} \cdot \mathbf{a} + \mathbf{c}, \quad (2.27)$$

where \mathbf{c} is a vector of noise waves that is added to the return signal from the multi-port.

Noise waves are the random signals generated by the multi-port network. It is evident from Equation 2.27 that in the absence of an incident wave \mathbf{a} , a noise wave vector \mathbf{c} is always present. \mathbf{c} is a vector of complex random variables whose values are determined by the noisy components inside the multi-port. Mathematically, it is modeled as a vector with each component being a continuous time Gaussian random variable. Each component can be correlated to others depending on the circuit components and topology. This correlation is captured by the noise correlation matrix

$$\mathbf{C}_s = \overline{\mathbf{c}\mathbf{c}^H}, \quad (2.28)$$

where the over bar denotes the mean value .

In the case of a 2-port network, $\mathbf{c} = \begin{bmatrix} c_1 & c_2 \end{bmatrix}^T$, with c_1 and c_2 correlated as de-

scribed by the correlation matrix

$$\mathbf{C}_s = \begin{bmatrix} \overline{|c_1|^2} & \overline{c_1 c_2^*} \\ \overline{c_2 c_1^*} & \overline{|c_2|^2} \end{bmatrix}. \quad (2.29)$$

The diagonal terms in \mathbf{C}_s are the auto-correlation of c_1 and c_2 , respectively, and the off-diagonal terms are the cross correlation of c_1 and c_2 . It is possible to determine this noise correlation matrix as described by Wedge and Rutledge [28]. It requires the knowledge of the network S-parameters (or other parameters such as Z-parameters that can be readily converted to S-parameters) [28]

$$\mathbf{C}_s = k_b T (\mathbf{I} - \mathbf{S}\mathbf{S}^H). \quad (2.30)$$

2-port networks are often encountered in LNA or power amplifier (PA) design where the circuit biasing has been determined and the LNA/PA can be described as having only the input and output port. Since Equation 2.30 can only be used for passive networks, a different method is required to find the noise correlation matrix for active 2-port networks.

2.12 Noise Waves and LNAs

LNAs are 2-port networks that provide large gain and add minimal noise to input signals. One of the main design goals for LNA designers is to keep the noise factor of this circuit as low as possible.

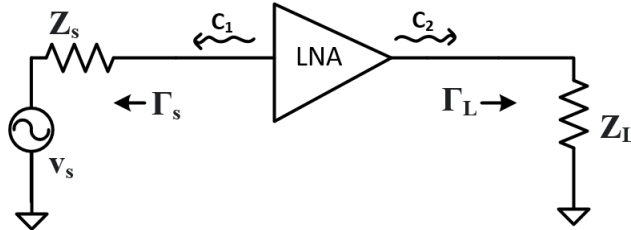


Figure 2.5: LNA noise waves.

A 2-port LNA, such as one in Figure 2.5, has a 2x2 S-parameter matrix, and a two-component noise-wave vector $\mathbf{c} = \begin{bmatrix} c_1 & c_2 \end{bmatrix}^T$, with c_1 emanating from the input port and c_2 emanating from the output port. c_1 is known as the forward noise wave and c_2 is known as the reverse noise wave. Consider the case when reverse gain and output reflection are both zero, $s_{12} = s_{22} = 0$, and LNA is terminated at the load end with $\Gamma_L = 0$. In this scenario, noise waves emanating from the input port get reflected back from the source with reflection coefficient Γ_s . In most LNAs, there is a correlation between c_1 and c_2 that LNA designers take advantage of to reduce the overall noise factor of the circuit. This is accomplished by reflecting the right amount of c_1 off of the source by carefully choosing the value of source impedance [30]. The correlation of forward and reverse noise waves can be expressed in terms of LNA S-parameters and noise parameters. From [28]:

$$\overline{|c_1|^2} = k_b T_0 B \left(\left(4N \frac{|1 - s_{11} \Gamma_{opt}|^2}{1 - |\Gamma_{opt}|^2} \right) - \frac{T_{min}}{T_0} (1 - |s_{11}|^2) \right) \quad (2.31)$$

$$\overline{|c_2|^2} = k_b T_0 B |s_{21}|^2 \left(\frac{T_{min}}{T_0} + 4N \frac{|\Gamma_{opt}|^2}{1 - |\Gamma_{opt}|^2} \right) \quad (2.32)$$

$$\overline{|c_1 \cdot c_2^*|} = -4k_b T_0 B N \frac{S_{21}^* \Gamma_{opt}^*}{1 - |\Gamma_{opt}|^2} + \frac{S_{11}}{S_{21}} \overline{|c_2|^2}, \quad (2.33)$$

where T_{min} (minimum noise temperature), N (Lange invariant), and Γ_{opt} (signal-source reflection coefficient for minimum noise) are LNA noise parameters, and T_0 is reference temperature.

2.13 Noise Parameters

The noise performance of any 2-port network, such as an LNA, can be described by their noise parameters [31]. There are several flavors of the noise parameters, but the most commonly known ones are F_{min} (minimum noise factor), Γ_{opt} or Y_{opt} , and R_n , where R_n is the equivalent noise resistance and Y_{opt} is the signal-source admittance for minimum noise.

Noise factor of any 2-port can be calculated by

$$F = F_{min} + \frac{4R_n |\Gamma_s - \Gamma_{opt}|^2}{Z_0 (1 - |\Gamma_s|^2) |1 + \Gamma_{opt}|^2}, \quad (2.34)$$

where Γ_s is the signal-source reflection coefficient.

To LNA designers, the F_{min} and Γ_{opt} of amplifying devices are of particular importance because a lower F_{min} means lower noise factor can be achieved and a reasonable Γ_{opt} means less effort in designing matching network to achieve noise factor near F_{min} . It can be seen from Equation 2.34 that $F = F_{min}$ is achieved when $\Gamma_s = \Gamma_{opt}$.

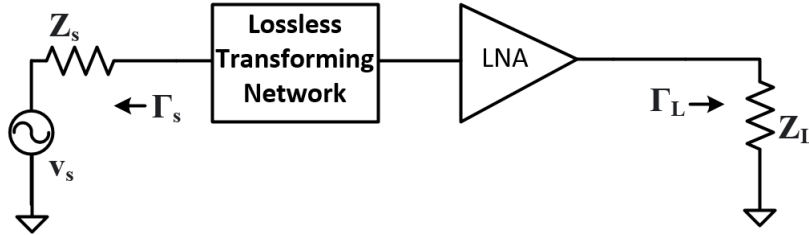


Figure 2.6: LNA with lossless transforming network at the input.

Equation 2.34 has a minor inconvenience built into it. R_n , unlike F_{min} and Γ_{opt} , is not invariant under lossless transformation at the input [32]. Consider the following case: when an LNA is attached to a matching network at the input side (Figure 2.6), the noise factor of the combined circuit is changed because the LNA is described using R_n which itself is dependent on Γ_{opt} . When Γ_{opt} changes as the lossless matching network changes, R_n also changes, which causes the noise factor of the circuit to change.

2.13.1 The Lange Invariant Noise Parameter

Matching networks are employed to transform the signal-source impedance Γ_s to Γ_{opt} in order to obtain lowest noise factor. F_{min} and Γ_{opt} are both invariant under lossless transformation; however, R_n is not. Lange introduced a new noise parameter in place of R_n that does remain invariant under lossless transformation [32]:

$$N = R_n \cdot \Re \{ Y_{opt} \}, \quad (2.35)$$

or

$$N = R_n \cdot G_{opt} \quad (2.36)$$

where $Y_{opt} = G_{opt} + jB_{opt}$.

Since N is invariant under lossless transformation, N is a more fundamental noise parameter than R_n [30]. N is known in literature as the Lange Invariant. This work uses N instead of R_n as the LNA noise parameter along with F_{min} or T_{min} , Γ_{opt} or Y_{opt} . It allows for changing Γ_{opt} by using a lossless transforming network at the LNA input while preserving the values of F_{min} and N .

The equation for noise factor using N , Y_{opt} , F_{min} is [33]

$$F = F_{min} + \frac{N}{G_{opt}G_s} |Y_{opt} - Y_s|^2, \quad (2.37)$$

where $G_s = \Re \{ Y_s \}$, Y_{opt} is the optimal source admittance, and Y_s is the signal-source admittance.

Equation 2.37 can be transformed from noise factor to equivalent noise temperature

$$T = T_{min} + \frac{NT_0}{G_{opt}G_s} |Y_{opt} - Y_s|^2. \quad (2.38)$$

2.14 Input and Output Referred Noise

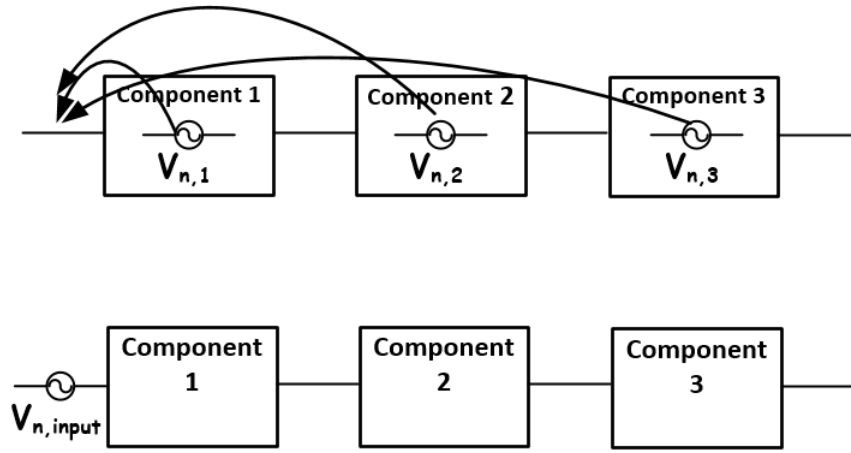


Figure 2.7: Input-referred noise in multi-component system.

System designers are often concerned with comparing their system noise performance with other systems of similar kind. Each component in the system can be noisy and these noise sources are independent of each other. Therefore, a comparison between systems that are not identical in architecture and components requires a way to isolate noise sources generated internally to the system and represent them as being independent and external to the system itself. This is done by referring the noise sources in each of the components to the input or output port such that the resulting noise source would produce identical noise performance to that of the original system (Figure 2.8).

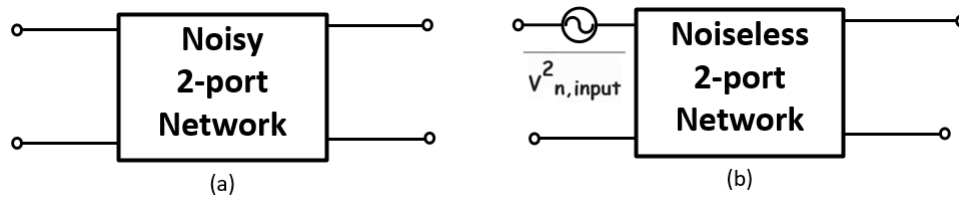


Figure 2.8: Input referred noise in 2-port network.

Consider a simple cascaded system such as one shown in Figure 2.7. The system consists of an amplifier at the input and output stage with a resistor in the middle and a noise-

less load at the output. Assume that the amplifiers are matched at the input and output. The noise generated in the resistor $v_{n,R}$ can be input referred by dividing $v_{n,R}$ by the input amplifier voltage gain A_1

$$v_{n,input} = v_{n,R}/A_1, \quad (2.39)$$

similarly, $v_{n,R}$ can be output referred by moving the noise source through the output amplifier

$$v_{n,output} = v_{n,R} \cdot A_2, \quad (2.40)$$

in both cases the overall system noise performance remains unchanged. Input-referred and output-referred noise allows for comparing different systems with different architectures in terms of how much noise they contribute to the system.

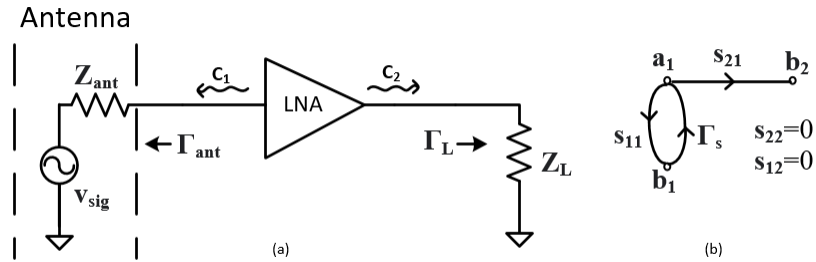


Figure 2.9: Antenna with LNA and matched load

A more complicated scenario, and one directly related to this work, is that of an LNA with an antenna as a source and a matched load at the output (Figure 2.9a). In this case, the LNA noise has to be referred to the input of the antenna such that it appears to be part of the signal picked up by the antenna itself.

Antennas can be modeled as signal source v_{sig} and antenna self-impedance Z_{ant} or Γ_{ant} looking towards the antenna port. LNA has noise waves c_1 and c_2 emanating from the input and output respectively, and these noise waves have to be input referred. Unlike the previous example, this LNA is not power matched at the input so the noise has to be referred to the input by means of signal flow graph (Figure 2.9b). This is accomplished by

first referring c_2 to the input of the LNA

$$c_{2,input} = c_2 \cdot \frac{1 - \Gamma_{ant} s_{11}}{s_{21}}. \quad (2.41)$$

Similarly, c_1 can be input referred using the signal flow graph

$$c_{1,input} = c_1 \cdot \Gamma_{ant}, \quad (2.42)$$

and the total input-referred noise is

$$c_{total,input} = c_1 \cdot \Gamma_{ant} + c_2 \cdot \frac{1 - \Gamma_{ant} s_{11}}{s_{21}}. \quad (2.43)$$

To verify that the output noise of the system with input referred noise remains the same, the output noise wave of the original system has to be determined. For that, the signal-flow graph can again be used to take c_1 to the output

$$c_{1,output} = c_1 \cdot \frac{\Gamma_{ant} s_{21}}{1 - \Gamma_{ant} s_{11}}. \quad (2.44)$$

Since the LNA is power matched to the output and the output reflection coefficient $s_{22} = 0$, the output noise wave remains unchanged at the output, $c_{2,output} = c_2$. Therefore, the total noise waves at the output is

$$c_{total,output} = c_1 \cdot \frac{\Gamma_{ant} s_{21}}{1 - \Gamma_{ant} s_{11}} + c_2. \quad (2.45)$$

Then, the input and output referred noise waves of the system should be related to each other by the gain of the system

$$c_{total,output} = A_{LNA} c_{total,input}, \quad (2.46)$$

where

$$A_{LNA} = \frac{s_{21}}{1 - s_{11}\Gamma_{ant}}. \quad (2.47)$$

Therefore,

$$c_{total,output} = \frac{s_{21}}{1 - s_{11}\Gamma_{ant}} c_{total,input} \quad (2.48)$$

$$c_{total,output} = \frac{s_{21}}{1 - s_{11}\Gamma_{ant}} \left(c_1 \cdot \Gamma_{ant} + c_2 \cdot \frac{1 - \Gamma_{ant}s_{11}}{s_{21}} \right), \quad (2.49)$$

and finally,

$$c_{total,output} = \left(c_1 \cdot \frac{s_{21}\Gamma_{ant}}{1 - s_{11}\Gamma_{ant}} + c_2 \right), \quad (2.50)$$

verifying that input referred noise from the LNA ports produces the same noise at the output of the system.

Referring noise to the input of a system is of particular importance in radio telescope design because beam equivalent noise directly affects how fast an astronomical observation can be made by the radio telescope (see the radiometer Equation 2.1).

2.14.1 Input Referred Noise Temperature

Input referred noise can be expressed in terms of noise temperature by using Nyquist's Equation 2.4. If the input referred noise temperature of each component in the receiver chain is known, and each component is power matched at the output, the beam equivalent system noise temperature can be found by using the Friis formula for noise temperature. Alternatively, if the beam equivalent noise temperature of each component in the receiver chain is known, the beam equivalent system noise temperature can be found by summing all the individual beam equivalent noise temperatures.

2.15 Traveling Noise Wave Delays in Transmission Lines

A noise wave $n(t)$ experiences time delay as it travel through a transmission line. Here, noise wave $n(t)$ is the same noise wave as in Equation 2.27; however, the noise wave is

now a function of time. The signal $n(t)$ travels through the transmission line at velocity v , which is the velocity factor v_p , $v_p \leq 1$, times the speed of light

$$v = c \cdot v_p. \quad (2.51)$$

As the signal travels through the transmission line, it is delayed by an amount proportional to the distance x traveled along the transmission line

$$n_x(t) = n(t) * \delta(t - \tau_d) = n(t - \tau_d) \quad (2.52)$$

where

$$\tau_d = \frac{x}{c \cdot v_p} \quad (2.53)$$

denotes the time a signal takes to travel a distance of x and $\delta(t)$ is the Dirac delta function. Note that $n(t)$ is convolved with the Dirac delta function to model the delay. This results in

$$n_x(f) = n(f) \cdot e^{-j2\pi f \tau_d}, \quad (2.54)$$

in the frequency domain where each frequency component is phase shifted by $-2\pi f \tau_d$.

It is important to note that the auto-correlation of the original noise $n(t)$ and the delayed noise $n(t - \tau_d)$ is no longer simply $\overline{n^2}$. Recall that noise is assumed to be WSS, which means that its correlation depends only on the difference in time. Thereby, the correlation of $n(t)$ and $n(t - \tau_d)$ is now a function of τ_d . An interesting observation here is that higher frequency components should go out of correlation faster than the low frequency components as τ_d is increased.

2.16 Conclusion

This chapter discusses electronic noise in detail. In particular, electronic noise as traveling noise waves is discussed as it will be used in later chapters to study the effects of delays on

antenna array noise. Important concepts related to noise in radiometers are also discussed.

Chapter 3

Antenna Array

3.1 Modeling Antennas as Circuit Elements

Circuit models of antennas tend to be simplistic regardless of antenna shape or operating frequency [25]. When an antenna is modeled as a transmitting antenna, it has a self-impedance Z_{self} and a radiation resistance R_{rad} in series (Figure 3.1a). The radiation resistance represents the losses attributed to the signals radiated away from the circuit and into free space. In the receiving antenna case, the received signal source is modeled as a voltage source in series with the antenna self-impedance [25]. The antenna self-impedance generally varies with frequency and sometimes quite drastically depending on antenna design (See Figure 4.4). The frequency varying antenna self-impedance can be viewed as a filter block when considering wideband design. This will become important when antenna arrays are discussed.

3.1.1 Antenna Losses, Matching, and Radiation Efficiency

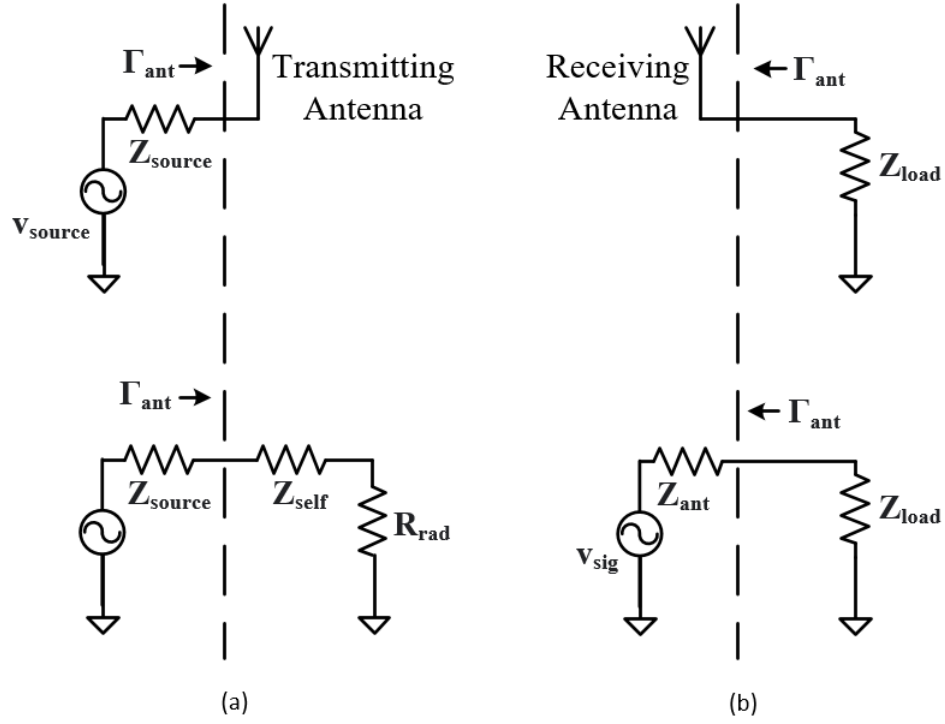


Figure 3.1: Circuit model of receiving and transmitting antennas with $Z_{ant} = Z_{self} + R_{rad}$.

The transmitting antennas have an impedance that needs to be matched to the driving source in order to deliver maximum power to the radiation element, R_{rad} , of the antenna. The radiation efficiency, η , of the antenna is the ratio of power radiated out to the sum of radiation power and power loss attributed to self-impedance. Radiation efficiency is most commonly expressed as

$$\eta = \frac{R_{rad}}{R_{rad} + R_{self}}, \quad (3.1)$$

where R_{self} is the real part of the antenna self-impedance, $R_{self} = \Re(Z_{self})$ [25].

In order to obtain maximum radiation strength in both receiving and transmitting antennas, the antenna has to be power matched to the load using the conjugate matching method

$$\Gamma_{ant} = \Gamma_s^*. \quad (3.2)$$

In many practical cases, antenna designers aim to match the antenna to the characteristic impedance of the system, which tends to be 50Ω . Designers who are more concerned with achieving low noise performance tend to transform the antenna impedance to the optimal impedance ($Z_{opt} = Y_{opt}^{-1}$) of the LNA that is used as a load to the antenna. Matching antenna to the load can be achieved by passive lumped elements or transmission line transformers of which there are several kind. An advantage of using lumped elements over transmission line transformers is that lumped elements take less space to implement.

This work focuses mainly on receiving antenna arrays, and as such all antennas will be modeled as signal voltage source in series with the antenna self-impedance as illustrated in Figure 3.1b.

3.2 Antenna Array

Arrays of antennas can be used to form a more sensitive antenna system if the received signal from each antenna is combined in phase. Antenna arrays increase the sensitivity of the receiver and allow for electronic steering of the main lobe of the antenna system without having to physically move the antenna or its reflector.

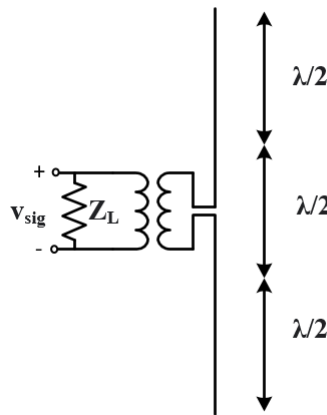


Figure 3.2: $3/2\lambda$ dipole antenna represented as a composite of 3 $1/2\lambda$ dipoles.

In order to develop an intuitive understanding of antenna arrays, consider the $3/2\lambda$ dipole antenna in Figure 3.2. The $3/2\lambda$ dipole antenna can be thought of as a composite

of three half-wave dipole antennas spaced $1/2\lambda$ apart. Assuming that the electromagnetic wave incident on the antenna is a plane wave with direction of propagation (Poynting vector) orthogonal to the antenna, then the current induced within the three half-wave antennas will be the same but with the phase offset corresponding to the half wavelength separation. The current from these 3 half-wave antennas is summed at the output port of the antenna (Figure 3.2)

$$I_{output} = I_0 + I_0e^{-j\pi} + I_0e^{-j\pi}. \quad (3.3)$$

For a general antenna of this type with $2 \cdot K + 1$ half-wave dipoles, the output current due to an orthogonal incident plane wave is

$$I = I_0 \left[2 \left(\sum_{k=1}^K e^{-j\pi k} \right) + 1 \right]. \quad (3.4)$$

The directivity of the antenna also increases by adding more half-wave dipoles. The individual elements have the directivity of 2.15 dBi, and the directivity of $3/2\lambda$ dipole is 3.5 dBi [34].

Dipole antennas have E-field pattern characterized by the equation

$$E_{\theta} = j\eta \frac{e^{-j\beta r}}{2\pi r} I_m \frac{\cos(\beta L/2 - \cos(\theta)) - \cos(\beta L/2)}{\sin(\theta)}, \quad (3.5)$$

where $\eta = \omega\mu/\beta$ is the impedance of free space, $\beta = 2\pi/\lambda$, I_m is the maximum current at feed point, r is distance from origin, and L is the length of dipole [34].

For a half-wave dipole antenna, $L = 1/2\lambda$, the E-field is

$$E_{\theta} = j\eta \frac{e^{-j\beta r}}{2\pi r} I_m \frac{\cos(\pi/2 \cdot \cos(\theta))}{\sin(\theta)}. \quad (3.6)$$

And for $L = 3/2\lambda$ the E-field is

$$E_{\theta} = j\eta \frac{e^{-j\beta r}}{2\pi r} I_m \frac{\cos(3\pi/2 \cdot \cos(\theta))}{\sin(\theta)}. \quad (3.7)$$

If the $L = 3/2\lambda$ antenna is modeled as a composite of 3 half-wavelength dipoles (Figure 3.2), the final E-field is the superposition of the individual E-field patterns of the three half-wave dipoles:

$$E_{\theta} = E_{\theta,1} + E_{\theta,2} + E_{\theta,3}, \quad (3.8)$$

$$E_{\theta} = \left[j\eta \frac{e^{-j\beta r}}{2\pi r} I_m \frac{\cos(\pi/2 \cdot \cos(\theta))}{\sin(\theta)} \right] + \left[j\eta \frac{e^{-j\beta(r-\lambda/2 \cdot \cos(\theta)) - j\pi}}{2\pi r} I_m \frac{\cos(\pi/2 \cdot \cos(\theta))}{\sin(\theta)} \right] + \left[j\eta \frac{e^{-j\beta(r+\lambda/2 \cdot \cos(\theta)) - j\pi}}{2\pi r} I_m \frac{\cos(\pi/2 \cdot \cos(\theta))}{\sin(\theta)} \right] \quad (3.9)$$

where the $-j\beta(r - \lambda/2 \cdot \cos(\theta))$ in the exponential of adjacent elements describes the phase change due to spatial distribution of the half-wave antennas, and $-j\pi$ models the phase shift of the signals as they travel from adjacent elements to the feed point of the middle antenna.

Further simplification of the above equation yields

$$E_{\theta} = \left[j\eta \frac{e^{-j\beta r}}{2\pi r} I_m \frac{\cos(\pi/2 \cdot \cos(\theta))}{\sin(\theta)} \right] \cdot \left[1 + e^{-j\beta(\lambda/2 \cdot \cos(\theta)) - j\pi} + e^{+j\beta(\lambda/2 \cdot \cos(\theta)) - j\pi} \right] \quad (3.10)$$

In Equation 3.10, the E-field expression of half-wave dipole antenna,

$\left(E_{\theta} = \left[j\eta \frac{e^{-j\beta r}}{2\pi r} I_m \frac{\cos(\pi/2 \cdot \cos(\theta))}{\sin(\theta)} \right] \right)$, can be distinguished from the array factor, which is

$$AF = \left[1 + e^{-j\beta(\lambda/2 \cdot \cos(\theta)) - j\pi} + e^{-j\beta(-\lambda/2 \cdot \cos(\theta)) - j\pi} \right]. \quad (3.11)$$

Equations 3.7 and 3.10 are equivalent models of a $3/2\lambda$ dipole antenna, ignoring the impedance of the two circuits. Figure 3.3 shows a polar plot of normalized E-field from equations 3.7 and 3.10. The two equations produce the same E-field patterns.

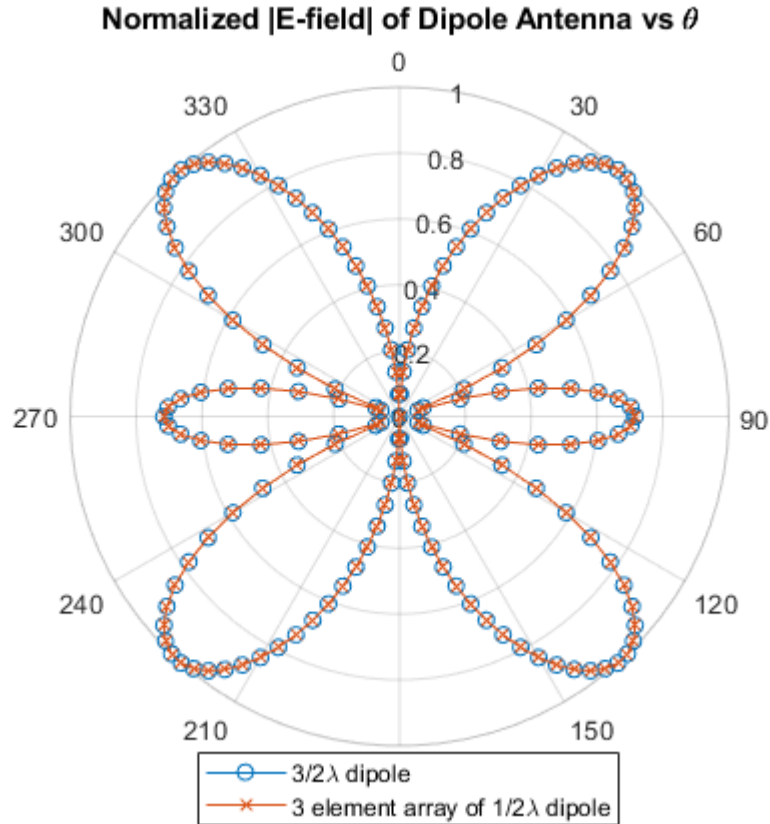


Figure 3.3: Plot of normalized E-field from equations 3.7 and 3.10.

Conventionally, antenna arrays incorporate LNAs, phase shifters, filters and signal summers. There are a few different architectures of antenna arrays, such as active phased array, passive phased array, and hybrid arrays. Another class of antenna array is the interferometer. In interferometers, signals from each array element, separated by a maximum distance d , are correlated rather than added at the output. In radio telescopes, the angular resolution obtained using this method is equal to that obtained using a single element telescope with aperture diameter of d [35]. Effectively, the array has the same angular resolution as a much larger telescope without having to physically construct it, where angular resolution θ , is obtained using $\theta = 1.22\lambda/d$. Interferometers, although similar to active phased arrays, are outside the scope of this work and are not considered further.

3.2.1 Active Antenna Arrays

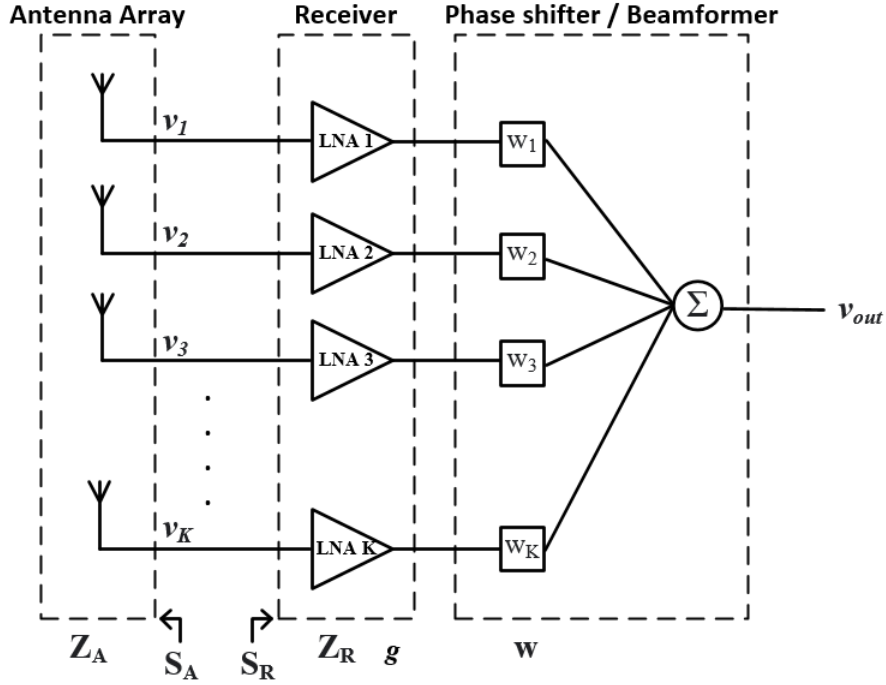


Figure 3.4: Simple receiving phased array

Active phased arrays, or active electronically scanned arrays, are gaining in popularity in radio telescope design [36] due to their beamforming ability. In an active phased array architecture, the signal from each antenna is amplified, phase shifted individually, and summed before the output (Figure 3.4). The phase shift and amplification at the output is referred to as the weight of the beamformer, $w_k = A_k e^{-j\phi_k}$, where A_k is the gain and ϕ_k is the phase shift introduced by the k^{th} weight. The beamformer is the part of the array that is typically located after the receivers as seen in Figure 3.4.

The output of the array can be expressed as

$$v_{out} = 0.5 \cdot \sum_{k=1}^K g \cdot v_k w_k, \quad (3.12)$$

where v_{out} is the output voltage of the array, v_k is the open circuit voltage of k^{th} antenna, w_k is the k^{th} beamformer weight, and g is the voltage gain of the receiver chain. This is

assuming that the receiver input impedance, \mathbf{Z}_R , and the antenna impedance matrix, \mathbf{Z}_A , are equal to the identity matrix, $\mathbf{Z}_A = \mathbf{Z}_R = \mathbf{I}$.

It is possible to alter the incoming signal from any one of the antenna elements to dampen out interference from that element or to increase the gain from others that might have better SNR. An important quality of active phased arrays is their ability to form and electronically steer a beam that is more directive than the maximum directivity of the individual elements. In more complex implementations, such as fire control radars, several beams can be independent steered simultaneously, or nulls (directions where gain is minimal) can be steered towards sources of deliberate interference such as jammers in order to reject the jamming signal.

The standard equation for voltage output of the array is [37]

$$v_{out} = g \cdot \mathbf{w}^H \mathbf{Z}_R (\mathbf{Z}_R + \mathbf{Z}_A)^{-1} \mathbf{v}, \quad (3.13)$$

where $\mathbf{w} = \begin{bmatrix} w_1 & w_2 & \cdots & w_K \end{bmatrix}^T$ is the beamformer weight vector and \mathbf{v} is a vector of open circuit voltages at the antenna outputs. In subsequent sections, the array in Figure 3.4 will be described using traveling power waves and S-parameters.

3.2.2 Beam Steering

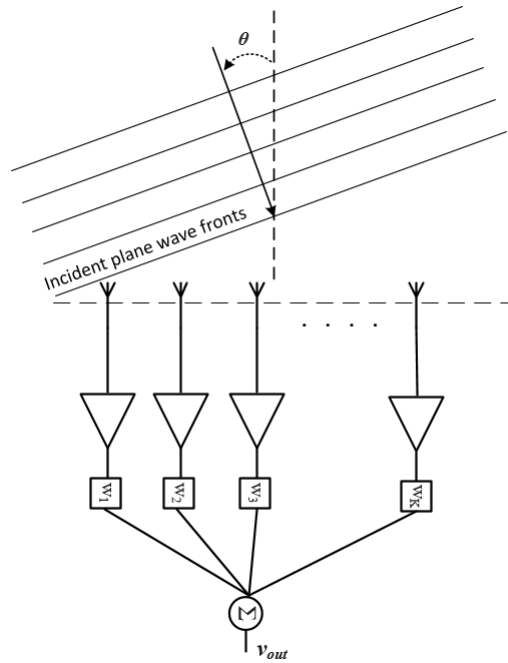


Figure 3.5: Receiving array with incident wave at an angle of θ .

One of the main advantages of phased antenna arrays is the ability to steer the main lobe of radiation pattern in different directions without having to physically move the array. This is accomplished by changing the phases from individual elements so that signals coming from a particular direction are constructively added and signals from other directions are destructively added creating direction of maximum directivity (lobes) and minimum directivity (nulls). Consider the array in Figure 3.5. A signal incident upon the array at angle θ arrives at the first element at time 0. The wave front arrives at the second element at a later time and with a phase shift corresponding to the extra path the signal takes. The phase shift is $\beta d \cos(\theta)$, where d is the distance of first element to the second element. In order to maximize the signal coming from the direction θ , the phase shifter has to shift the phases of each element such that signals from that direction add constructively at the output.

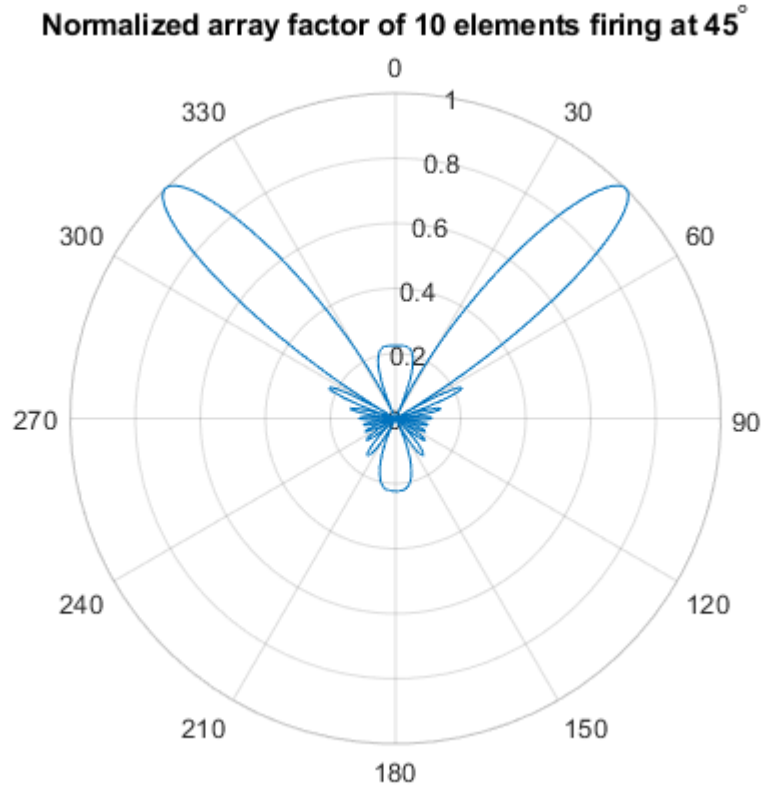


Figure 3.6: Plot of array factor pattern with array operating at 45° .

One way of achieving this is by setting the n^{th} beamformer phase of an equally spaced linear array (ESLA) to $n \cdot \beta d \cos(\theta)$ (assuming all feed lines are of equal length). The resulting pattern would look like the one in Figure 3.6 given that the antenna elements are isotropic. Notice that the field pattern of the active array is completely different from the individual isotropic antennas. There are numerous and more effective algorithms for beam steering and beamforming that have been developed since arrays were first invented; however, these methods are outside the scope of this work.

3.2.3 Noise in Antenna Arrays

In the field of radio astronomy, beam equivalent noise temperature is one of the primary ways of expressing noise performance of antenna arrays. Beam equivalent noise temperature is the noise output of the array referred to the output of the antenna ports per unit

bandwidth expressed as noise temperature under isotropic environment temperature [37]

$$T_{sys} = T_{iso} \frac{P_N}{P_{t,iso}}, \quad (3.14)$$

where P_N represents the power of noise sources in the active array, $P_{t,iso}$ is the isotropic thermal noise power of the array under thermal equilibrium, and T_{iso} the isotropic environment temperature of the array. P_N is comprised of noise due to ohmic losses, the receiver noise, and the noise external to the array. Noise sources that are external to the array are referenced to the outside of the array; that is, before the self-impedance of the array and outside the array itself [15].

3.3 Array Factor

Antenna arrays can be constructed with any antenna type provided the signals are combined in the end. The underlying geometry of the array and electronic architecture of the beamformer can be separated from the antenna elements themselves and analyzed separately. As discussed in Section 3.2, the E-field pattern of half-wave dipole array is composed of two terms multiplied together. One of the terms, Equation 3.6, is the E-field of the original $1/2\lambda$ dipole and the other term, Equation 3.10, is the array factor. This quantity is a multiplicative factor that describes the array pattern with isotropic antenna elements. Array factor allows for the analysis and description of an array architecture without having to complicate the analysis with complex field patterns of constituent antenna type. The final field pattern of the array can then be determined by multiplying the array factor by the field pattern of constituent antennas provided all the elements are identical. The array factor equation of ESLA spaced apart by d and with feed line delay of α is

$$AF = \sum_{n=0}^N A_n w_n \cdot e^{-jn(\beta d \cos(\theta) + \alpha_n)}, \quad (3.15)$$

where w_n is the n^{th} complex beamformer weight and A_n is the complex gain of n^{th} LNA.

Array factor of 2 dimensional arrays can be constructed by first making an array factor of elements in one direction and multiplying it by the array factor of the other direction. The antennas in each row and column of the 2D array must be equally spaced apart and each row and column must have the same number of elements.

3.4 Antenna S-parameters

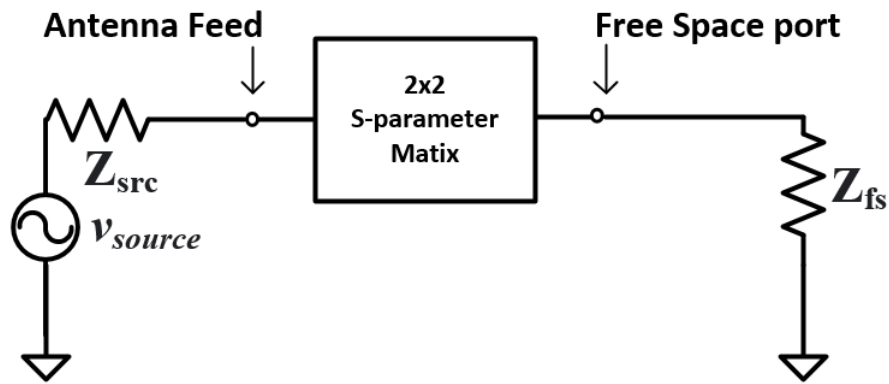


Figure 3.7: Antenna modeled with free space port.

An antenna can be thought of as a 2-port network with the feed point being one of the ports and free space (or other medium the antenna is designed for) being the other port. An antenna driven by a signal can be modeled as the 2-port network driven by a source at the feed port and free space impedance at the output port (Figure 3.7) [38]. In this model, s_{11} is the reflection coefficient of the antenna also known as Γ_{ant} , and s_{21} is the transmission coefficient of the fed signal to free space, which is related to the antenna operating in the transmitting mode. s_{12} is that transmission coefficient from free space to the antenna feed, which is related to the antenna operating in the receiving mode. And s_{22} is the reflection coefficient of the free space port, which is related to the antenna radar cross section.

3.5 Antenna-Array Mutual Impedance and Mutual Coupling

Antenna arrays are naturally multi-port devices. An array with M elements can be described as an M -port network. Antenna arrays are mostly described using the Z, Y, and S-parameters; however, S-parameters are most suitable for high frequency antennas owing to the difficulty of measuring Z or Y parameters at high frequencies. The antenna S-parameter matrix is an $M \times M$ matrix. The diagonal entries of the matrix, describe the reflection coefficient of each antenna port and the off diagonal entries, $s_{mn}, n \neq m$, quantify mutual coupling from the n^{th} element to the m^{th} element.

Mutual impedance or mutual coupling is a well-known phenomenon in antenna arrays, whose analysis is dating back to the 1960's [39, 40]. Antenna elements in many arrays are spaced close together, which causes signals to couple from one antenna to another via the near field and far field. Antenna arrays must have element spacing less than $\lambda/2$ in order to avoid grating lobes (secondary main lobes) [34]. Mutual impedance decreases as element spacing increases [41]. In most applications, mutual impedance is also considered to be an undesired side effect of closely spaced antenna elements. Large mutual impedance also reduces the overall efficiency of the array in transmitting mode and by reciprocity in receiving mode [39]. One of the first efforts to decouple the array elements from each other was by Andersen et al. [42]. They described a simple $2M$ port lossless network inserted between the array and the receiver that decoupled the array. However, the method required that the mutual coupling of the array to be purely reactive and worked in very narrowband cases. This method, although insightful, did not describe a practical means of decoupling an array. In more recent works, it is shown that it is possible, at least theoretically, to decouple the antenna array using a lossless matching network between antenna ports and receiver inputs [43,44]. The central focus of these methods is to design a matching network for the array that “diagonalizes” the array in such a way that it presents $\Gamma_{opt}\mathbf{I}$ array to the LNAs, where Γ_{opt} is the optimal reflection coefficient for LNAs that minimizes LNA noise.

Such matching networks are complex to compute and even more complex to construct for large arrays. Again, such a network would only work in narrowband case. Another problem with this decoupling method is that when a different beam angle is used, the decoupling network can no longer be used to obtain optimal noise match for the array.

An array scattering matrix that is diagonal implies that the radiation pattern of each element is orthogonal to the others [40]. Conversely, an array scattering matrix with mutual coupling has elemental radiation pattern that are not orthogonal to the other elements. This implies that a matching network that “diagonalizes” the array is in effect changing the overall active radiation pattern of each element in order to add the non-orthogonal components of the radiation pattern in a destructive manner in order to cancel them out [43].

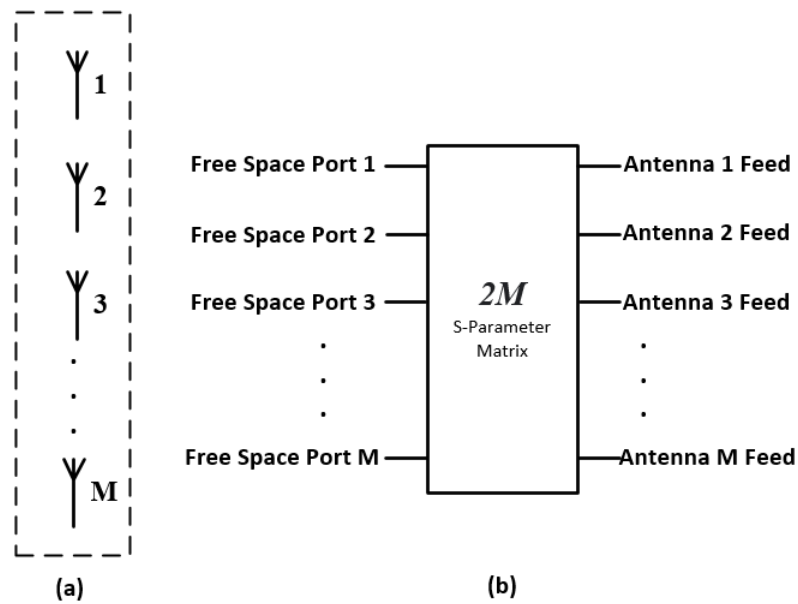


Figure 3.8: N-element array modeled as 2M-port network.

Much like a single antenna, an antenna array with M elements can be modeled using a $2M$ port network [38]. In this model, mutual coupling is described by a coupling matrix S_{Mu} existing in the free space between the antennas (Figure 3.9). The free space port of each antenna in the M antenna array is terminated with Z_{fs} (impedance of free space) and it is connected to the mutual coupling matrix. The $2M$ -port antenna-array network is constructed from the antenna S-parameters and the mutual coupling matrix S_{Mu} . Half of

the ports, ports 1 to M , are antenna feed points, and the rest, ports $M + 1$ to $2M$, represent free space ports. In transmitting mode, the array is fed from sources at each of the M feed ports of the array, and ideally, the M free space ports are terminated with Z_{fs} . In receiving mode, the free space ports are driven by the signal source via Z_{fs} and the feed ports of the antennas are terminated in load impedance (Figure 3.9).

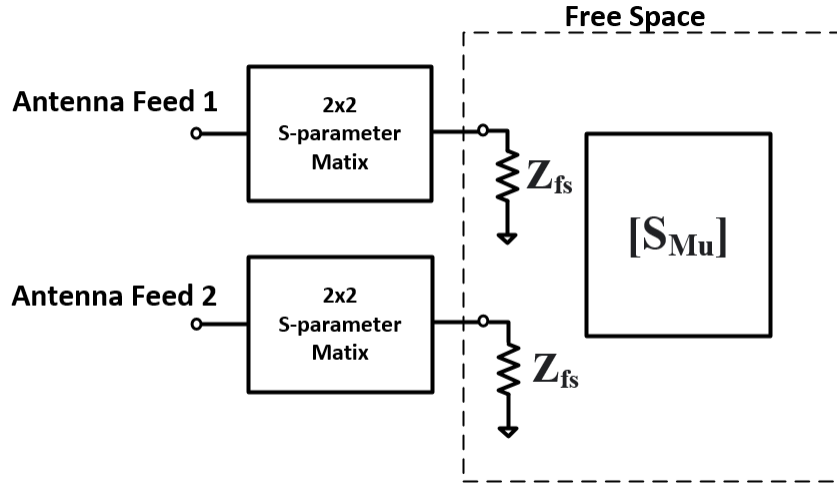


Figure 3.9: 2-element array model with free-space mutual-coupling matrix.

One advantage of modeling antenna arrays using the $2M$ ports method is that it allows for describing signal coupling from one antenna to another via free space, which includes the far field and also the near field effects. Consider an antenna array with two elements, $M = 2$ (Figure 3.9). The array is a 4 port network with two of the ports dedicated to free space. With this array operating in receiving mode with reflection-less terminations at the feed ports, consider now a signal incident upon the free space port $n = M + 1 = 3$. This signal can take a few paths. It can be reflected back to free space via s_{33} , transmitted to either of the antenna feed ports via s_{13} or s_{23} , or be coupled to the second antenna and radiated out to free space again via s_{43} . The last two cases occur when the signal couples from one antenna to another due to mutual coupling matrix S_{Mu} .

Although this method of modeling antenna arrays provides a way to characterize the mutual coupling, the coupling of signals to free space can be safely ignored when analyzing

signals within the array, for example, the LNA noise signal that is generated internally to the receiver. It is not of concern if these noise signals radiate out to free space and do not return.

3.6 Effects of Mutual Coupling on Array Noise

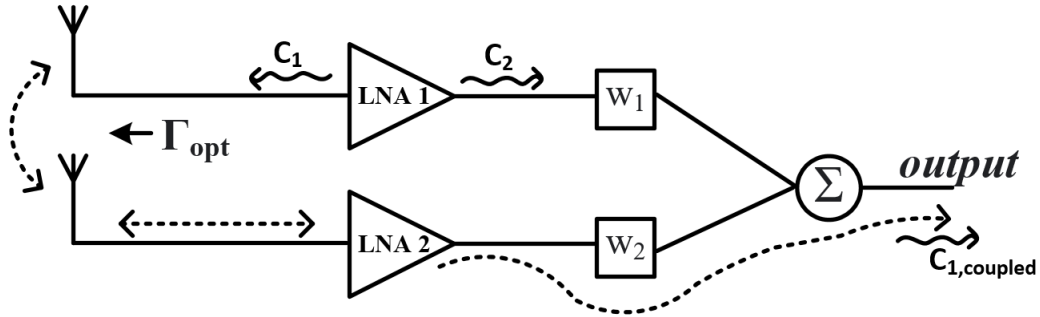


Figure 3.10: 2-element array with forward noise-wave coupling to the output via mutual impedance path in the array.

Mutual coupling is an inevitable consequence of constructing antenna arrays with dense spacing. It is important to understand how noise propagates within the array in the presence of mutual coupling. Consider a 2-element array of the kind shown in Figure 3.10, with non-negligible mutual coupling, operating in the absence of incident radiation. The LNAs generate partially correlated noise waves at their input and output ports. If the output port of the LNA is terminated properly, $Z_{load} = Z_0$, then in order to obtain minimum noise for each LNAs the input port must see Γ_{opt} looking towards the array. This allows the right amount of noise wave c_1 with the proper phase to be reflected back towards the LNA in order to cancel some of the correlation between c_1 and c_2 out and minimize the overall LNA noise [30]. However, due of mutual coupling, c_1 gets added to the output of array via beamformer, which increases the overall noise temperature of the system. This scenario shows that matching the LNA to the self-impedance of the array is not the optimal noise matching condition for arrays with significant mutual coupling. Arrays with mutual coupling present a more complex flow of noise signals that require a more detailed analysis.

For a receiving phased array, the standard equation for determining beam equivalent receiver noise temperature is [37]

$$T_{rec} = T_{iso} \frac{\mathbf{w}^H \mathbf{R}_{rec} \mathbf{w}}{\mathbf{w}^H \mathbf{R}_t \mathbf{w}}, \quad (3.16)$$

where \mathbf{R}_{rec} is the receiver noise correlation matrix, T_{iso} is the isotropic environment temperature, and \mathbf{R}_t is the array thermal noise correlation matrix defined as

$$\mathbf{R}_t = k_b T_{iso} B \cdot \mathbf{G} (\mathbf{I} - \mathbf{S}_A \mathbf{S}_A^H) \mathbf{G}^H, \quad (3.17)$$

where \mathbf{S}_A is the array S-parameter matrix, and B is bandwidth, and

$$\mathbf{G} = g \sqrt{Z_0} (\mathbf{I} + \mathbf{S}_R) (\mathbf{I} - \mathbf{S}_A \mathbf{S}_R)^{-1}, \quad (3.18)$$

where g is voltage gain of receiver, and $\mathbf{S}_R = \mathbf{I} \cdot S_{LNA,11}$ is the receiver S-parameter matrix (Figure 3.4). Notice the presence of \mathbf{S}_A term in \mathbf{R}_t and \mathbf{G} as the off-diagonal terms of \mathbf{S}_A that quantify mutual coupling play a significant role in determining receiver noise temperature.

3.6.1 Mutual Coupling and Antenna Separation Distance

There is a reciprocal relationship between mutual coupling and array element separation distance. Ivashina et al. discuss this adverse relationship between separation and mutual coupling in [45]. Of particular importance in that paper is the result that the array system temperature, T_{sys} , increases drastically when element separation falls below 0.5λ . This is attributed to an increase in the array self-impedance and array active impedance. The system temperature levels off as the distance between elements increases to more than $\sim 0.7\lambda$. Interestingly, Ivashina et al. focused on the effects of separation on s_{11} and active reflection coefficient for a 2 and 3 element dipole array. They chose not to discuss s_{21} of the array as the separation is decreased its effect on array noise temperature. Although

active reflection coefficient includes s_{21} , it also includes quantities such as LNA s_{11} and beamformer weights. This obscures the reason behind the increase of T_{sys} . As will be shown in Chapter 4 in Figure 4.5b, the separation between 2-dipole elements decreases, the magnitude of array s_{21} increases very fast below 0.5λ . The curve in Figure 4.5b is similar to the system temperature curve in [45] suggesting the primary mechanism of T_{sys} increase maybe due to the increase of s_{21} of the array.

3.7 Active Array Impedance

Much like mutual coupling, active impedance and its effect on array noise had been well-known for some time [39,40]. One of the reasons why setting the LNA Γ_{opt} to the array s_{mm} does not minimize array noise is that the m^{th} LNA does not see the passive array impedance Z_{mm} looking towards the array. Rather, it sees the entire active array, which includes the mutual impedance, LNA input impedance, and the beamformer weights. Therefore, in order to minimize overall array noise, each LNA must be matched to the active array impedance rather than the passive array impedance. Active array impedance, and active reflection coefficient $\Gamma_{act,m}$, is difficult to measure directly and can only be calculated based on measured values of array and receiver network parameters because introducing measurement apparatus into an active array changes the active array and it no longer represents the original system.

There have been recent attempts at measuring Γ_{act} with the use of directional couplers [46, 47]. However, these methods also change the underlying system and cannot directly measure Γ_{act} accurately due to the non ideal nature of directional couplers. There are several definitions in literature for Γ_{act} with the common theme of defining Γ_{act} as

$$\Gamma_{act,m} = \frac{b_m(\theta, \phi)}{a_m(\theta, \phi)}, \quad (3.19)$$

where b_m and a_m are both dependent on the beam angles θ and ϕ [48]. Although this def-

inition for Γ_{act} is for a transmitting array, due to reciprocity it can also be used to describe the Γ_{act} for receiving array.

3.7.1 Active Reflection Coefficient Matching

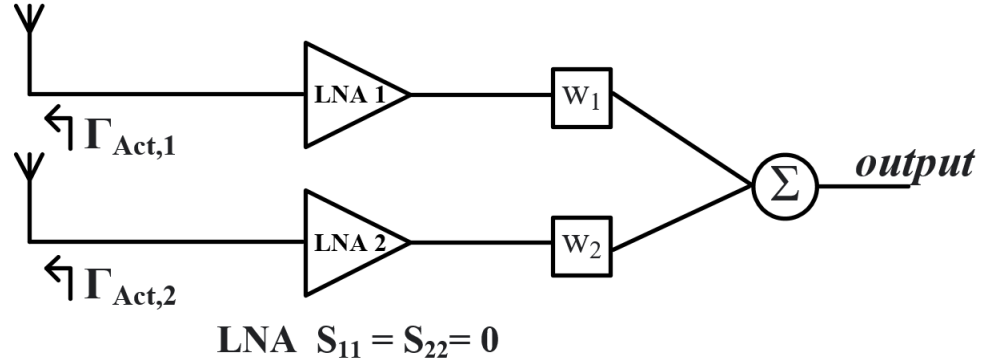


Figure 3.11: 2-element array with identical LNAs having $s_{11} = s_{22} = 0$.

Active array impedance and active reflection coefficient had been well-known for a long time; however, matching to it was not concretely described in literature until Maaskant and Woestenbergh described it using traveling noise waves [14]. The analysis was done using a simple 2-element array, similar to one in Figure 3.11, with LNA $s_{11} = s_{22} = 0$ and phase shifter that change the weights of the beamformer. They described Γ_{act} of m^{th} antenna as the sum of passive antenna reflection coefficient, s_{mm} , and the forward transmissions s_{km} phase shifted by the beamformer. Then, they matched the LNAs to these $\Gamma_{act,m}$ in order to minimize the overall system noise temperature to lower than what is possible with matching to s_{mm} .

Maaskant et al. described Γ_{act} as follows [14]

$$\Gamma_{act,m} = \frac{1}{w_m^*} \left(\sum_{k=1}^M S_{km} \cdot w_k^* \right). \quad (3.20)$$

This definition assumes that the LNA's $s_{11} = 0$, so it is not a general definition for Γ_{act} . Nevertheless, Maaskant et al. showed through mathematics and simulation that it is in fact

possible to noise match the LNAs to the active reflection coefficient and obtain an array noise performance near the absolute minimum possible for the receiver and the array.

A problem in this matching scheme, and one that was immediately recognized by Maaskant, is that minimum noise is only attainable for a particular scan direction corresponding to single set of beamformer weights. Maaskant et al. acknowledged that matching to the passive reflection coefficient produces a lower overall receiver noise temperature for a larger scan volume [14].

Another problem, which has more to do with practicality, is that the active reflection coefficients are different for each array element. The array designer will have to design as many LNAs as there are antenna elements in the array. Although this problem is not insurmountable given adequate resources, most designers tend to use identical LNAs in receivers and such a drastic departure from established design methods is unlikely to be widely adopted.

Since Maaskant's original work, there have been attempts to use the active reflection coefficient to obtain a lower receiver noise temperature [16, 17, 49]. An attempt that stands out in literature is by Warnick et al. who tried to optimize the receiver noise over several scan directions [16]. More on this method in Chapter 4. Warnick also presented a novel way of calculating the Γ_{act} that was more general than Maaskant's definition in the fact that it included LNAs that had $s_{11} \neq 0$. The definition relied heavily on Warnick's convention of using matrix transformations that transform various quantities to the output of the receiver, for example

$$v = \mathbf{Q}v_{oc}, \quad (3.21)$$

where \mathbf{Q} transforms open circuit voltages (v_{oc}) at the array ports to voltages at the output of the receiver (v). Warnick et al. definition, which is similar to Maaskant's, is [16]

$$\Gamma_{act,m} = \frac{1}{\mathbf{w}_{f,m}^*} \left(\sum_{k=1}^M S_{km} \cdot \mathbf{w}_{f,k}^* \right), \quad (3.22)$$

where $w_{f,m}$ are the beamformer weights referred to the input of LNAs via the transformation matrix \mathbf{G} :

$$\mathbf{w}_f = \mathbf{G}^H \mathbf{w}$$

A more detailed description of both \mathbf{Q} and \mathbf{G} can be found in Chapter 4.

There are other definitions in literature that describe Γ_{act} but arrive at it using different approaches. Belostotski et al. used mutual coupling parameters (M-parameters) to derive Γ_{act} [17] and arrived at the same results.

3.8 Conclusion

Antenna arrays are versatile devices that provide electronic beam steering and increased directivity. Antenna arrays have an active impedance that must be taken into consideration when designing receivers in order to optimize array noise. This chapter discusses prerequisite concepts in antenna array theory that will be used in the next chapter.

Chapter 4

Propagation Delays in Antenna Array

The analysis of delays in antenna array and their impact on array noise and noise matching had not been discussed in literature prior to [50] (a publication resulting from this work). Delays in antenna arrays are an intrinsic part of the array S-parameters provided that they are measured correctly. Conventionally, array S-parameters are measured by assuming the passive array as an M-port network using vectored network analyzer (VNA). The array S-parameters can be used to calculate the theoretical noise power at the output due to the array thermal noise. They are also used to design LNAs with Γ_{opt} that minimizes the receiver noise. In this chapter, propagation delays are incorporated in the analysis of array noise, and a study of impact of noise delays on Γ_{act} and T_{rec} is performed. And finally, a method is developed for matching the active array to identical LNAs that optimize the overall noise of the active array.

4.1 Modeling Propagation Delays in Antenna Array

S-parameters of an array with M elements can be described as an $M \times M$ matrix with complex entries s_{ij} that have an amplitude S_{ij} and a phase θ , $s_{ij} = S_{ij} \cdot e^{j\theta_{ij}}$. The quantity s_{ij} is the ratio of traveling power wave emanating from port i to the traveling power wave incident on port j given all other ports are terminated properly with reflection-less terminations and the array is not excited by an external source [51]. Using this definition, s_{ij} naturally contain the delays a narrowband signal experiences while traveling from port j (p_j) to port i (p_i). Observing Figure 4.1, there are two cases to consider while following signal propagation. First is when $i = j$ and the second is when $i \neq j$.

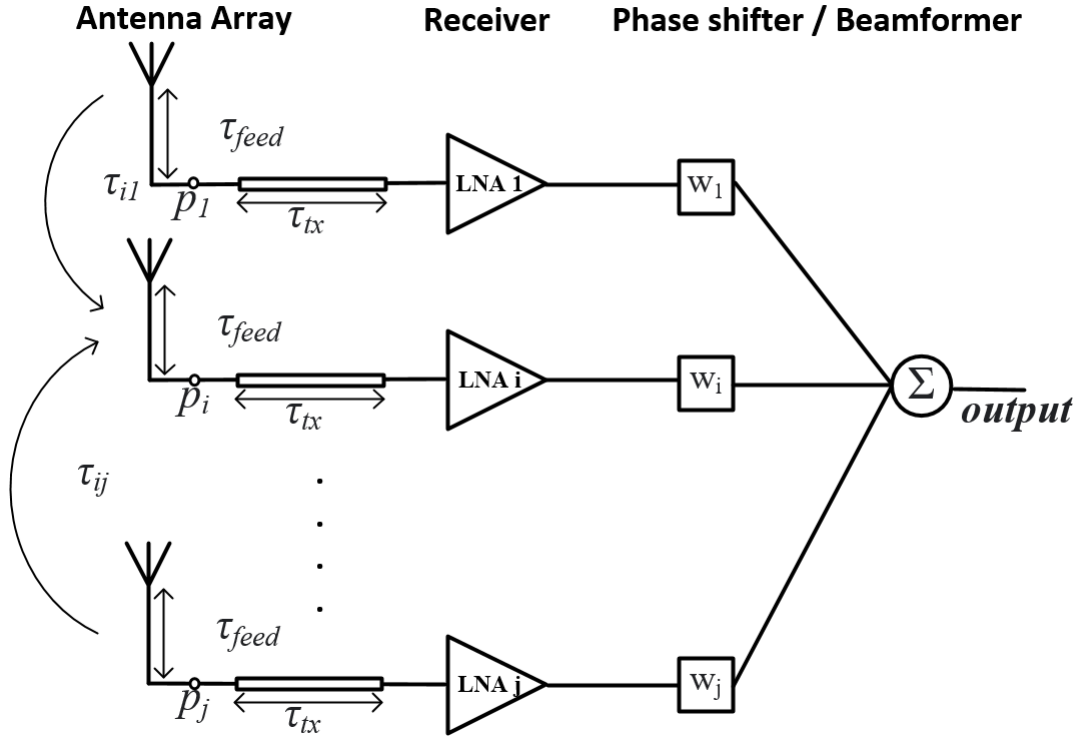


Figure 4.1: Antenna array with transmission line, antenna feed, and inter antenna delay.

Consider the $i = j$ case where the s_{ii} represents the reflection coefficient of port i . In this case, the delay a noise signal experiences is comprised of transmission line delay and the delay between antenna port and feed of the antenna. The delay term and the intrinsic reflection coefficient can be expressed separately in the antenna S-parameters

$$s_{ii} = S_{ii} \cdot e^{j\theta_{ii}} = S_{ii} e^{j\phi_{ii}} \cdot e^{-j2\pi f \tau_{delay}}, \quad (4.1)$$

where ϕ_{ii} is the phase shift of the reflected signal excluding the delay phase shift. Note that $\phi_{ii} - j2\pi f_0 \tau_{delay}$ equals θ_{ii} because s_{ii} has to be correct at the frequency, f_0 , it was measured at.

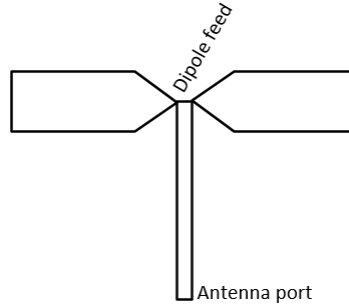


Figure 4.2: Simplified diagram of thick dipole antenna with long feed line.

So far, a result like this can be derived from a well-known equation for transmission line S-parameters found in popular microwave design texts such as [51]. However, to further demonstrate that signal delays are indeed present within antenna elements, consider Figure 4.2. It shows a simplified diagram of thick dipole antenna found in [49]. The antenna port is at the bottom and dipole feed point at the top in the diagram. The antenna port cannot physically be at the antenna feed point. It is usually some distance away from it for reasons of practicality. The distance d between the port and the feed, translates to a signal delay of $\tau_d = \frac{d}{v_p}$ with v_p being the propagation velocity of the antenna feed line. It is noteworthy to recognize the feed line delay as distinct from transmission line delay because the propagation velocities in these areas can be different causing different delay times for the same length of propagation medium. A noise signal injected into the antenna port experiences delay twice within the feed line. First, while propagating towards the antenna feed point, and second, while propagating back to the port after being reflected at the antenna if the signal is not transmitted completely into free space.

Now consider the $i \neq j$ case. In this case a noise signal injected into the j^{th} port is observed as it appears at the i^{th} port. As shown in Figure 4.1, the signal propagates along the transmission line to the antenna feed and experiences the delay $\tau_d + \tau_{tx}$. It then enters the antenna, and this time, it propagates to the i^{th} antenna. Antenna i is placed at some distance d_{ij} away from the j^{th} antenna. The signal leaves antenna j and arrives at antenna i after some time τ_{ij} , which is calculated by assuming speed of light (c) as propagation

velocity, $\tau_{ij} = \frac{d_{ij}}{c}$. Because the signal propagates in air, assuming the speed of light as propagation velocity is reasonable. As with the feed line propagation delay derived earlier, the inter-element delay τ_{ij} can be separated from the narrowband S-parameter of the array

$$s_{ij} = S_{ij}e^{j\phi_{ij}} \cdot e^{-j2\pi f \cdot 2\tau_d} \cdot e^{-j2\pi f \tau_{ij}} \cdot e^{-j2\pi f \cdot 2\tau_{ix}} \quad (4.2)$$

$$s_{ij} = S_{ij}e^{j\phi_{ij}} \cdot e^{-j2\pi f (2\tau_d + \tau_{ij} + 2\tau_{ix})}. \quad (4.3)$$

Again, the intrinsic transmission coefficient $S_{ij}e^{j\phi_{ij}}$ is assumed to be constant over the frequency band under consideration. This assumption is reasonable because it can be used for a frequency range where the antenna intrinsic transmission coefficient is relatively constant.

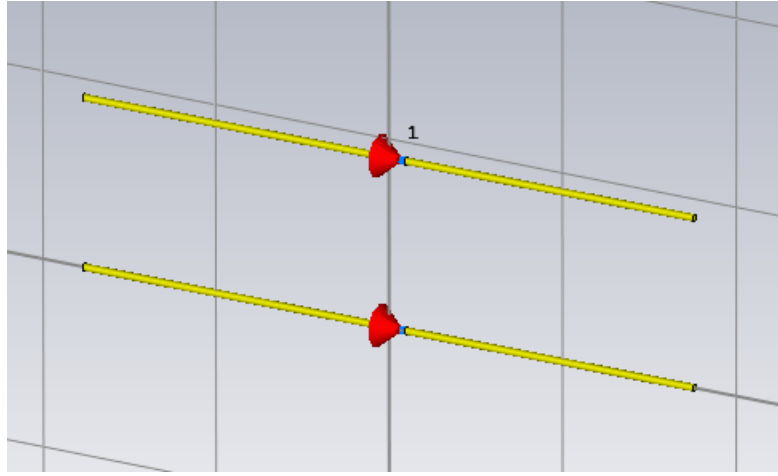


Figure 4.3: CAD model of $1/2\lambda$ dipole 1-GHz antenna array in CST.

It is not clear whether the overall effect of delays is as simple as $e^{-j2\pi f_0(2\tau_d + \tau_{ij} + 2\tau_{ix})}$, that is, it depends primarily on the distance between the array elements and propagation velocity. To verify this assumption, an experiment was setup in CST electromagnetic simulation software. In this experiment, a simple two-element half-wave dipole array was setup operating at 1-GHz with each antenna fed with a separate port (Figure 4.3). Next, the S-parameters of the array were extracted using CST built-in functions. Figure 4.4 shows the phase of s_{21} of this setup with antennas separated by 0.9λ . Observe that the expected $-2\pi f(\tau_{ij})$ curve is embedded in the phase curve that would otherwise not exist in the

absence of the delay caused by the 0.9λ separation (Figure 4.4).

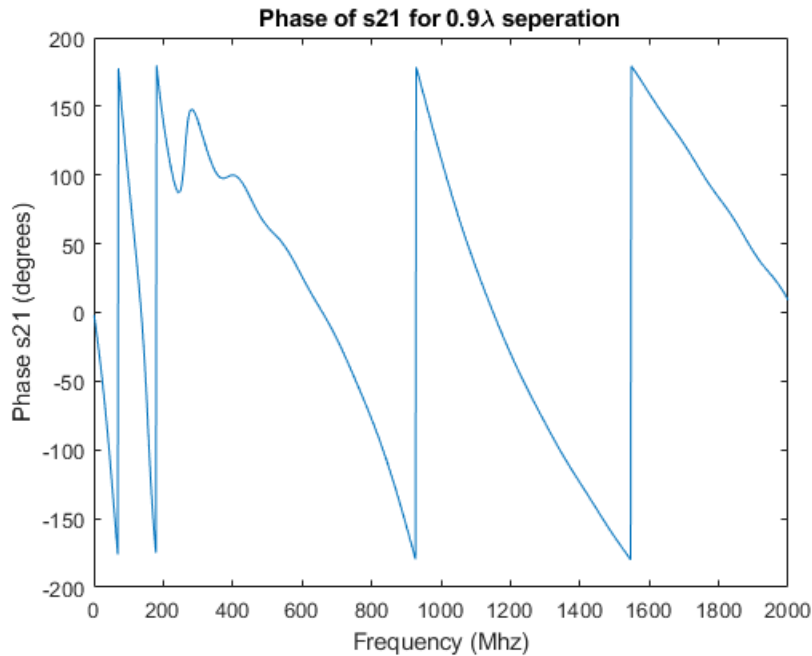
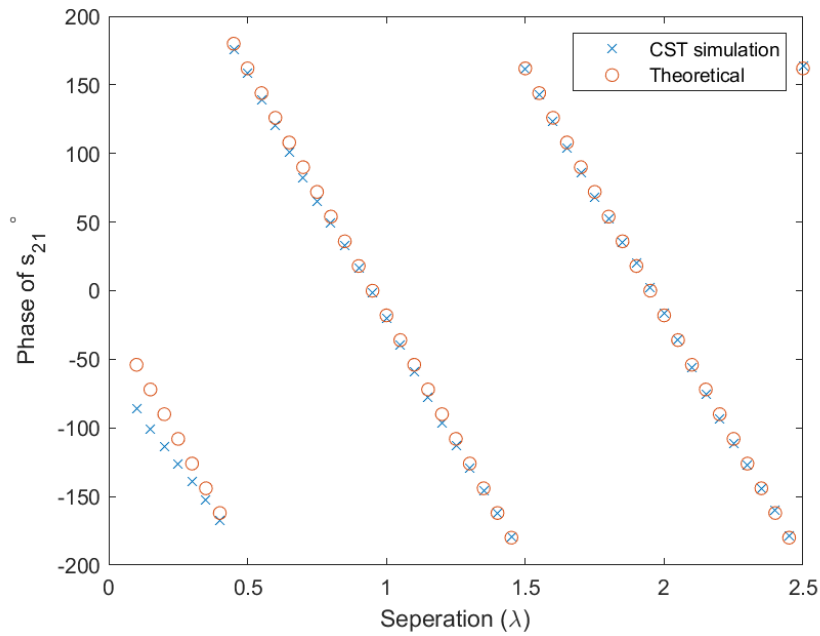


Figure 4.4: CST simulation results for 0.9λ separation of 2-element dipole array showing phase of s_{21} of the array as a function of frequency.

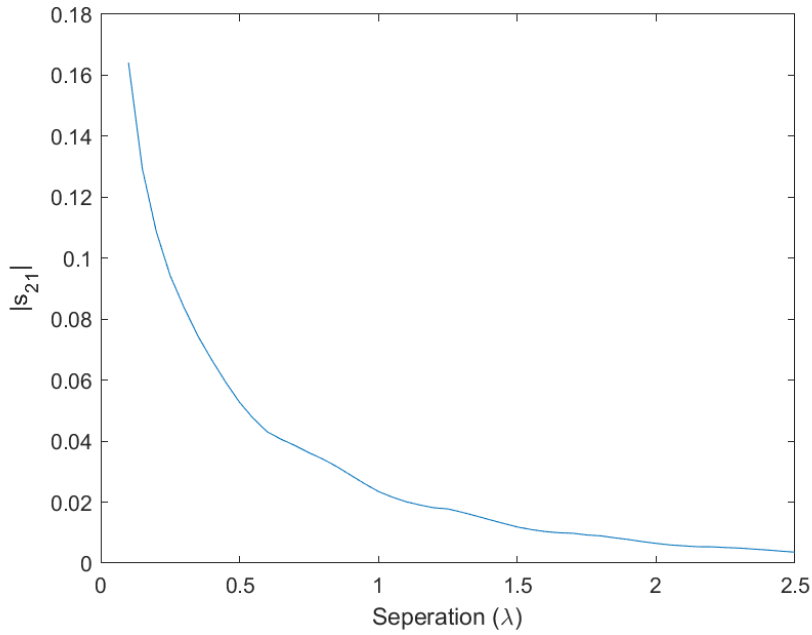
In order to discern the delay phase curve from intrinsic phase curve of the s_{21} , another simulation was conducted using CST. In this simulation, the second antenna was moved from 0.1λ to 2.5λ in increments of 0.05λ steps, and the phase of s_{21} was simulated and recorded. Figure 4.5a illustrates the result of this CST simulation and theoretical phase of s_{21} as calculated using Equation 4.3. As expected, the phase of s_{21} changed almost exactly as predicted due to the delay caused by the separation (Figure 4.5a). Therefore, it was verified that the downwards sloping of s_{21} phase curve was due, in part, to the propagation delay.

Although this simulation was conducted using half wave dipole antennas, it can be readily extended to other antenna types. Nevertheless, the propagation velocity and the propagation paths may not be as simple for other antenna types. For example, an array of patch antennas on the same PCB with element separation of less than λ may be more complex to analyze. Electromagnetic waves radiate from the patch antenna from its fringes.

Further, the PCB material, Rogers RO5240 for example, which has an $\epsilon_r = 2$, will slow down the propagation of electromagnetic waves from one patch antenna to another. Due to the complexity of such scenarios, this work will instead focus on the inter-element time delay τ_{ij} while ignoring the details of signal propagation path and propagation velocity that depends primarily on the array geometry and the materials used in the construction of the array.



(a) Phase of s_{21} as distance between dipoles is increased from 0.1λ to 2.5λ at 1 GHz.



(b) $|s_{21}|$ as distance between dipoles is increased from 0.1λ to 2.5λ at 1 GHz.

Figure 4.5: Dipole array delay simulation.

4.2 Effects of Delays on Noise Output of Beamforming Arrays

With propagation delay τ_{ij} established, it is now possible to observe its effects on the array, and, to explore how the delays effect noise propagation in the array. In this section, the array model used in derivation and analysis will be a receiving array typically found in radio telescopes with the following components: the antenna array, the feed and transmission lines, LNAs, receiver, phase shifters or beamformers, and a band-pass filter at the output of the array (Figure 4.6). An array of this type has become the standard receiving array model in literature. Most real receiving arrays will deviate from this model; however, this model can be readily used for most receiving arrays with minor modifications.

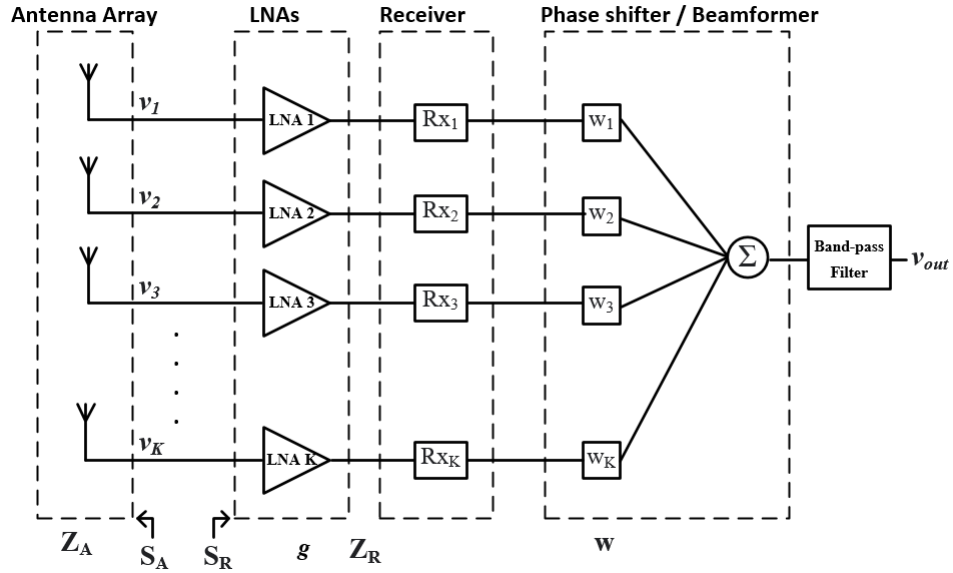


Figure 4.6: Simplified model of receiving array with band-pass filter at the output.

Because the noise from antenna array, LNAs, and the receiver are assumed to be uncorrelated, the PSD contribution from each of the components can be added to arrive at the total PSD

$$PSD_{total} = PSD_{Antenna} + PSD_{LNA} + PSD_{rec} + PSD_{beamformer}. \quad (4.4)$$

There are 2 main sources of noise in this system. First is the noise generated by the array, and second is the noise generated by the LNAs. The receiver is assumed to not

contribute significantly to the overall noise PSD of the system because it appears in the receiver chain after the LNAs, which provide large gain and minimize the noise contribution from the receiver and beamformer in accordance with Friis's formula. Beamformers or phase shifters also contribute noise but are assumed to be insignificant for the purpose of this analysis. The receiver S-parameter matrix is set to identity, $S_{rec} = \mathbf{I}$. The LNAs are assumed to be terminated at the output with $\Gamma_L = 0$ and the output reflection coefficient of each LNA is zero, $s_{22} = 0$. The LNAs also have a non-zero input reflection coefficient, $s_{11} \neq 0$, and the forward transmission is greater than zero, $|s_{21}| > 0$. All LNAs are assumed to be identical for simplicity.

4.2.1 Noise Due to LNAs

The LNA noise is dependent on noise parameters N , T_{min} , and Γ_{opt} , where N is invariant under lossless transformation at the input of LNA [32]. Traveling noise waves are used in this analysis with c_1 denoting forward noise waves emanating from LNA input and c_2 denoting reverse noise waves emanating from the LNA output. The noise waves c_1 and c_2 are correlated with the correlation matrix $\mathbf{C}_s = \overline{\mathbf{c}\mathbf{c}^\dagger}$, where $\mathbf{c} = \begin{bmatrix} c_1 & c_2 \end{bmatrix}^T$, and \dagger is the hermitian conjugate. It is noteworthy that noise waves from different LNAs are not correlated, i.e. $\overline{c^1 c^{2\dagger}} = 0$, where \mathbf{c}^1 and \mathbf{c}^2 are the noise wave vector of LNA #1 and LNA #2, respectively. Due to close proximity of the LNAs in a realizable array, it is possible that the noise waves from different LNAs are slightly correlated. However, this correlation is expected to be very weak and can be safely ignored.

In ordinary analysis of problem of this kind, a signal flow graph is constructed and the vector of noise waves is simply transformed by using the rules of signal flow graph analysis. Another approach is to use algebraic manipulation to convert outgoing noise waves at the input of LNA to the output of LNA. However, to fully grasp the nature of noise delays, it is insightful to track the noise waves as they propagate through the array and appear at the output.

Consider a scenario where only one of the LNAs in Figure 4.6 is noisy and the rest are noiseless. Forward noise wave emanating from the input of this LNA travels along the transmission line and is delayed during propagation as $c_f(t) * \delta(t - \tau_{tx})$. For brevity, c_f is equivalent to c_1 and $c_{f,j}^K$ denotes the forward noise wave of K^{th} LNA as it appears at the j^{th} LNA input. The delayed wave now arrives at the array port and is delayed by the antenna feed $\delta(t - \tau_d)$. It then arrives at the point of intrinsic array S-parameters and is partially reflected back towards the input and is partially transmitted to other antennas onward via the transmission line to the input of other LNAs. As it does so, it experiences delays $\delta(t - \tau_{i,j})$ for each inter-element path it takes in addition to a second delay by the transmission line and the antenna feed $\delta(t - \tau_d - \tau_{tx})$.

Combining all the delays and intrinsic S-parameters yields

$$c_{f,j}^K = \sum_{i=1}^M c_f^K(t) * \delta(t - \tau_d - \tau_{tx}) * S_{ij} e^{j\phi_{ij}} * \delta(t - \tau_{ij}) * \delta(t - \tau_d - \tau_{tx}), \quad (4.5)$$

where K is the index of the noisy LNA and c_f^K is the original forward noise wave due to K^{th} LNA.

The noise waves now have two paths to take. First path is via the s_{21} of the LNA to the output, and the other is back towards the array via LNA s_{11} . The noise waves that are reflected again undergo a delay and coupling via the transmission line and the array. However this time they also interfere with the incoming noise signals from the array because these signals are correlated. This process is mathematically repeated an infinite number of times, and the resulting transformed, delayed, reflected, and interfered noise wave that originated at the input of K^{th} LNA finally appears at the output where it combines and interferes with the reverse noise wave c_r^K that originates from the output of K^{th} LNA. However, at the output of the noisy LNA, only some instances of multiple transformed copies of the original forward noise wave interfere with the reverse noise wave. The other copies of noise wave that coupled to different LNAs combine with the reverse noise wave at the

output of the beamformer where all signals are combined. At this point, the total power of the very complicated signal is arrived at by integrating the signal over time.

Noise waves can be analyzed in time domain; however, the resulting calculations will be riddled with convolution operators (*). Because the convolution of two time domain functions is the same as multiplication of the two functions in frequency domain, $f_1(t) * f_2(t) \xrightarrow{\mathcal{F}} F_1(f) \cdot F_2(f)$, the derivation of PSD can be done in the frequency domain for ease of computation.

Before the full derivation of noise PSD can be done, the antenna array S-parameters have to be slightly modified in order to embed the delay terms in them. Each term in the antenna S-parameters now has the antenna feed line delay τ_d , inter-element delay τ_{ij} , and transmission line delay τ_{tx} embedded in them. And, these are functions of frequency

$$s_{ij}(f) = S_{ij} e^{j\phi_{ij}} \cdot e^{-j2\pi f(\tau_{ij} + 2\tau_d + 2\tau_{tx})}, \quad (4.6)$$

where $\tau_{ij} + 2\tau_d + 2\tau_{tx}$ is the delay a signal experiences as it travels from the input of j^{th} LNA to the input of i^{th} LNA, which includes the transmission lines.

The PSD derivation begins by expressing the forward and reverse noise waves of all LNAs as vectors

$$\mathbf{c}_f = \begin{bmatrix} c_f(f)_1 \\ c_f(f)_2 \\ \vdots \\ c_f(f)_M \end{bmatrix}, \mathbf{c}_r = \begin{bmatrix} c_r(f)_1 \\ c_r(f)_2 \\ \vdots \\ c_r(f)_M \end{bmatrix} \quad (4.7)$$

In this convention, the bold style lower case letter denote a vector of length M .

The forward noise waves emanate from the LNA inputs and are coupled to other LNAs via the array S-parameter matrix $\mathbf{S}_A \mathbf{c}_f$. Some of the signal is transferred to LNA output via the LNA s_{21} and some of it is reflected back via s_{11} . The n^{th} reflection off the LNAs is denoted by subscript n in $\mathbf{c}_{f,n}$. The output transmitted portion of the first reflection can be

expressed as $\mathbf{S}_{21}\mathbf{S}_A\mathbf{c}_f$, while the reflected portion is described as

$$\mathbf{c}_{f,1} = \mathbf{S}_{11}\mathbf{S}_A\mathbf{c}_f = \mathbf{S}_{11}\mathbf{S}_A\mathbf{c}_{f,0}, \quad (4.8)$$

where $\mathbf{S}_{11} = s_{11,LNA} \cdot \mathbf{I}$ and $\mathbf{S}_{21} = s_{21,LNA} \cdot \mathbf{I}$. Note that $\mathbf{c}_{f,0} = \mathbf{c}_f$ and it has not yet reflected off the LNAs.

The reflected waves experience antenna array S-parameters again. Therefore, the second reflection is

$$\mathbf{c}_{f,2} = \mathbf{S}_{11}\mathbf{S}_A\mathbf{c}_{f,1} \quad (4.9)$$

$$\mathbf{c}_{f,2} = \mathbf{S}_{11}\mathbf{S}_A\mathbf{c}_{f,1} = \mathbf{S}_{11}\mathbf{S}_A\mathbf{S}_{11}\mathbf{S}_A\mathbf{c}_{f,0}. \quad (4.10)$$

A pattern to be noted here is that the n^{th} reflection can always be described as

$$\mathbf{c}_{f,n} = \mathbf{S}_{11}^n \mathbf{S}_A^n \mathbf{c}_f, \quad (4.11)$$

while the n^{th} transmission to the outputs can always be written as

$$Transmission_n = \frac{\mathbf{S}_{21}}{\mathbf{S}_{11}} \mathbf{c}_{f,n}, \quad (4.12)$$

where the superscript in \mathbf{S}_A^n denotes the n^{th} power of \mathbf{S}_A . Recall that each element of \mathbf{S}_A is a function of frequency, see Equation 4.6, which contains the delay terms $e^{-j2\pi f_0(\tau_{ij}+2\tau_d+2\tau_{ix})}$. Therefore, each reflection is delayed successively for each time it reflects from the LNA. It is not evident at this point how the delayed reflections play a part in the output PSD of the LNAs. For that, it is required to sum up all the transmissions of the noise waves across the LNAs to obtain

$$\sum_{n=1}^{\infty} Transmission_n = \frac{\mathbf{S}_{21}}{\mathbf{S}_{11}} \sum_{n=1}^{\infty} \mathbf{c}_{f,n} = \frac{\mathbf{S}_{21}}{\mathbf{S}_{11}} \sum_{n=1}^{\infty} \mathbf{S}_{11}^n \mathbf{S}_A^n \mathbf{c}_f. \quad (4.13)$$

And at this point, the forward noise waves of LNAs mix with the reverse noise waves \mathbf{c}_r

$$c_{output} = \frac{\mathbf{S}_{21}}{\mathbf{S}_{11}} \sum_{n=1}^{\infty} \mathbf{S}_{11}^n \mathbf{S}_A^n \mathbf{c}_f + \mathbf{c}_r. \quad (4.14)$$

Since $\Gamma_L = s_{22} = 0$, all the noise power is transferred to the beamformer represented by weight vector, $\mathbf{w} = \begin{bmatrix} w_1 & w_2 & \cdots & w_M \end{bmatrix}^T$. The output is summed in the process of beamforming to result in

$$c_{output} = \mathbf{w}^T \left(\frac{\mathbf{S}_{21}}{\mathbf{S}_{11}} \sum_{n=1}^{\infty} \mathbf{S}_{11}^n \mathbf{S}_A^n \mathbf{c}_f + \mathbf{c}_r \right). \quad (4.15)$$

Note that the row vector \mathbf{w}^T and the column vector $\frac{\mathbf{S}_{21}}{\mathbf{S}_{11}} \sum_{n=1}^{\infty} \mathbf{S}_{11}^n \mathbf{S}_A^n \mathbf{c}_f + \mathbf{c}_r$ are multiplied using matrix multiplication, which sums the output implicitly.

In order to deal with the sum in Equation 4.15 it is assumed that the array is passive, i.e. the array does not amplify signals that are incident upon it. For example, if the array is excited by a signal source with signal power p_{source} at one of the array ports, the resulting reflected signals should not have a combined power of greater than p_{source} . Mathematically, this can be described as

$$\sum_{i=1}^M |s_{A,ij}| \leq 1, \quad (4.16)$$

for all j . Intuitively, it is possible to conclude that the expression $\sum_{n=1}^{\infty} \mathbf{S}_{11}^n \mathbf{S}_A^n \mathbf{c}_f$ is bounded assuming that $|s_{11}| < 1$. Next, using the following identity for the sum of a matrix geometric series

$$\lim_{n \rightarrow \infty} \sum_{k=0}^n \mathbf{T}^k = (\mathbf{I} - \mathbf{T})^{-1}, \quad (4.17)$$

where $\mathbf{T}^0 = \mathbf{I}$, the sum in Equation 4.15 can be simplified to

$$c_{output} = \mathbf{w}^T \left(\mathbf{S}_{21} \mathbf{S}_A (\mathbf{I} - \mathbf{S}_{11} \mathbf{S}_A)^{-1} \mathbf{c}_f + \mathbf{c}_r \right). \quad (4.18)$$

This result is not unforeseen, and it could have been arrived at using signal flow graph.

However, doing so would have hidden the physical reality of signals reflecting inside the array and summing at the output.

Finally, the Einstein-Wiener-Khinchin theorem can be used to get the PSD of the LNAs at the output. Recall that the PSD of a signal is the Fourier transform of the auto-correlation of the signal

$$PSD = \mathcal{F}(f \times f) = \mathbf{F}^* \cdot \mathbf{F} = |\mathbf{F}|^2, \quad (4.19)$$

Because Equation 4.18 is already in frequency domain, the only step left is to find the auto-correlation of the expression, which is

$$R = c_{output}^* c_{output}, \quad (4.20)$$

that yields

$$R_{output} = \mathbf{w}^H \left[\left(\mathbf{S}_{21} \mathbf{S}_A (\mathbf{I} - \mathbf{S}_{11} \mathbf{S}_A)^{-1} \mathbf{c}_f + \mathbf{c}_r \right) \left(\mathbf{c}_f^H (\mathbf{I} - \mathbf{S}_{11}^H \mathbf{S}_A^H)^{-1} \mathbf{S}_A^H \mathbf{S}_{21}^H + \mathbf{c}_r^H \right) \right] \mathbf{w}, \quad (4.21)$$

where R traditionally denotes the auto-correlation of functions and R_{output} is the auto-correlation of c_{output} .

4.2.2 Total Noise Power of Receiver with Delays

The total power of the LNA noise P_N can be found by integrating Equation 4.21 over the bandwidth $B = f_H - f_L$

$$P_{N,rec} = \int_{f_L}^{f_H} \mathbf{w}^H \left[\left(\mathbf{S}_{21} \mathbf{S}_A (\mathbf{I} - \mathbf{S}_{11} \mathbf{S}_A)^{-1} \mathbf{c}_f + \mathbf{c}_r \right) \left(\mathbf{c}_f^H (\mathbf{I} - \mathbf{S}_{11}^H \mathbf{S}_A^H)^{-1} \mathbf{S}_A^H \mathbf{S}_{21}^H + \mathbf{c}_r^H \right) \right] \mathbf{w} \cdot df \quad (4.22)$$

Comparing Equation 4.22 to the usual way of computing total output noise of the array due to LNAs, which is to simply multiply by the bandwidth, it can be seen that Equation 4.22 captures the frequency dependence of the noise delays by using integration.

R_{output} can be reorganized to deal with the correlation between c_1 and c_2 and can be rewritten as

$$R_{output} = \mathbf{w}^H \left[|s_{21}|^2 N_1 \mathbf{S}_A (\mathbf{I} - \mathbf{S}_{11} \mathbf{S}_A)^{-1} (\mathbf{I} - \mathbf{S}_{11}^H \mathbf{S}_A^H)^{-1} \mathbf{S}_A^H + \right. \quad (4.23)$$

$$\left. \rho^* \sqrt{N_1 N_2} (\mathbf{I} - \mathbf{S}_{11}^H \mathbf{S}_A^H)^{-1} \mathbf{S}_A^H \mathbf{S}_{21}^H + \rho \sqrt{N_1 N_2} \mathbf{S}_{21} \mathbf{S}_A (\mathbf{I} - \mathbf{S}_{11} \mathbf{S}_A)^{-1} + N_2 \mathbf{I} \right] \mathbf{w},$$

where N_1 is the auto-correlation of forward noise wave $\overline{|c_f|^2}$, i.e. $\overline{|c_1|^2}$ of LNAs, N_2 the auto-correlation of reverse noise wave $\overline{|c_r|^2}$, i.e. $\overline{|c_2|^2}$ of the LNAs, and $\rho \sqrt{N_1 N_2}$ is the cross correlation between forward and reverse noise waves $\overline{c_1 c_2^*}$.

The total power output can be expressed as

$$P_{N,rec} = \int_{f_L}^{f_H} \mathbf{w}^H \left[|s_{21}|^2 N_1 \mathbf{S}_A (\mathbf{I} - \mathbf{S}_{11} \mathbf{S}_A)^{-1} (\mathbf{I} - \mathbf{S}_{11}^H \mathbf{S}_A^H)^{-1} \mathbf{S}_A^H + \right. \quad (4.24)$$

$$\left. \rho^* \sqrt{N_1 N_2} (\mathbf{I} - \mathbf{S}_{11}^H \mathbf{S}_A^H)^{-1} \mathbf{S}_A^H \mathbf{S}_{21}^H + \rho \sqrt{N_1 N_2} \mathbf{S}_{21} \mathbf{S}_A (\mathbf{I} - \mathbf{S}_{11} \mathbf{S}_A)^{-1} + N_2 \mathbf{I} \right] \mathbf{w} \cdot df$$

The closed-form integral in Equation 4.24 could not be found due to the inverse matrix term $(\mathbf{I} - \mathbf{S}_{11} \mathbf{S}_A)^{-1}$, and, it will be left in the integral form.

4.2.3 Total Noise Power of Array with Delays

For the array noise, a similar approach can be used to refer the array noise at the array ports to the output of the receiver. There are however a couple differences. First is that the noise waves emanating from the array are incident upon the LNAs, whereas the LNA forward noise waves are incident upon the array. This difference is accounted for by the exclusion of the \mathbf{S}_A term from the noise wave output equation when compared to Equation 4.22 as in

$$c_{output} = \mathbf{w}^T (\mathbf{S}_{21} (\mathbf{I} - \mathbf{S}_{11} \mathbf{S}_A)^{-1} \mathbf{c}_A), \quad (4.25)$$

where \mathbf{c}_A is the vector of noise waves emanating from the array ports.

The second difference is that the individual noise components of the noise vector \mathbf{c}_A are correlated, and the correlation matrix $\mathbf{C}_{s,A}$ is found using Bosma's theorem [27]

$$\mathbf{C}_{s,A} = k_b T_0 (\mathbf{I} - \mathbf{S}_A \mathbf{S}_A^H). \quad (4.26)$$

The auto-correlation of array output noise vector is

$$\mathbf{R}_{output} = |s_{21}|^2 \mathbf{w}^H [(\mathbf{I} - \mathbf{S}_{11} \mathbf{S}_A)^{-1} \mathbf{C}_{s,A} (\mathbf{I} - \mathbf{S}_{11}^H \mathbf{S}_A^H)^{-1}] \mathbf{w}, \quad (4.27)$$

and the noise PSD due to array is then

$$P_t = |s_{21}|^2 k_b T_0 \int_{f_L}^{f_H} \mathbf{w}^H [(\mathbf{I} - \mathbf{S}_{11} \mathbf{S}_A)^{-1} (\mathbf{I} - \mathbf{S}_A \mathbf{S}_A^H) (\mathbf{I} - \mathbf{S}_{11}^H \mathbf{S}_A^H)^{-1}] \mathbf{w} \cdot df, \quad (4.28)$$

while acknowledging that the array S-parameters are functions of frequency and delay.

4.2.4 Receiver Noise Temperature with Delays

The beam equivalent receiver noise temperature can be expressed in terms of auto-correlation of traveling noise waves. Starting with

$$T_{rec} = T_{iso} \frac{P_{rec}}{P_{t,iso}}, \quad (4.29)$$

from [15], where $P_{t,iso}$ is the array noise under thermal equilibrium with temperature $T_{iso} = T_0$, and substituting the Equations 4.28 and 4.22 into Equation 4.29, the beam equivalent receiver noise temperature with delays can be expressed as

$$T_{rec} = \frac{\int_{f_L}^{f_H} \mathbf{w}^H \left[|s_{21}|^2 (N_1 \mathbf{S}_A (\mathbf{I} - \mathbf{S}_{11} \mathbf{S}_A)^{-1} (\mathbf{I} - \mathbf{S}_{11}^H \mathbf{S}_A^H)^{-1} \mathbf{S}_A^H + \right.}{|s_{21}|^2 k_b \times} \quad (4.30)$$

$$\left. \rho^* \sqrt{N_1 N_2} (\mathbf{I} - \mathbf{S}_{11}^H \mathbf{S}_A^H)^{-1} \mathbf{S}_A^H \mathbf{S}_{21}^H + \rho \sqrt{N_1 N_2} \mathbf{S}_{21} \mathbf{S}_A (\mathbf{I} - \mathbf{S}_{11} \mathbf{S}_A)^{-1} + N_2 \mathbf{I} \right] \mathbf{w} \cdot df}{\int_{f_L}^{f_H} \mathbf{w}^H [(\mathbf{I} - \mathbf{S}_{11} \mathbf{S}_A)^{-1} (\mathbf{I} - \mathbf{S}_A \mathbf{S}_A^H) (\mathbf{I} - \mathbf{S}_{11}^H \mathbf{S}_A^H)^{-1}] \mathbf{w} \cdot df}.$$

Note that this equation differs from [15] by a factor of k_b because k_b is assumed to be part of N_1 and N_2 and as such cannot explicitly cancel with k_b in the denominator.

4.2.5 Verification Using Simulation

In order to verify Equation 4.30, a numerical simulation in MATLAB was conducted with identical LNAs. The array was taken from [49]. An LNA from [52] with the following noise parameters and scattering matrix was chosen: $Z_{opt} = (71.2 + j15.7) \Omega$, $T_{min} = 6.29 \text{ K}$, $R_n = 0.706 \Omega$, $s_{11} = 0.2$, $s_{21} = 10$, and $s_{12} = s_{22} = 0$. The array was a 19 element thick dipole array with array pattern as illustrated in Figure 4.7. A cable of length λ at f_0 of 1GHz was inserted between the array ports and LNAs in order to simulate transmission line delays. The transmission line was chosen to be of length λ so that the antenna s-parameters would be the same as seen from the LNAs at the operating frequency. In order to focus on the effects of delays on output noise, all beamformer weights were set to 1. The array S-parameters were modified with the delay terms by calculating the inter-element delay using the separation distance of each element described in Figure 4.7. The simulation was setup such that the narrowband S-parameters of the array were same as the ones measured for the array. Then, for each LNA, a set of forward and reverse noise waves samples were generated for each frequency component. A total of 20000 non-correlated independent Gaussian distributed samples were generated. Then, using the MATLAB Cholsky matrix-decomposition function, the signals were correlated using correlation matrix generated using the LNA noise parameters and Bosma's theorem. The signals were propagated through the array and reflected back and forth, by using matrix multiplication, from the array and the LNAs for a total of 10 times. This was done to ascertain good convergence. Using a maximum of 20000 samples ensured that the simulation time was kept reasonable while maintaining low simulation noise. The simulated beam equivalent receiver noise temperature, T_{rec} , of this array was calculated and plotted. The simulation result was compared against Equation 4.30 and narrowband equation from [16].

Figure 4.8b shows the simulation results. There is a good agreement between the derived equation and the simulation. More importantly, the simulated T_{rec} is not flat and the total noise power cannot be determined simply by multiplying the 1-Hz bandwidth result of Equation 4.22 by the bandwidth. Moreover, for this particular array under the simulated beamformer weights, if a bandwidth of greater than 750MHz is considered, the noise temperature is as much as 13.6% higher than what would be calculated using the equations from [15].

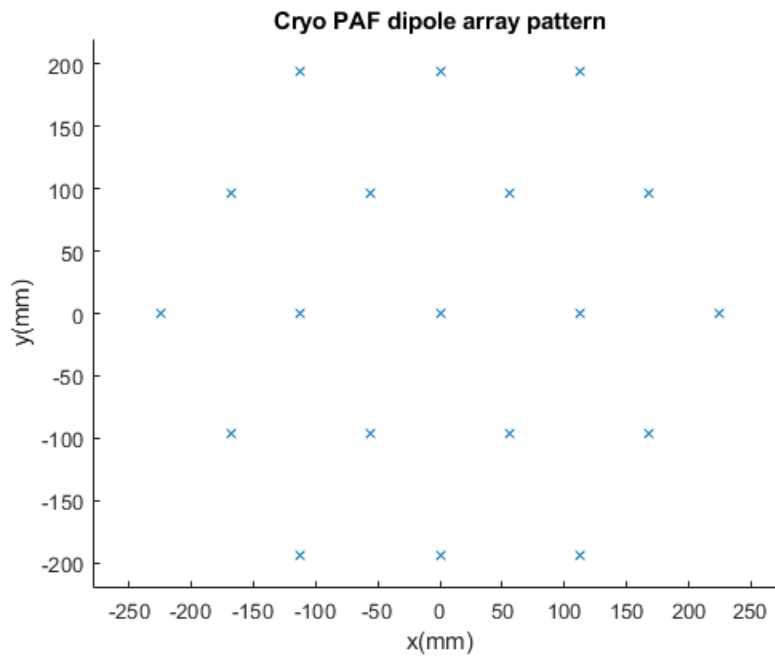
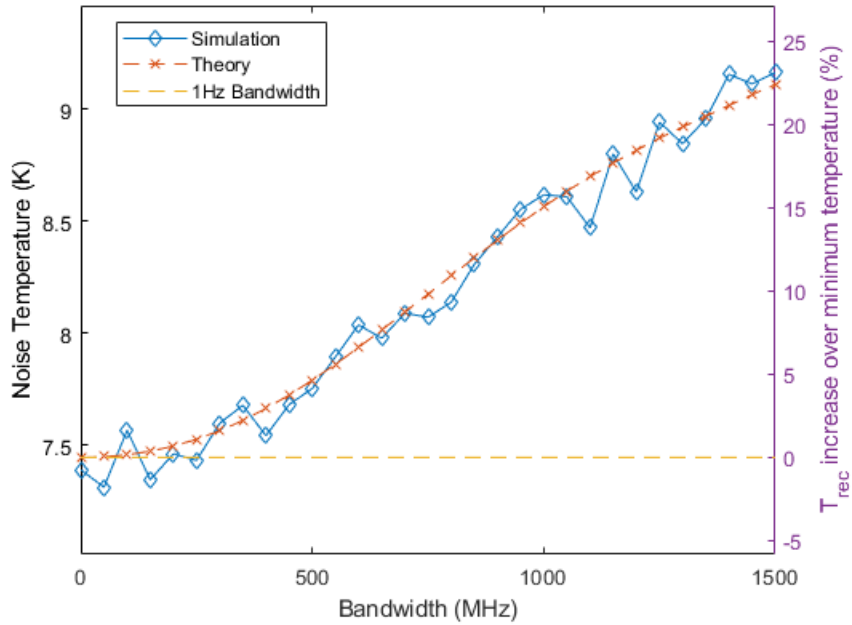
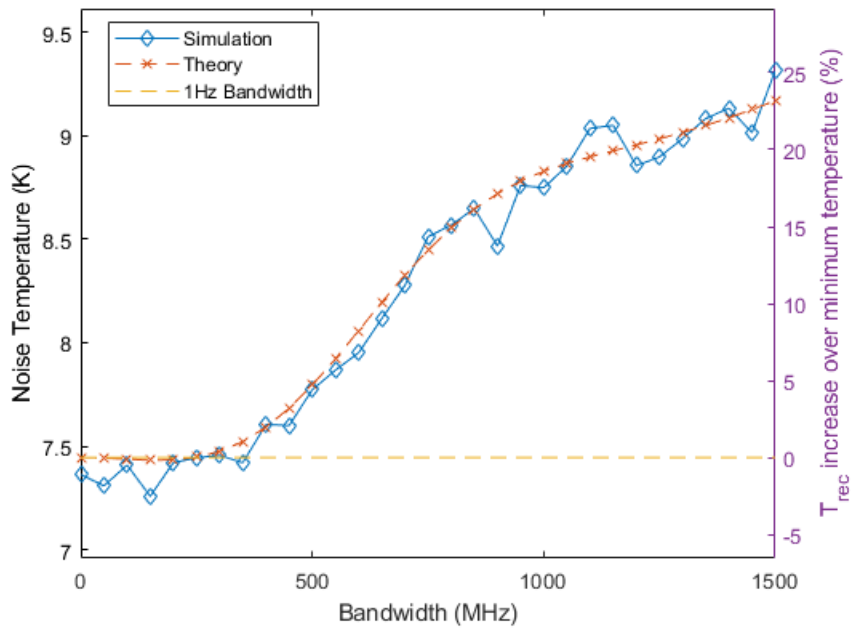


Figure 4.7: Antenna displacement pattern of the 19 element array.

This simulation confirms that there is a non linear relationship between array thermal and receiver noise and the bandwidth of the array. And, the relationship is due to the delays present within the receiving array. The relationship is significant enough that over a large bandwidth, the narrowband formula for T_{rec} diverges quickly from this simulation. The relationship is significant even in the absence of long feed lines (greater than 1λ) that its contribution cannot be ignored in wideband array design. See Appendix A for simulation code.



(a) Numerical simulation results of 19 element array from [49] without transmission lines



(b) Numerical simulation results of 19 element array from [49] with λ length transmission lines

Figure 4.8: Wideband 19-element array simulation

4.3 Γ_{act} with Delays and Γ_{act} Matching

The active reflection coefficient Γ_{act} is understood to be a function of beam angle. Due to delays, Γ_{act} also becomes a function of frequency. Many receiving arrays are designed to target specific operating frequencies with a configurable bandwidth. As discussed in Section 3.7, matching to the active reflection coefficient is used to match the LNAs of the receiver to the array when it is operating at a particular beam angle. This section contains a discussion of how delays and bandwidths affect Γ_{act} matching including verification of this Γ_{act} matching using simulation.

In Section 4.1 it was discussed that the phases of antenna S-parameters exhibit frequency dependency consistent with what is expected due to time delays. This frequency dependence of the antenna S-parameters can be readily incorporated in the conventional equations for Γ_{act} . Starting with [16]

$$\Gamma_{act,m} = \frac{1}{\mathbf{w}_{f,m}^*} \left(\sum_{k=1}^M S_{A,km} \cdot \mathbf{w}_{f,k}^* \right), \quad (4.31)$$

where $\mathbf{w}_{f,m}$ are the beamformer weights referred to the input of LNAs via the transformation matrix \mathbf{G}

$$\mathbf{w}_f = \mathbf{G}^H \mathbf{w}. \quad (4.32)$$

For a receiving array of the type shown in Figure 4.6,

$$\mathbf{G} = g\sqrt{Z_0}(\mathbf{I} + \mathbf{S}_R)(\mathbf{I} - \mathbf{S}_R\mathbf{S}_A)^{-1}, \quad (4.33)$$

where g is voltage gain of the receiver and \mathbf{S}_R is the receiver S-parameter matrix [16], $\mathbf{S}_R = s_{11}\mathbf{I}$. It is apparent from the above equations that Γ_{act} is dependent on the signal delays in the array. Substituting the \mathbf{S}_A in Equation 4.31 with \mathbf{S}_A with delays and expressing

the equation as a function of frequency yields

$$\Gamma_{act,m}(f) = \frac{1}{\mathbf{w}_{f,m}^*(f)} \left(\sum_{k=1}^M S_{A,km}(f) \cdot \mathbf{w}_{f,k}^*(f) \right), \quad (4.34)$$

and

$$\mathbf{w}_f(f) = \mathbf{G}^H(f) \mathbf{w} \quad (4.35)$$

$$\mathbf{G}(f) = g\sqrt{Z_0}(\mathbf{I} + \mathbf{S}_R)(\mathbf{I} - \mathbf{S}_R\mathbf{S}_A(f))^{-1}, \quad (4.36)$$

where $\mathbf{S}_A(f)$ represents the antenna S-parameters as a function of delay and frequency

$$s_{A,ij}(f) = S_{ij}e^{j\phi_{ij}}e^{-j2\pi f(\tau_{ij}+2\tau_d+2\tau_{rx})}, \quad (4.37)$$

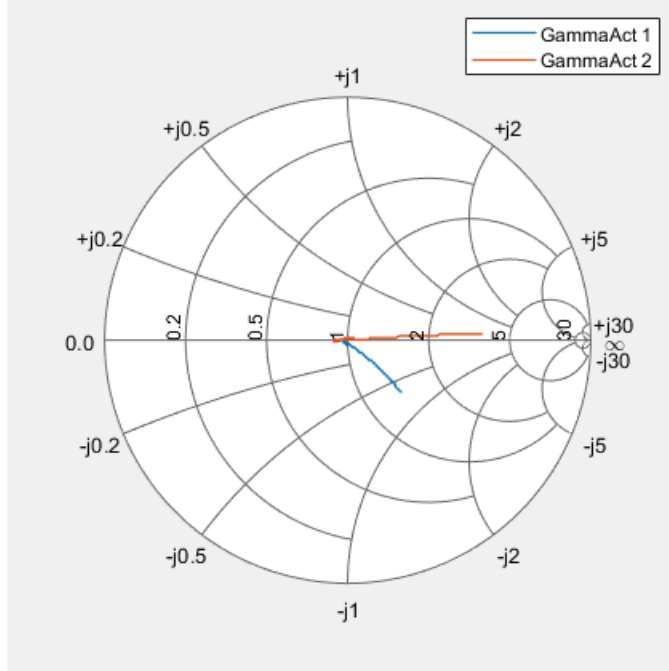
with $S_{ij}e^{j\phi_{ij}}$ being independent of frequency.

It is difficult to see how the delay dependence of $\Gamma_{act}(f)$ can affect the active reflection coefficient matching. However, what is clear is that the notion of matching a wideband array to the narrowband Γ_{act} may not be ideal. And, in some cases where the LNA noise is very sensitive to the source reflection coefficient, matching to narrowband Γ_{act} may produce much higher than expected noise output.

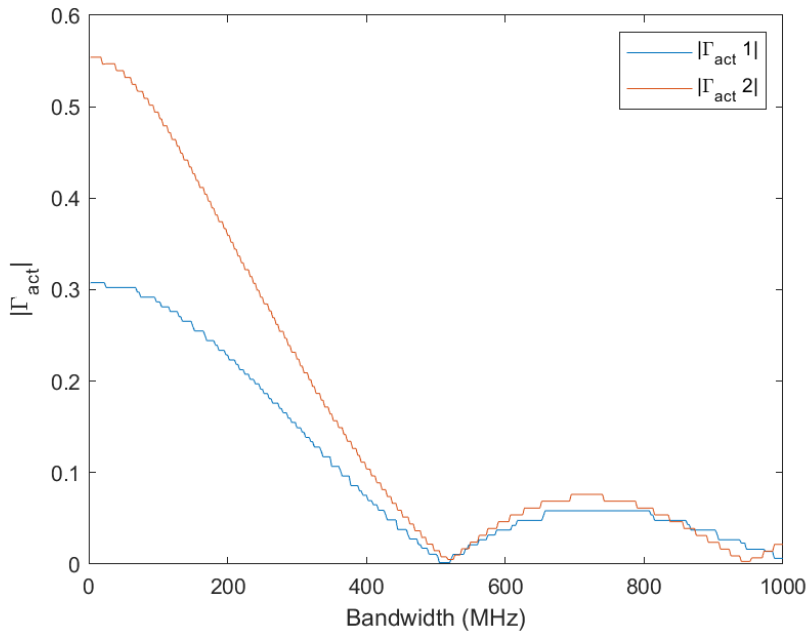
In order to further understand how the delays change Γ_{act} , a numerical simulation in MATLAB was conducted with a fictitious array of 2 elements with element spacing of λ and a $1/2\lambda$ transmission line (at f_0 of 1GHz) connecting to the LNAs. A $1/2\lambda$ transmission line was chosen so that the array S-parameters at f_0 remain the same as for no delay case. The array S-parameters were $s_{11} = 0.5048 - j0.2436$, $s_{12} = -0.1516 + j0.2177$, $s_{21} = -0.1516 + j0.2177$, and $s_{22} = 0.5030 - j0.2338$. In this simulation, and unlike the previous simulation, the Γ_{opt} of both LNAs were swept to find the Γ_{act} as bandwidth is slowly increased. This was possible because N is invariant under lossless transformation unlike R_n [32]. The beamformer weights were set to $\mathbf{w} = \begin{bmatrix} 1 & e^{-j\pi/4} \end{bmatrix}^T$. The LNAs had noise parameters as follows: $T_{min} = 15$ and $N = 0.024$, and the following S-parameters: $s_{11} = 0.1$,

$s_{21} = 10$, and $s_{12} = s_{22} = 0$. Under these conditions, the narrowband Γ_{act} is calculated to be $\Gamma_{act,1} = 0.2337 - j0.2013$ and $\Gamma_{act,2} = -0.5539 + j0.0176$ using Equation 4.31. The bandwidth was increased in small steps from 5 MHz to 1 GHz and the Γ_{act} was found by observing where in the space of Γ_{opt} the noise is the lowest. Since lowest noise in an active array occurs when $\Gamma_{opt,m} = \Gamma_{act,m}$, finding Γ_{opt} that minimize the array noise is equivalent to finding Γ_{act} .

A Smith chart of simulated Γ_{act} is shown in Figure 4.9a as the bandwidth is increased. The wideband Γ_{act} shows deviation from the narrowband case as the bandwidth increases. As bandwidth is increased, both Γ_{act} fall towards the center of the Smith chart. Both Γ_{act} reach the middle of Smith chart at about 500 MHz which is a moderately large bandwidth.



(a) Smith chart with simulated Γ_{act} plotted as bandwidth is increased from 5MHz to 1 GHz, Γ_{act} occurs where the array obtains the least noise as Γ_{opt} of both LNAs are swept through the entire Γ_{act} space.



(b) Plot of $|\Gamma_{act}|$ with vs bandwidth. Both $|\Gamma_{act}|$ fall to 0 as bandwidth is increased.

Figure 4.9: Results of 2-element dipole array simulations with varied bandwidth

The search for wideband Γ_{act} in this manner is computationally intensive because for

an array of size M there are $2 \cdot M$ variables that need to be resolved to search the entire Γ_{act} space. If the search space is divided into 100 steps for each variable, i.e, the real and imaginary components are swept at an interval of 0.02 step size from $-1j$ to $1j$ and -1 to 1 , the total number of simulations required would be 100^4 or a hundred million. To complicate matters further, because the simulation is a wideband noise simulation, which requires discrete noise signals with up to a 10^4 noise samples for each LNA, and, each noise sample needs to be propagated up to 10 times between the LNAs and the array, the final number of computations required is enormous. Roughly speaking, for an antenna array of M elements, a search step size of 0.02, simulation bandwidth of 50 MHz, and for reflection count of 10, the total number of matrix multiplications required would be in excess of 10^{4M+5} . Even for an array of 2 elements, a modest search for Γ_{act} for just 1 of the element spacing would take a long time. Therefore, to speed up simulation, a windowed search method was employed. In this method, the search space consisted of 4 variables: the amplitudes and phases of $\Gamma_{act,1}$ and $\Gamma_{act,2}$. Starting from the known values of narrowband $\Gamma_{act,1}$ and $\Gamma_{act,2}$, a small window of search space was created around them that was a mere 0.001% of the entire search space. The starting Γ_{act} was found for the 1 Hz case using Equation 4.31. Then, the bandwidth of the array was changed by a slight amount and a new search window was created around the old Γ_{act} . Then, the window was searched to find the new Γ_{act} by searching for lowest array noise output. This method allowed relatively fast simulation of the array under various scenarios without having to wait many days for a single simulation. See Appendix B for simulation code.

4.4 Impact of Noise Bandwidth on Antenna Array Matching

It was discussed in Section 4.3 that matching a wideband array to the LNAs using the narrowband Γ_{act} (a vector quantity) may not always produce the lowest receiver noise temperature for a given beam angle. Also, designing each LNA differently for each antenna element is impractical, especially because it restricts the array to perform at lowest noise

level only for one scan direction. In most practical arrays, identical LNAs for each antenna are used instead. In this section, a method for matching identical LNAs to the active array is discussed, including the incorporation of delays and bandwidth in the derivation. This scalar Γ_{opt} is referred to as the “optimal Γ_{act} ” as it attempts to accomplish the same goal as matching to narrowband Γ_{act} , which is to produce the lowest T_{rec} for a given bandwidth and element separation distance using identical LNAs while remaining frequency invariant in the bandwidth. Afterwards, a method for finding Γ_{act} for multiple scan directions, which was first discussed in [16], is modified to include the delays and bandwidth effect. Next, optimal Γ_{act} for multiple scan directions is derived. Finally, a method to give precedence to certain scan directions while finding multi-beam optimal Γ_{act} is presented.

In the literature, the standard way of representing receiving array system noise temperature is by expressing it as beam equivalent noise temperature [15, 16, 37]

$$T_{sys} = T_{iso} \frac{P_{noise}}{P_{t,iso}}, \quad (4.38)$$

where P_{noise} is comprised of noise from external source, receiver noise and noise due to ohmic losses in the system. Noise due to external sources is ignored in this analysis; however, they can be readily incorporated into the analysis due to the additive nature of uncorrelated noise. The beam equivalent receiver noise temperature is defined as

$$T_{rec} = T_{iso} \frac{P_{N,rec}}{P_{t,iso}}, \quad (4.39)$$

where $P_{N,rec}$ is the receiver noise power and $P_{t,iso}$ is the array thermal noise power under thermal equilibrium in isotropic noise environment at temperature T_{iso} .

Expanding Equation 4.39 produces

$$T_{rec} = T_{iso} \frac{\mathbf{w}^H \mathbf{R}_{rec} \mathbf{w}}{\mathbf{w}^H \mathbf{R}_t \mathbf{w}}, \quad (4.40)$$

where \mathbf{R}_t is antenna thermal noise correlation matrix at the receiver output [15].

The array thermal noise correlation matrix can be written as

$$\mathbf{R}_{t,f} = k_b T_{iso} B (\mathbf{I} - \mathbf{S}_A \mathbf{S}_A^H),$$

using Bosma's theorem [27], where $\mathbf{R}_{t,f}$ denotes correlation of forward noise waves at the array ports.

Forward noise waves correlation matrix $\mathbf{R}_{t,f}$ at the LNA input can be transformed to noise wave correlation matrix at the output of the receiver, \mathbf{R}_t , by using \mathbf{G} [16]

$$\mathbf{R}_t = \mathbf{G} \mathbf{R}_{t,f} \mathbf{G}^H, \quad (4.41)$$

where $\mathbf{G} = \sqrt{Z_0} (\mathbf{I} + \mathbf{S}_R) (\mathbf{I} - \mathbf{S}_R \mathbf{S}_A)^{-1}$ for the array type under consideration. The output noise power due to thermal array noise is then

$$P_{t,iso} = k_b T_{iso} B \cdot \mathbf{w}^H \mathbf{G} (\mathbf{I} - \mathbf{S}_A \mathbf{S}_A^H) \mathbf{G}^H \mathbf{w}. \quad (4.42)$$

Note that transformation matrix \mathbf{G} described from hereon differs from \mathbf{G} in [16], which is a matrix that transforms forward noise wave amplitudes at the amplifier inputs to *voltages* at the receiver output. While \mathbf{G} hereon transforms forward noise waves at the LNA inputs to *noise waves* at the output of the receiver. Using noise waves instead of noise voltages has notional benefits as working with voltages necessitates carrying around factors such as $\sqrt{Z_0}$ or having the cumbersomeness of converting scatter waves to voltages via the equations $a = \frac{(V+Z_0I)}{2\sqrt{Z_0}}, b = \frac{(V-Z_0I)}{2\sqrt{Z_0}}$. Ultimately, these factors cancel out in the final steps of analysis thereby negating the need to use voltages and currents in the analysis in the first place. Therefore, the following definition is used in this thesis

$$\mathbf{G} = (\mathbf{I} + \mathbf{S}_R) (\mathbf{I} - \mathbf{S}_R \mathbf{S}_A)^{-1}, \quad (4.43)$$

where \mathbf{G} transforms forward noise waves at the LNA inputs to the output of receiver.

By expanding the denominator of Equation 4.39 and using the new \mathbf{G} ,

$$P_{l,iso} = k_b T_{iso} B \cdot \mathbf{w}^H \mathbf{G} (\mathbf{I} - \mathbf{S}_A \mathbf{S}_A^H) \mathbf{G}^H \mathbf{w}. \quad (4.44)$$

It can be seen that Equation 4.44 is similar to Equation 4.28 in Section 4.2.4, but the integral is simplified by using B instead. This equation assumes that all quantities are frequency independent.

Substituting Equation 4.44 into 4.39 yields

$$T_{rec} = \frac{P_{N,rec}}{k_b B \cdot \mathbf{w}^H \mathbf{G} (\mathbf{I} - \mathbf{S}_A \mathbf{S}_A^H) \mathbf{G}^H \mathbf{w}}. \quad (4.45)$$

Next, expanding the numerator of Equation 4.45 gives

$$P_{N,rec} = \mathbf{w}^H \mathbf{R}_{rec} \mathbf{w} \quad (4.46)$$

$$P_{N,rec} = \mathbf{w}^H \mathbf{G} \mathbf{R}_{rec,f} \mathbf{G}^H \mathbf{w}, \quad (4.47)$$

where $\mathbf{R}_{rec,f}$ is the noise wave correlation matrix of the LNA at the input of LNAs. Expressing $\mathbf{R}_{rec,f}$ using traveling wave noise parameters yields

$$P_{N,rec} = k_b B \cdot \mathbf{w}^H \mathbf{G} \left[\mathbf{T}_\alpha + \mathbf{S}_A \mathbf{T}_\beta \mathbf{S}_A^H + \mathbf{T}_\gamma \mathbf{S}_A + \mathbf{T}_\gamma^H \mathbf{S}_A^H \right] \mathbf{G}^H \mathbf{w}, \quad (4.48)$$

where $\mathbf{T}_\alpha = E \{a_n \cdot a_n^*\} / k_b B$, $\mathbf{T}_\beta = E \{b_n \cdot b_n^*\} / k_b B$, $\mathbf{T}_\gamma = E \{a_n \cdot b_n^*\} / k_b B$ from [16].

The three noise parameter correlation matrices are

$$\mathbf{T}_\alpha = T_{min} + T_0 \frac{N}{G_{opt} R_0} |1 - R_0 Y_{opt}|^2 \quad (4.49)$$

$$\mathbf{T}_\beta = -T_{min} + T_0 \frac{N}{G_{opt} R_0} |1 + R_0 Y_{opt}|^2 \quad (4.50)$$

$$\mathbf{T}_\gamma = T_0 \frac{N}{G_{opt} R_0} (1 + R_0 Y_{opt}) (1 - R_0 Y_{opt}^*). \quad (4.51)$$

Inserting the matrices into Equation 4.45 yields [16]

$$T_{rec} = \frac{\mathbf{w}^H \mathbf{G} \left[\mathbf{T}_\alpha + \mathbf{S}_A \mathbf{T}_\beta \mathbf{S}_A^H + \mathbf{T}_\gamma \mathbf{S}_A + \mathbf{T}_\gamma^H \mathbf{S}_A^H \right] \mathbf{G}^H \mathbf{w}}{\mathbf{w}^H \mathbf{G} (\mathbf{I} - \mathbf{S}_A \mathbf{S}_A^H) \mathbf{G}^H \mathbf{w}}. \quad (4.52)$$

Note that in this equation, $k_b B$ in the numerator cancels out the $k_b B$ in the denominator. This equation is accurate for narrowband case where the frequency response of array, LNAs, and beamformer weights are constant. An assumption hidden in this equation is that the bandwidth under consideration is $B = 1\text{Hz}$ [15]. Despite this assumption, the equation applies to all cases where the antenna S-parameters and LNA noise parameters are constant over the bandwidth under consideration.

Equation 4.52 is now fully expanded to explicitly show all terms with \mathbf{S}_A and \mathbf{G} that can be converted to frequency dependent terms by embedding delays in them. As described in Section 4.2.1, the antenna array S-parameters can be written as a function of frequency

$$\mathbf{S}_A(f) = \begin{bmatrix} s_{11} e^{-j2\pi f(\tau_{11} + 2\tau_d + 2\tau_x)} & \dots & s_{1m} e^{-j2\pi f(\tau_{1m} + 2\tau_d + 2\tau_x)} \\ \vdots & \ddots & \vdots \\ s_{n1} e^{-j2\pi f(\tau_{n1} + 2\tau_d + 2\tau_x)} & \dots & s_{nm} e^{-j2\pi f(\tau_{nm} + 2\tau_d + 2\tau_x)} \end{bmatrix}, \quad (4.53)$$

where the lower case s_{ij} denote the complex intrinsic frequency invariant component of array S-parameters. It is assumed that the self delay of each antenna element is zero, $\tau_{ii} = 0$. The antenna feeds are assumed to be the same for each element, therefore the feed line delay τ_d is the same. And, the transmission line from LNA inputs to antenna ports are the same, so the transmission line delay τ_x is the same for all elements as well.

Next, the modified S-parameters (Equation 4.53) are inserted into Equation 4.52 to get

$$T_{rec} = \frac{\int_{f_L}^{f_H} \left[\mathbf{w}^H \mathbf{G}(f) \left[\mathbf{T}_\alpha + \mathbf{S}_A(f) \mathbf{T}_\beta \mathbf{S}_A^H(f) + \mathbf{T}_\gamma \mathbf{S}_A(f) + \mathbf{T}_\gamma^H \mathbf{S}_A^H(f) \right] \mathbf{G}^H(f) \mathbf{w} \right] df}{\int_{f_L}^{f_H} \left[\mathbf{w}^H \mathbf{G}(f) (\mathbf{I} - \mathbf{S}_A(f) \mathbf{S}_A^H(f)) \mathbf{G}^H(f) \mathbf{w} \right] df}. \quad (4.54)$$

Equation 4.54 replaces the constant B with integral $\int_{f_L}^{f_H} (\dots) df$ in both numerator and denominator to capture the frequency dependence of $\mathbf{S}_A(f)$ and $\mathbf{G}(f)$. Equation 4.54 uses the function notation with matrices, $\mathbf{S}_A(f)$ and $\mathbf{G}(f)$, to denote that the matrix entries are frequency dependent quantities. This notation will be dropped from hereon until the end of this section for convenience. The definite bounds of the integral, f_L and f_H , are the lower and upper frequencies respectively of the band-pass filter at the output. Again, such an integral does not have a closed-form solution and will be left in the following form

$$T_{rec} = \frac{\int_{f_L}^{f_H} \left[\mathbf{w}^H \mathbf{G} \left[\mathbf{T}_\alpha + \mathbf{S}_A \mathbf{T}_\beta \mathbf{S}_A^H + \mathbf{T}_\gamma \mathbf{S}_A + \mathbf{T}_\gamma^H \mathbf{S}_A^H \right] \mathbf{G}^H \mathbf{w} \right] df}{\int_{f_L}^{f_H} \left[\mathbf{w}^H \mathbf{G} (\mathbf{I} - \mathbf{S}_A \mathbf{S}_A^H) \mathbf{G}^H \mathbf{w} \right] df} \quad (4.55)$$

With Equation 4.55, it is now possible to find an optimal Γ_{act} for the scan direction associated \mathbf{w} . When all the LNAs are matched to this optimal Γ_{act} , the array produces the lowest noise output for bandwidth of $B = f_H - f_L$ and beamformer weight vector \mathbf{w} . The derivation begins by representing optimal Γ_{act} in admittance form and breaking it down to its real and imaginary components

$$Y_{act} = G_{act} + jB_{act}. \quad (4.56)$$

The lowest receiver noise occurs when

$$\frac{\partial (T_{rec})}{\partial G_{act}} = 0 \quad (4.57)$$

and

$$\frac{\partial (T_{rec})}{\partial B_{act}} = 0. \quad (4.58)$$

The 3 correlation matrices, \mathbf{T}_α , \mathbf{T}_β , and \mathbf{T}_γ can be expressed in terms of the noise parameters $G_{opt} + jB_{opt}$, N , and T_{min} , when $G_{act} + jB_{act}$ is substituted for $G_{opt} + jB_{opt}$,

$$\mathbf{T}_\alpha = T_{min} + T_0 \frac{N}{G_{act} R_0} |1 - R_0 (G_{act} - jB_{act})|^2 \quad (4.59)$$

$$\mathbf{T}_\beta = -T_{min} + T_0 \frac{N}{G_{act} R_0} |1 + R_0 (G_{act} + jB_{act})|^2 \quad (4.60)$$

$$\mathbf{T}_\gamma = T_0 \frac{N}{G_{act} R_0} (1 + R_0 (G_{act} + jB_{act})) (1 - R_0 (G_{act} - jB_{act})) \quad (4.61)$$

First, $\frac{\partial (T_{rec})}{\partial B_{act}} = 0$ is found to occur when

$$B_{act} = \frac{-2\mathbf{w}^H \left[\int_{f_L}^{f_H} \mathbf{G} \Im \{ \mathbf{S}_A \} \mathbf{G}^H df \right] \mathbf{w}}{R_0 \mathbf{w}^H \left[\int_{f_L}^{f_H} \mathbf{G} [\mathbf{I} + \mathbf{S}_A \mathbf{S}_A^H + 2\Re \{ \mathbf{S}_A \}] \mathbf{G}^H df \right] \mathbf{w}}, \quad (4.62)$$

and the resulting expression for B_{act} is used to find G_{act} ,

$$G_{act}^2 = \frac{-2\mathbf{w}^H \left[\int_{f_L}^{f_H} \mathbf{G} [(1 + R_0^2 B_{act}^2) (\mathbf{I} + \mathbf{S}_A \mathbf{S}_A^H) - (1 + 2jZ_0 B_{opt} - Z_0^2 B_{opt}^2) \mathbf{S}_A] \right] \mathbf{w}}{\mathbf{w}^H \left[\int_{f_L}^{f_H} \mathbf{G} [\mathbf{I} + \mathbf{S}_A \mathbf{S}_A^H + 2\Re \{ \mathbf{S}_A \}] \mathbf{G}^H df \right] \mathbf{w} \times} \quad (4.63)$$

$$\frac{- (1 + 2jZ_0 B_{opt} - Z_0^2 B_{opt}^2)^* \mathbf{S}_A^H \mathbf{G}^H df \mathbf{w}}{R_0^2}$$

Finally, Equations 4.62 and 4.63 are combined to get Y_{act}

$$Y_{act} = G_{act} + jB_{act}. \quad (4.64)$$

For detailed derivation, see Appendix C

Equations 4.62 and 4.63 are fairly complex and made even more complex due to the integral and G_{act}^2 term. Nonetheless, they do provide a way to find a single Γ_{opt} for all LNAs that minimizes the array noise as opposed to finding individual Γ_{opt} for each LNA.

4.4.1 Simulation of 71 Element Array with Optimal Γ_{act}

In order to verify optimal Γ_{act} derived previously and to determine its usefulness, a numerical simulation in MATLAB was conducted using the 71-element dual polarized Vivaldi focal-plane array for a Square Kilometer Array receiver demonstrator as described in [53]. The model was described for several operating frequencies, and, the 1.4GHz model was chosen as it would allow for a large simulation bandwidth. A suitable LNA with $T_{min} = 15K$, and $N = 0.024$ was chosen from [54]. The Lange noise parameter $N = R_n G_{opt}$, which, like T_{min} , is invariant under lossless transformation, allowed for generating of a large number of nearly identical LNAs that have different Γ_{opt} but the same noise performance. These LNAs can be simulated with the array in search for the lowest T_{rec} without changing the overall power of the noise sources present in the array.

The Vivaldi array has 71 elements: 36 are vertically polarized and 35 are horizontally polarized. Each polarization has its own beamformer network. The beamformer weights associated with the 35 horizontally polarized elements were set to 0, while the weights associated with the vertically polarized array elements were set to 1. The scan direction to be simulated was therefore the one associated with unity gain beamformer weights for the vertically polarized elements of the array. The delay between the array elements was calculated based on separation distance and assuming speed of light as signal propagation velocity. The phase shifts caused by delays in the array were removed from each S-parameter of the array. This was done to ensure that all S-parameters of the array were kept the same at the operating frequency when phase shifts due to delays were introduced back into the S-parameters during simulation.

Due to tight spacing of antennas in the array, it is possible that the propagation velocity

of signals between elements is much slower than c . This could be because of coupling between elements that are closely spaced together. For the vertically polarized antennas separated by a horizontally polarized antenna, there is much conductive material in the way for signal propagation to happen at c . The antenna distances were calculated by using the center of one antenna to the center of another antenna; however, it is possible that propagation path for signals is not this simple. For example, the coupling observed in the array S-parameters may happen near the feed of the antenna rather than at the point of radiation. Despite these concerns, and in order to narrow the focus of the simulation to the impact of noise bandwidth and delays on T_{rec} and Γ_{act} , propagation velocity was assumed to be c , and antenna centers were used to calculate propagation distances between antennas in order to find inter-element delays τ_{ij} .

The LNAs in receiver were fed from the antenna ports using transmission lines. In order to keep the array S-parameters invariant as seen by the LNAs at f_0 , the identical transmission line lengths were restricted to $\left\{n\frac{\lambda}{2} \mid n \in \mathbb{N}\right\}$. For a transmission line of length $d = n\frac{\lambda}{2}$, the S-parameters at the operating frequency remains the same.

$$\tau = \frac{d}{c}, d = n\frac{\lambda}{2} \therefore \tau = \frac{n\lambda}{2c}, \tau = \frac{n}{2f_0} \quad (4.65)$$

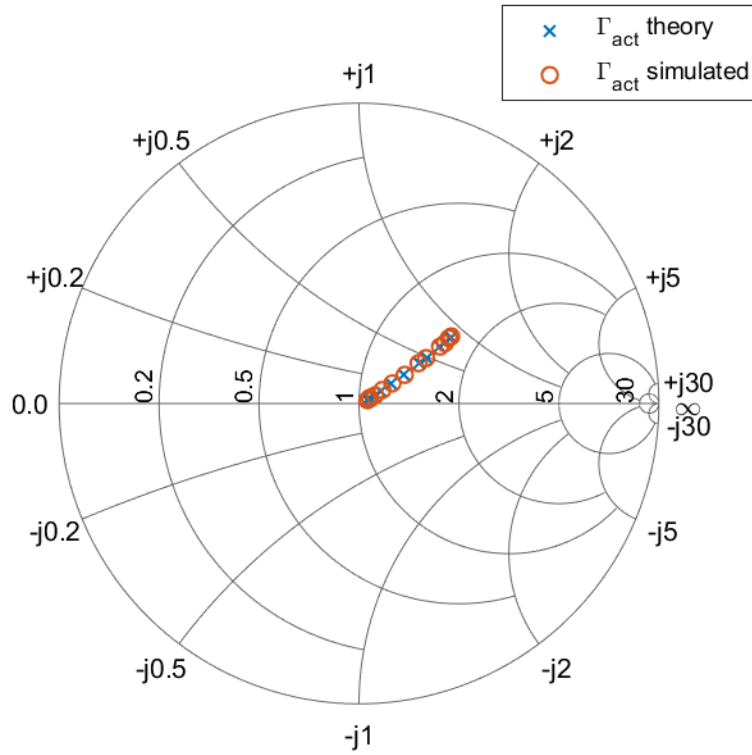
where τ is one way transmission line delay.

The effect of $\left\{n\frac{\lambda}{2} \mid n \in \mathbb{N}\right\}$ transmission line on S-parameters is

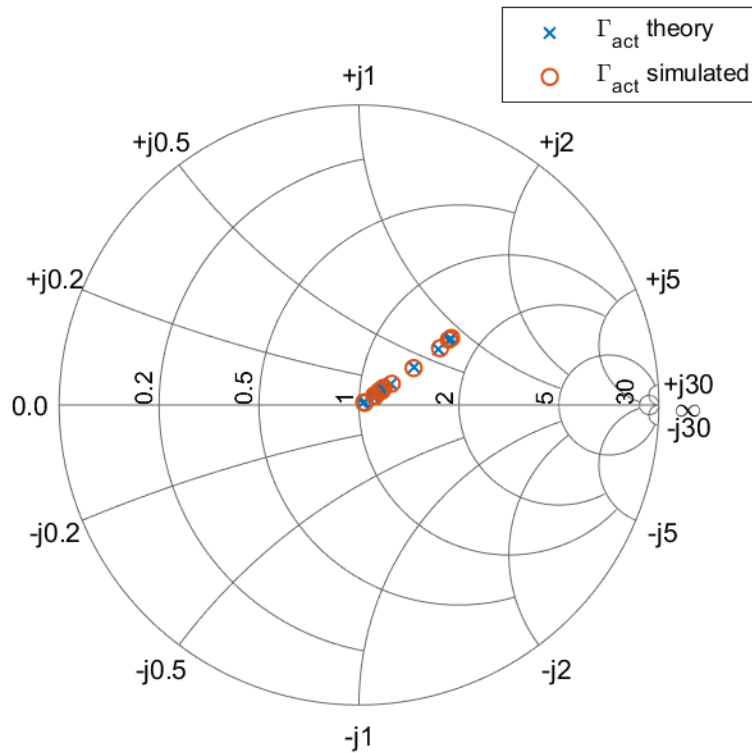
$$s(f_0)_{ix} = s(f_0) \cdot e^{-j2\pi f_0 2\tau} = s(f_0) \cdot e^{-j2\pi f_0 2\frac{n}{2f_0}} = s(f_0) \cdot e^{-j2\pi n} = s(f_0), \quad (4.66)$$

where the factor of 2 with τ signifies that time of flight for the signal is twice the one way propagation delay. Then, $s(f_0) = s \cdot e^{-j2\pi f_0 n} = s$ if $n \in \mathbb{N}$.

All LNAs in the simulation were generated using N and T_{min} , so all LNAs are realizable due to the bounding equation $2\frac{T_{min}}{T_0} > 4N \geq \frac{T_{min}}{T_0}$ from [55].



(a) Smith chart of simulated and theoretical optimal Γ_{act} with no transmission line as bandwidth is increased from 1Hz to 300MHz.



(b) Smith chart of simulated and theoretical optimal Γ_{act} with 2.5λ transmission line as bandwidth is increased from 1Hz to 300MHz.

Figure 4.10: Search of optimal Γ_{act} using simulation.

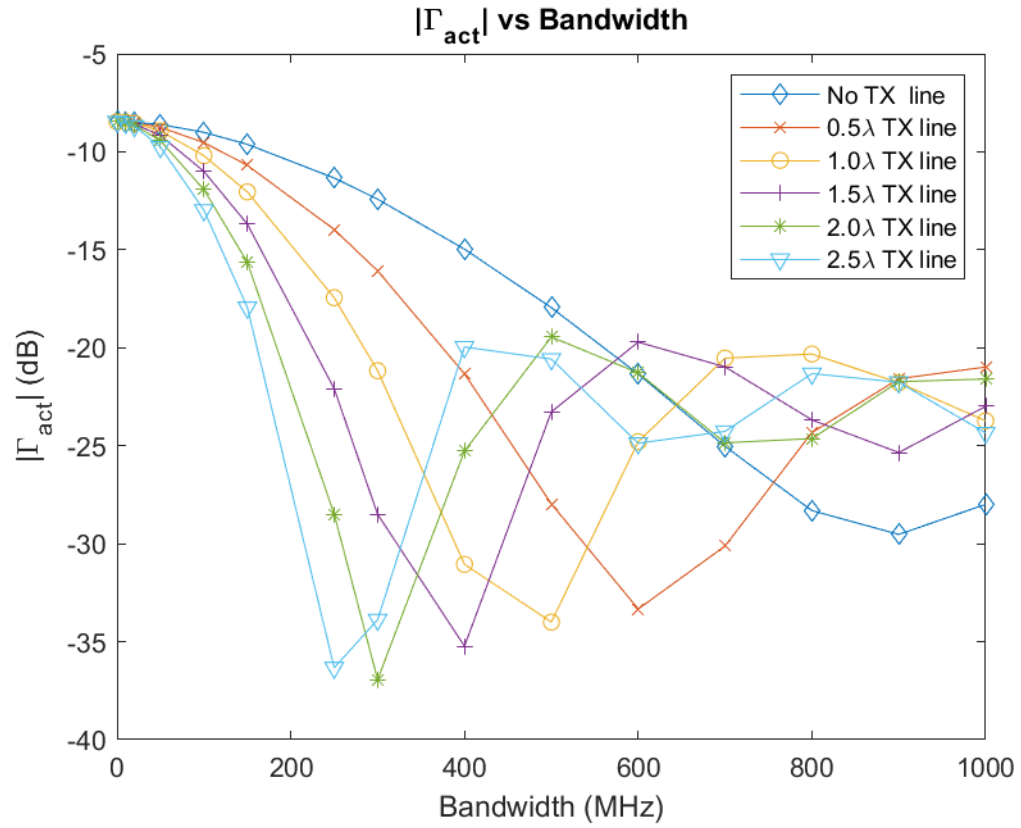


Figure 4.11: Plot of $|\Gamma_{act}|$ vs bandwidth for various transmission line lengths.

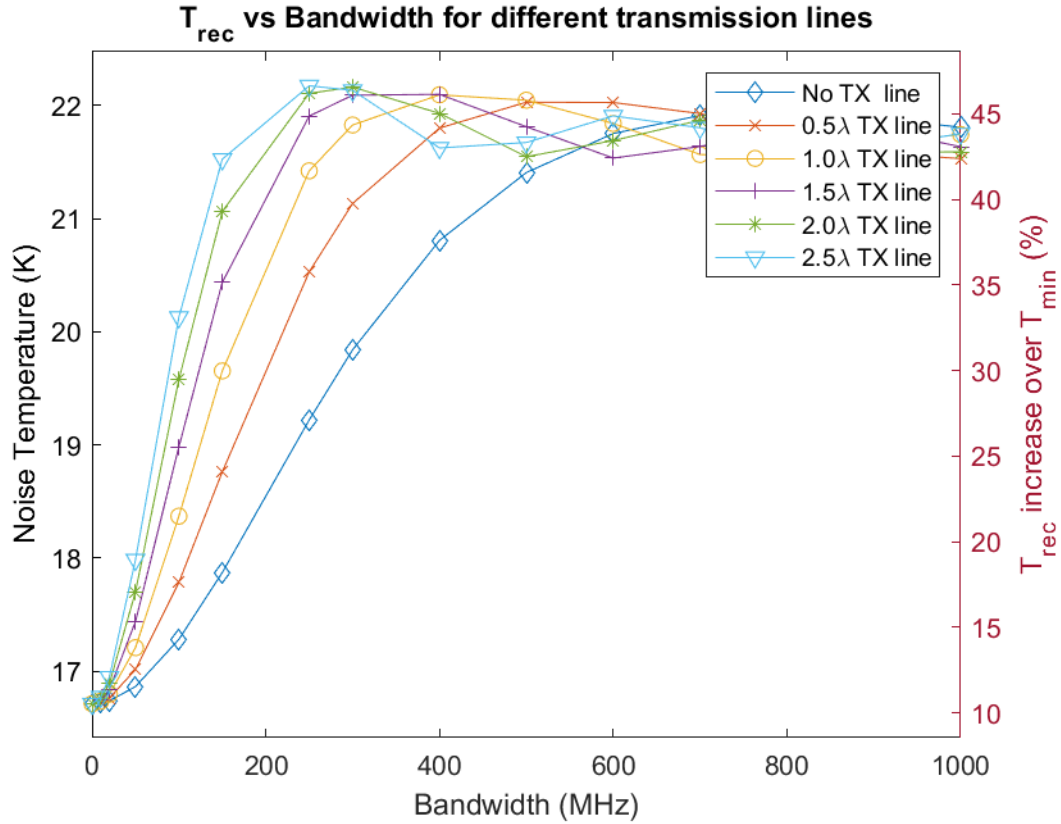


Figure 4.12: Plot of T_{rec} vs bandwidth for various transmission line lengths.

The optimal Γ_{act} was found by sweeping the entire Γ_{opt} space and finding where in the space of Γ_{opt} the T_{rec} was lowest. After optimal Γ_{act} was found using simulation, it was compared to the theoretical optimal Γ_{act} calculated using Equations 4.62, 4.63, and 4.64 by converting Y_{act} to Γ_{act} . Figure 4.10a shows the comparison of theoretical optimal Γ_{act} to the simulated optimal Γ_{act} as bandwidth is increased from 1Hz to 1GHz. The narrowband Γ_{act} agrees with both the simulated and derived optimal Γ_{act} in the 1-Hz case. Then, as the bandwidth increases, both the simulated and theoretical optimal Γ_{act} diverge from narrowband Γ_{act} as predicted and settle to the middle of Smith chart. As the bandwidth approaches 300MHz, Γ_{act} approaches the point of Z_0 on the Smith chart. Figure 4.10b shows the same simulation except with a transmission line of 2.5λ . In this case, the trajectory of Γ_{act} on Smith chart is the same but it approaches the center much faster than the first case with no transmission line. Figure 4.12 shows the effects of bandwidth on T_{rec} for different lengths

of transmission line. Observe that in all cases, T_{rec} is the same for $B = 1$ Hz case. In all cases, as the bandwidth is increased, T_{rec} goes up and settles to about 45% higher than T_{min} . For longer transmission lines, T_{rec} approaches the highest temperature much faster than the smaller transmission lines.

The simulation validates the derived equation for optimal Γ_{act} and that it indeed minimizes T_{rec} in the active array case when matching the array to identical LNAs. The rise in T_{rec} can be attributed to the decorrelation of forward and reverse noise waves of LNAs when larger delays in the system are introduced or bandwidth is increased. This result also strengthens the simulation results obtained in Section 4.3 because the Γ_{act} in that simulation also fall to the center of Smith chart as bandwidth is increased.

This simulation was conducted in frequency domain because it is not computationally possible to search through the entire Γ_{act} space for lowest array noise in time domain. The frequency space was split into many smaller intervals. These intervals were small enough that the array S-parameters did not vary significantly in them. For each frequency interval, the narrowband Equation 4.40 was used to produce the receiver noise temperature. And, for each interval, \mathbf{S}_A was re-calculated for the center frequency in the interval. The resulting receiver temperatures were summed to produce the overall beam equivalent receiver noise temperature for the original bandwidth. This process is the same as numerical integration using the midpoint rule when the narrowband Equation 4.52 is used and B is replaced with integration over frequency. See Appendix D for simulation code.

4.5 Optimizing For Multiple Scan Directions

Warnick et al. presented a method for minimizing the array noise over multiple scan directions in [16]. The method involved summing the output noise of the array operating under different scan directions, and finding $Y_{opt,m}$ that minimize average receiver noise temperature of the array. They defined the multi-beam average receiver noise temperature T_{av}

as

$$T_{av} = \frac{1}{P} \sum_{p=1}^P T_{rec}^p, \quad (4.67)$$

where T_{rec}^p is the receiver noise temperature when array is operating with p^{th} beamformer weight vector. Next, they found the $Y_{opt,m}$ for the multi-beam average temperature T_{av} as follows:

$$\frac{\partial T_{av}}{\partial Y_{opt,m}^*} = 0. \quad (4.68)$$

This type of optimization has the benefit of lowering the array noise temperature over several operating modes of the array. However, much like the narrowband $\Gamma_{act,m}$, this method requires matching individual LNAs to each antenna in the array, which is not practical. For this reason, an optimal Γ_{act} needs to be derived that can minimize the multi-beam average receiver noise temperature. The derivation of multi-beam optimal Γ_{act} starts in much the same way as [16]

$$T_{av} = \frac{1}{P} \sum_{p=1}^P T_{rec}^p, \quad \frac{\partial T_{av}}{\partial Y_{opt,m}^*} = 0 \quad (4.69)$$

However, this time T_{rec}^p is given as

$$T_{rec}^p = \frac{\int_{f_L}^{f_H} \left[\mathbf{w}_p^H \mathbf{G} \left[\mathbf{T}_\alpha + \mathbf{S}_A \mathbf{T}_\beta \mathbf{S}_A^H + \mathbf{T}_\gamma \mathbf{S}_A + \mathbf{T}_\gamma^H \mathbf{S}_A^H \right] \mathbf{G}^H \mathbf{w}_p \right] df}{\int_{f_L}^{f_H} \left[\mathbf{w}_p^H \mathbf{G} (\mathbf{I} - \mathbf{S}_A \mathbf{S}_A^H) \mathbf{G}^H \mathbf{w}_p \right] df}, \quad (4.70)$$

where \mathbf{w}_p are now the beamformer weights associated with the p^{th} scan direction. Next, substituting Equation 4.70 into 4.69 yields

$$T_{av} = \frac{1}{P} \sum_{p=1}^P \frac{\int_{f_L}^{f_H} \left[\mathbf{w}_p^H \mathbf{G} \left[\mathbf{T}_\alpha + \mathbf{S}_A \mathbf{T}_\beta \mathbf{S}_A^H + \mathbf{T}_\gamma \mathbf{S}_A + \mathbf{T}_\gamma^H \mathbf{S}_A^H \right] \mathbf{G}^H \mathbf{w}_p \right] df}{\int_{f_L}^{f_H} \left[\mathbf{w}_p^H \mathbf{G} (\mathbf{I} - \mathbf{S}_A \mathbf{S}_A^H) \mathbf{G}^H \mathbf{w}_p \right] df}, \quad (4.71)$$

Equation 4.71 is the multi-beam average beam referred receiver noise temperature that

includes the frequency varying nature of \mathbf{S}_A . Equation 4.71 can be used to find the multi-beam optimal Γ_{act} by using $Y_{act} = G_{act} + jB_{act}$ and finding the derivatives $\frac{\partial(T_{av})}{\partial G_{act}} = 0$ and $\frac{\partial(T_{av})}{\partial B_{act}} = 0$. Because of the distributive nature of derivative operator, multi-beam optimal B_{act} is found to be

$$B_{act} = \frac{\sum_{p=1}^P \left[\frac{-2\mathbf{w}_p^H \int_{f_L}^{f_H} \mathbf{G} \Im\{\mathbf{S}_A\} \mathbf{G}^H df \mathbf{w}_p}{\mathbf{w}_p^H \int_{f_L}^{f_H} \mathbf{G} (\mathbf{I} - \mathbf{S}_A \mathbf{S}_A^H) \mathbf{G}^H df \mathbf{w}_p} \right]}{\sum_{p=1}^P \left[\frac{R_0 \mathbf{w}_p^H \int_{f_L}^{f_H} \mathbf{G} [\mathbf{I} + \mathbf{S}_A \mathbf{S}_A^H + 2\Re\{\mathbf{S}_A\}] \mathbf{G}^H df \mathbf{w}_p}{\mathbf{w}_p^H \int_{f_L}^{f_H} \mathbf{G} (\mathbf{I} - \mathbf{S}_A \mathbf{S}_A^H) \mathbf{G}^H df \mathbf{w}_p} \right]} \quad (4.72)$$

and

$$G_{act}^2 = \frac{\sum_{p=1}^P \left[\frac{-2\mathbf{w}_p^H \left[\int_{f_L}^{f_H} \mathbf{G} \left[(1 + R_0^2 B_{act}^2) (\mathbf{I} + \mathbf{S}_A \mathbf{S}_A^H) - 2\Re\{ (1 + 2jZ_0 B_{opt} - Z_0^2 B_{opt}^2) \mathbf{S}_A \} \right] \mathbf{G}^H df \right] \mathbf{w}_p}{\mathbf{w}_p^H \int_{f_L}^{f_H} \mathbf{G} (\mathbf{I} - \mathbf{S}_A \mathbf{S}_A^H) \mathbf{G}^H df \mathbf{w}_p} \right]}{\sum_{p=1}^P \left[\frac{R_0^2 \mathbf{w}_p^H \int_{f_L}^{f_H} \mathbf{G} [\mathbf{I} + \mathbf{S}_A \mathbf{S}_A^H + 2\Re\{\mathbf{S}_A\}] \mathbf{G}^H df \mathbf{w}_p}{\mathbf{w}_p^H \int_{f_L}^{f_H} \mathbf{G} (\mathbf{I} - \mathbf{S}_A \mathbf{S}_A^H) \mathbf{G}^H df \mathbf{w}_p} \right]} \quad (4.73)$$

See Appendix E for complete derivation. Equations 4.72 and 4.73 are fairly complex and cannot be simplified easily. Because of the complexity of these equations, it is postulated that the multi-beam optimal Γ_{act} will fall to the center of Smith chart faster as B increases, much like optimal Γ_{opt} falls to the center of Smith chart.

4.6 Weighted Average Multi-beam Optimization

Many arrays are designed to operate with beam steering capabilities. If all the possible scan directions are known at the time of the receiver design, and the bandwidth of operation is known, then it is possible to produce a receiver with identical LNAs that minimizes the overall noise of the array using Equations 4.72 and 4.73. This approach can be taken further to include the fact that some beam angles may be more important and more used, so more preference is given to that particular beam when calculating optimal Γ_{act} .

If a beam angle associated with a p^{th} beamformer weight vector is used more often,

then, it can be weighted more in the averaging Equation 4.71. Define a weight vector \mathbf{z} as

$$\mathbf{z} = [z_1, z_2, \dots, z_p]^T, \quad (4.74)$$

$$\{z_p \geq 0 \mid z_p \in \mathbb{R}\}, \|\mathbf{z}\| = 1, \quad (4.75)$$

where z_p corresponds to the importance given to the p^{th} beam. The higher the weight z_p the more the beam direction associated with it is expected be used or is of importance. Then, the average multi-beam receiver noise temperature T_{av} is

$$T_{av} = \mathbf{T}_{rec}\mathbf{z} \quad (4.76)$$

$$\mathbf{T}_{rec} = [T_{rec}^1, T_{rec}^2, \dots, T_{rec}^p] \quad (4.77)$$

where T_{av} is not a true average receiver temperature as the scaling of each T_{rec}^p term is different. This T_{av} can then be used in Equation 4.71 to arrive at a multi-beam optimal Γ_{act} that is better suited for some scan directions than others.

4.7 Conclusion

This chapters discusses the effects of delays on antenna array and receiver noise. Equation for T_{rec} is developed that incorporate the delays and bandwidths, which had not previously been discussed in literature. Optimal Γ_{act} is presented as a new method of array noise optimization, and multi-beam optimal Γ_{act} is also presented. The developed methods and equations are verified using simulation.

Chapter 5

Discussion

Analyzing noise delays in antenna arrays in the manner discussed in Chapter 4 illustrates the breaking down of traditional equations found in [16,37] when wideband antenna arrays with frequency varying S-parameters are considered. In Section 4.4.1, it is shown that for an array with modest bandwidth of 300MHz, T_{rec} can increase of up to 45% more than T_{min} of LNA when delays are not ignored. In [49], the measured output noise of the array is higher than calculated; this difference is not properly explained. It is possible that some of the discrepancy in measured and calculated array output noise can be accounted for by including bandwidth and delay effects in the analysis and by using frequency dependent S-parameters.

The simulation in Section 4.4 was done using the array developed in [54]. For other arrays, it is entirely possible that the effects of bandwidth and delays on T_{rec} may be more or less adverse. Therefore, the 45% increase in T_{rec} over T_{min} for the simulated array may not be representative of majority of the arrays. Although the focus of the simulation in Section 4.4 was strictly on the effects of bandwidth and delays on T_{rec} and Γ_{act} , array noise is inexorably linked to the array and LNA S-parameters which are obviously different for different types of arrays. Nonetheless, it is clear that generally noise delays have an adverse effect on array noise temperature.

There is a dual effect of delay and bandwidth on noise in antenna arrays. Intuitively, increasing the bandwidth or increasing the element spacing has an effect on the phase of antenna S-parameters. Changing of element separation creates an obvious effect on phase of $\mathbf{S}_A(f)$ by compressing or expanding the delay phase curve along the frequency domain. Changing the bandwidth includes or excludes more of the delay curve on either side of operating frequency f_0 . Theoretically, either increasing bandwidth or increasing separation distance should have the same effect, however in real systems, where the antenna

S-parameters are not constant over the bandwidth of interest, increasing bandwidth means including more of the frequency varying nature of antenna and LNA S-parameters that are attributed to physical effects other than delays. Therefore, care must be taken in interpreting these results. Most LNAs do not exhibit constant gain or phase distortion over large bandwidth and the same is true of other components.

For some applications, such as MIMO communications systems, T_{rec} is a small component of the overall system noise and the effects of delays and bandwidth on the increase of T_{rec} may not be significant. The increase of T_{rec} is only of concern in applications where T_{rec} forms a significant component of the overall system noise temperature, such as highly sensitive radiometers and receivers.

The concept of matching the LNAs in the receiver to $\Gamma_{act,m}$, which has been developed and discussed in literature for some time, is also discovered to be less effective when it comes to wideband matching or for arrays with large delays. Matching to $\Gamma_{act,m}$ to obtain lowest receiver noise temperature seems promising at first, but is impractical. When bandwidth and delays are taken into account, $\Gamma_{act,m}$ shift closer to the center of Smith chart. When bandwidth dependence of array and LNA (and other components in receiver chain) S-parameters is considered, $\Gamma_{act,m}$ moves even closer to the center of Smith chart. This suggests that the frequency dependence of S-parameters decorrelates c_1 and c_2 of LNAs, and this decorrelation is exacerbated with increasing bandwidth or increasing delays in the array. The movement of $\Gamma_{act,m}$ to the center of Smith chart signifies that for wideband arrays a good strategy for minimizing T_{rec} is to use identical LNAs with $\Gamma_{opt} = 0$. This may seem counter intuitive at first, but recall that LNA noise matching occurs when part of c_1 is optimally reflected back towards the LNA so that it can cancel out with some of correlated portion of c_2 . In arrays with significant delays and large bandwidth, c_1 and c_2 are highly decorrelated, and having as little part of c_1 as possible reflect back is good for noise optimization. Some portion of c_1 will get radiated out and some portion will couple back to other LNAs via mutual coupling. However, this type of coupling is always present

in tightly spaced arrays and the only option is to not have c_1 reflect back directly from the array and add to the total noise at the beamformer output as discovered in this work.

Chapter 6

Conclusion

This thesis presented a method of incorporating bandwidth and delays in antenna array matching and array noise analysis, which had not been discussed in literature prior to this work. It expands the analysis of receiving arrays to include frequency varying nature of antenna S-parameters due to delays. It is shown through derivation and simulation that array output noise in broadband arrays will be higher than that calculated using traditional narrowband equations, and this is due to the frequency varying nature of array S-parameters. This analysis naturally required the extension of narrowband equations for T_{rec} and Γ_{act} to frequency dependent terms presented in this work. It is shown that including the frequency varying nature of antenna S-parameters moves Γ_{act} to the center of Smith chart. The method of finding Γ_{act} for multiple beam angles found in [16] is extended to include frequency varying terms and a new method for finding a single Γ_{act} for multiple beam angles while including frequency dependent S-parameters is also presented. Finally, a method is developed that weights certain scan directions more in the aforementioned multi-beam averaging method in order to give more priority to those scan directions when designing the receiver.

Bibliography

- [1] J. A. de Zwart, P. J. Ledden, P. Kellman, P. van Gelderen, and J. H. Duyn, "Design of a SENSE-optimized high-sensitivity MRI receive coil for brain imaging," *Magnetic Resonance in Medicine*, vol. 47, pp. 1218–1227, June 2002.
- [2] G. Krieger, N. Gebert, and A. Moreira, "Multidimensional waveform encoding: A new digital beamforming technique for synthetic aperture radar remote sensing," *IEEE Transactions on Geoscience and Remote Sensing*, vol. 46, pp. 31–46, January 2008.
- [3] T. Heath, R. Kerr, G. Hopkins, B. Sharp, B. Meadows, and J. Cothorn, "Simultaneous, multi-frequency synchronous oscillator antenna," in *IEEE Military Communications Conference*, (San Diego), pp. 1–7, 16-19 November 2008.
- [4] P. Dewdney, P. Hall, R. Schilizzi, and T. Lazio, "The Square Kilometre Array," vol. 97, pp. 1482–1496, August 2009.
- [5] R. Zhang, T. J. Lim, Y.-C. Liang, and Y. Zeng, "Multi-antenna based spectrum sensing for cognitive radios: A GLRT approach," *IEEE Transactions on Communications*, vol. 58, pp. 84–88, January 2010.
- [6] E. Brookner, "Never ending saga of phased array breakthroughs," in *IEEE International Symposium on Phased Array Systems and Technology (ARRAY)*, (Waltham, MA), pp. 61–73, 12-15 October 2010.
- [7] D. Heo and K. F. Warnick, "Integrated eight element Ku band transmit/receive beamformer chipset for low-cost commercial phased array antennas," in *IEEE International Symposium on Phased Array Systems and Technology (ARRAY)*, (Waltham, MA), pp. 653–659, 12-15 October 2010.

- [8] A. Natarajan, S. Reynolds, M.-D. Tsai, S. Nicolson, J.-H. Zhan, D. G. Kam, D. Liu, Y.-L. Huang, A. Valdes-Garcia, and B. Floyd, "A fully-integrated 16-element phased-array receiver in SiGe BiCMOS for 60-GHz communications," vol. 46, pp. 1059–1075, May 2011.
- [9] O. Inac, F. Golcuk, T. Kanar, and G. Rebeiz, "A 90-100-GHz phased-array transmit/receive silicon RFIC module with built-in self-test," vol. 61, pp. 3774–3782, October 2013.
- [10] T. S. Rappaport, Y. Xing, O. Kanhere, S. Ju, A. Madanayake, S. Mandal, A. Alkhatieb, and G. C. Trichopoulos, "Wireless communications and applications above 100 GHz: Opportunities and challenges for 6G and beyond," *IEEE Access*, vol. 7, pp. 78729–78757, 2019.
- [11] N. Rajatheva *et al.*, "White paper on broadband connectivity in 6G."
- [12] W. Turner, "SKA PHASE 1 SYSTEM (LEVEL 1) REQUIREMENTS," tech. rep., 2015.
- [13] A. Sheldon, L. Belostotski, G. Messier, and A. Madanayake, "Impact of Noise Bandwidth on Noise Figure," *IEEE Transactions on Instrumentation and Measurement*, vol. 68, pp. 2662–2664, jul 2019.
- [14] R. Maaskant and E. E. M. Woestenburg, "Applying the active antenna impedance to achieve noise match in receiving array antennas," *IEEE Antennas and Propagation Society, AP-S International Symposium (Digest)*, pp. 5889–5892, 2007.
- [15] K. F. Warnick, M. V. Ivashina, R. Maaskant, and B. Woestenburg, "Unified definitions of efficiencies and system noise temperature for receiving antenna arrays," *IEEE Transactions on Antennas and Propagation*, vol. 58, no. 6, pp. 2121–2125, 2010.

- [16] K. F. Warnick, B. Woestenburg, L. Belostotski, and P. Russer, “Minimizing the noise penalty due to mutual coupling for a receiving array,” *IEEE Transactions on Antennas and Propagation*, vol. 57, no. 6, pp. 1634–1644, 2009.
- [17] L. Belostotski, B. Veidt, K. F. Warnick, and A. Madanayake, “Low-noise amplifier design considerations for use in antenna arrays,” *IEEE Transactions on Antennas and Propagation*, vol. 63, no. 6, pp. 2508–2520, 2015.
- [18] A. R. Thompson, J. M. Moran, and G. W. Swenson Jr., *Interferometry and Synthesis in Radio Astronomy*. New York: John Wiley & Sons, 1986.
- [19] J. B. JOHNSON, “Thermal Agitation of Electricity in Conductors,” *Nature*, vol. 119, pp. 50–51, jan 1927.
- [20] H. Nyquist, “Thermal agitation of electric charge in conductors,” *Physical Review*, vol. 32, no. 1, pp. 110–113, 1928.
- [21] W. Schottky, “Über spontane Stromschwankungen in verschiedenen Elektrizitätsleitern,” *Annalen der Physik*, vol. 362, no. 23, pp. 541–567, 1918.
- [22] R. F. Voss and J. Clarke, “Flicker (1/f) noise: Equilibrium temperature and resistance fluctuations,” *Physical Review B*, vol. 13, pp. 556–573, jan 1976.
- [23] P. H. Handel, “Turbulence Theory for the Current Carriers in Solids and a Theory of 1/f Noise,” *Physical Review A*, vol. 3, pp. 2066–2073, jun 1971.
- [24] I. Lundström, D. McQueen, and C. Klason, “On low frequency and 1/f noise from diffusion like processes,” *Solid State Communications*, vol. 13, pp. 1941–1944, dec 1973.
- [25] S. Rogers, J. Aberle, and D. Auckland, “Two-port model of an antenna for use in characterizing wireless communications systems obtained using efficiency measure-

- ments,” in *IEEE Antennas and Propagation Society International Symposium (IEEE Cat. No.02CH37313)*, vol. 3, pp. 730–733, IEEE, 2002.
- [26] B. F. Burke, F. Graham-Smith, and P. N. Wilkinson, *An Introduction to Radio Astronomy*. Cambridge University Press, jul 2019.
- [27] H. Bosma, *On the theory of linear noisy system*. 1967.
- [28] S. W. Wedge and D. B. Rutledge, “Noise Waves and Passive Linear Multiports,” 1991.
- [29] R. P. Hecken, “Analysis of Linear Noisy Two-Ports Using Scattering Waves,” *IEEE Transactions on Microwave Theory and Techniques*, vol. 29, pp. 997–1004, oct 1981.
- [30] L. Belostotski, “No Noise Is Good Noise: Noise Matching, Noise Canceling, and Maybe a Bit of Both for Wide-Band LNAs,” *IEEE Microwave Magazine*, vol. 17, no. 8, pp. 28–40, 2016.
- [31] R. Lane, “The determination of device noise parameters,” *Proceedings of the IEEE*, vol. 57, no. 8, pp. 1461–1462, 1969.
- [32] J. Lange, “Noise Characterization of Linear Twoports in Terms of Invariant Parameters,” *IEEE Journal of Solid-State Circuits*, vol. 2, pp. 37–40, jun 1967.
- [33] L. Belostotski, “On the Number of Noise Parameters for Analyses of Circuits With MOSFETs,” *IEEE Transactions on Microwave Theory and Techniques*, vol. 59, pp. 877–881, apr 2011.
- [34] W. L. Stutzman, *Antenna theory and design*. Hoboken, NJ: Wiley, 2013.
- [35] A. A. Michelson, “I. On the application of interference methods to astronomical measurements,” *The London, Edinburgh, and Dublin Philosophical Magazine and Journal of Science*, vol. 30, pp. 1–21, jul 1890.

- [36] K. F. Warnick, R. Maaskant, M. V. Ivashina, D. B. Davidson, and B. D. Jeffs, *Phased Arrays for Radio Astronomy, Remote Sensing, and Satellite Communications*. Cambridge University Press, jul 2018.
- [37] K. F. Warnick and B. D. Jeffs, “Efficiencies and system temperature for a beamforming array,” *IEEE Antennas and Wireless Propagation Letters*, vol. 7, pp. 565–568, 2008.
- [38] S. de Silva, M. Okoniewski, and L. Belostotski, “Antenna-Array Network Model,” *IEEE Transactions on Antennas and Propagation*, vol. 68, pp. 5387–5394, jul 2020.
- [39] P. Hannan, “The element-gain paradox for a phased-array antenna,” *IEEE Transactions on Antennas and Propagation*, vol. 12, pp. 423–433, jul 1964.
- [40] S. Stein, “On cross coupling in multiple-beam antennas,” *IRE Transactions on Antennas and Propagation*, vol. 10, pp. 548–557, sep 1962.
- [41] R. C. Hansen, *Phased Array Antennas*. Wiley Series in Microwave and Optical Engineering, New York, USA: John Wiley & Sons, Inc., jan 1998.
- [42] J. Andersen and H. Rasmussen, “Decoupling and descattering networks for antennas,” *IEEE Transactions on Antennas and Propagation*, vol. 24, pp. 841–846, nov 1976.
- [43] K. F. Warnick and M. A. Jensen, “Optimal noise matching for mutually coupled arrays,” *IEEE Transactions on Antennas and Propagation*, vol. 55, no. 6 II, pp. 1726–1731, 2007.
- [44] M. L. Morris and M. A. Jensen, “Network model for MIMO systems with coupled antennas and noisy amplifiers,” *IEEE Transactions on Antennas and Propagation*, vol. 53, no. 1 II, pp. 545–552, 2005.

- [45] M. V. Ivashina, E. E. Woestenburger, and E. A. Redkina, "Effects of the element separation on the noise performance of receiving antenna arrays," *2007 6th International Conference on Antenna Theory and Techniques, ICATT'07*, no. 1, pp. 82–86, 2007.
- [46] C. Zhang, Q. Lai, and C. Gao, "Measurement of active S-parameters on array antenna using directional couplers," in *2017 IEEE Asia Pacific Microwave Conference (APMC)*, pp. 1167–1170, IEEE, nov 2017.
- [47] N. Colon-Diaz, D. Janning, T. Corigliano, L. Wang, and J. Aberle, "Measurement of Active Reflection Coefficient for Co-Located MIMO Radar Using Dual Directional Couplers," *2018 AMTA 2018 Proceedings, AMTA 2018*, pp. 1–4, 2019.
- [48] J. Weem and Z. Popovic, "A method for determining noise coupling in a phased array antenna," *2001 IEEE MTT-S International Microwave Symposium Digest (Cat. No.01CH37157)*, vol. 1, pp. 4–7, 2001.
- [49] K. F. Warnick, D. Carter, T. Webb, J. Landon, M. Elmer, and B. D. Jeffs, "Design and characterization of an active impedance matched low-noise phased array feed," *IEEE Transactions on Antennas and Propagation*, vol. 59, no. 6 PART 1, pp. 1876–1885, 2011.
- [50] R. Ali, L. Belostotski, G. G. Messier, A. Madanayake, and A. T. Sutinjo, "Impact of bandwidth on antenna array noise matching," *Electronics Letters*, vol. 57, pp. 158–160, feb 2021.
- [51] G. Gonzalez, *Microwave transistor amplifiers : analysis and design*. Prentice Hall, 2nd ed., 1997.
- [52] S. Weinreb, J. Bardin, H. Mani, and G. Jones, "Matched wideband low-noise amplifiers for radio astronomy," *Review of Scientific Instruments*, vol. 80, p. 044702, apr 2009.

- [53] R. Sarkis, B. Veidt, and C. Craeye, “Fast numerical method for Focal Plane Array simulation of 3D Vivaldi antennas,” in *2012 International Conference on Electromagnetics in Advanced Applications*, pp. 772–775, IEEE, sep 2012.
- [54] A. J. Beaulieu, L. Belostotski, T. Burgess, B. Veidt, and J. W. Haslett, “Noise Performance of a Phased-Array Feed with CMOS Low-Noise Amplifiers,” *IEEE Antennas and Wireless Propagation Letters*, vol. 15, no. c, pp. 1719–1722, 2016.
- [55] K. O. N. Micro, “Noise Parameters,” *Electronic Noise and Interfering Signals*, no. 9, pp. 69–112, 2006.

Appendix A

19 element array simulation code

The following program listing is MATLAB code for simulating noise signals as they propagate in the 19 element array. The code generates noise signals for both the array and the LNAs. The noise signals are then propagated through out the array by means of matrix multiplication in frequency domain. Next the signals are combined at the output of the beam former in order to calculate the receiver and array noise power. Finally, the array and receiver noise are used to calculate the beam equivalent receiver noise temperature.

Listing A.1: 19 Element array simulation MATLAB code

```
clf;
clear all;

Nel = 19;

load cryo_paf_kite_2010_data
ZA = ZA(1:Nel,1:Nel);

weight = w_boresight_cryo_model(1:Nel);
weight = weight(1:Nel);
%weight = ones(Nel,1);

% Constants
Z0 = 50;
T0 = 290;
kb = 1.38064852e-23;
I = eye(Nel);
```

```

c = 3e8; % speed of light in vacuum
Er = 2.4; % relative dielectric constant of PTFE for measurement cable
j = sqrt(-1);
fc = 1.6e9;

% sim parameters
nSmp = 20000; % Number of noise samples to generate.
numReflections = 10; % Number of times the signal reflects off the
    ↪ antenna.

% Amplifier noise parameters (Weinreb, cryo LNA)
Tmin = 6.29;
Rn = 0.706;
Zopt = 71.2+j*15.7;
GammaOpt = z2s(Zopt,Z0);

% maaskant
%Tmin = 100;
%Rn = 25;
%Zopt = 25+j*25;
%GammaOpt = (Zopt - Z0)/(Zopt + Z0);

% array s parameters
%SA = I*GammaOpt;
SA = z2s(ZA,Z0);
%SR = (Z0*I + ZR)\(ZR - Z0*I);

```

```

% S Parameters of Measured LNA
%s11 = 1e-12+0.266*exp(1j*(pi/180)*75.87); % Reflection coefficient
    ↪ for LNA input.
s11 = 0.1;
s21 = 10;
s12 = 0;
s22 = 0;
% gain = abs(s21)^2; % Amplifier gain
%maaskant
%s11 = 0;
%s21 = 10;
%s12 = 0;
%s22 = 0;
SLNA = [s11 s12;
        s21 s22];
ZLNA = s2z(SLNA, Z0);
SR = I*s11;

% antenna delays
antenna_standoff_height = (69.37 + 20.6)/1000;
%Generate array index and positions
y_diff = sqrt(112^2 - (112/2)^2);
array_pos_vec(1,:) = [-2*112 0];
array_pos_vec(2,:) = [-112 0];
array_pos_vec(3,:) = [0 0];
array_pos_vec(4,:) = [112 0];

```

```

array_pos_vec(5,:) = [2*112 0];
array_pos_vec(6,:) = [-1.5*112 y_diff];
array_pos_vec(7,:) = [-0.5*112 y_diff];
array_pos_vec(8,:) = [0.5*112 y_diff];
array_pos_vec(9,:) = [1.5*112 y_diff];
array_pos_vec(10,:) = [-1.5*112 -y_diff];
array_pos_vec(11,:) = [-0.5*112 -y_diff];
array_pos_vec(12,:) = [0.5*112 -y_diff];
array_pos_vec(13,:) = [1.5*112 -y_diff];
array_pos_vec(14,:) = [-112 2*y_diff];
array_pos_vec(15,:) = [0 2*y_diff];
array_pos_vec(16,:) = [112 2*y_diff];
array_pos_vec(17,:) = [-112 -2*y_diff];
array_pos_vec(18,:) = [0 -2*y_diff];
array_pos_vec(19,:) = [112 -2*y_diff];
array_pos_vec = array_pos_vec / 1000;

% make delay matrix
for n = 1:Nel
    for m = 1:Nel
        tau_ij(n,m) = sqrt((array_pos_vec(n,1) - array_pos_vec(m,1))^2
            ↪ + (array_pos_vec(n,2) - array_pos_vec(m,2))^2)/c;
    end
end
end

```

```

% Constants to calculate the cable delay
%cableL = 1.8288; % length of cable at the front end of the LNA in
    ↪ meters
tau_d = antenna_standoff_height/c; %One way propagation delay (sec) so
    ↪ round trip is 2\tau. (1.36ns/ft*6 ft) %(\sqrt(Er)/c)*cableL
    ↪ *100;
%tau_t = [0 tau*0.1; tau*0.1 0];
tau_tx = 0;

% remove phase shift due to delays from measured s paramters
for n = 1:Nel
    for m = 1:Nel
        SA_no_delay(n,m) = SA(n,m)/exp(-2*j*pi*fc*(tau_ij(n,m)+2*tau_d)
            ↪ );
    end
end

% Noise wave power and correlation coefficient from calculated from
% measured data
c1Psd = (kb*Tmin*(abs(s11)^2-1)+(4*kb*T0*Rn/Z0)*abs(1-s11*GammaOpt)^2/
    ↪ abs(1+GammaOpt)^2); % Power spectral density of input noise (W/
    ↪ Hz)
c2Psd = (abs(s21)^2*(kb*Tmin+(4*kb*T0*Rn/Z0)*abs(GammaOpt)^2/abs(1+
    ↪ GammaOpt)^2)); % Power spectral density of output noise (W/Hz)
rho = (-conj(s21)*conj(GammaOpt)*(4*kb*T0*Rn/Z0)/abs(1+GammaOpt)^2+(

```

```
↪ s11/s21)*c2Psd)/sqrt(c1Psd*c2Psd); % Cross correlation of the  
↪ input and output noise.
```

```
BW_arr = [1e-6 50:50:1500]*1e6;  
for b = 1:length(BW_arr)  
    b  
    W = BW_arr(b);  
    BW_arr(b)  
    tic  
    freq_space = fftshift(linspace(-BW_arr(b)/2,BW_arr(b)/2,nSmp));  
  
    %% generate random samples LNA noise  
    mixingWeights = chol(...  
        [ c1Psd (rho)*sqrt(c1Psd*c2Psd); ...  
          conj(rho)*sqrt(c1Psd*c2Psd) c2Psd ]);  
  
    for ant = 1:Nel  
        w1 = (randn(nSmp,1)+j*randn(nSmp,1))/sqrt(2);  
        w2 = (randn(nSmp,1)+j*randn(nSmp,1))/sqrt(2);  
        w_v = [ w1 w2 ] * conj(mixingWeights);  
        c1(:,ant) = fft(w_v(:,1));  
        c2(:,ant) = fft(w_v(:,2));  
    end;  
  
    %% generate random samples array noise
```

```

for ant = 1:Nel
    w_ant(:,ant) = fft((randn(nSmp,1)+j*randn(nSmp,1))/sqrt(2));
end;
parfor (s = 1:nSmp,8)
    SA_f = SA_no_delay.*exp(-j*2*pi*(fc+freq_space(s))*(tau_ij + 2*
        ↪ tau_d));
    Cant = kb*T0*(I - SA_f*SA_f');
    mixingWeightsAnt = chol(Cant);
    c_ant(s,:) = w_ant(s,:) * conj(mixingWeightsAnt);
    reflection_ant(s,:) = (exp(-j*2*pi*(fc+freq_space(s))*(tau_tx))
        ↪ *c_ant(s,:).').'*s11;
    %for ant = 1:Nel
    % c_ant(s,ant) = w_v_ant(s,ant);
    %end;
end;

a = zeros(size(c1));
reflection = c1;
%reflection_ant = (c_ant);
%b_ant = reflection_ant*s21;
b_ant = zeros(size(c1));
for r = 1:numReflections
    b_ant = b_ant + reflection_ant*s21/s11;
    parfor (s = 1:nSmp, 8);
        SA_f = SA_no_delay.*exp(-j*2*pi*(fc+freq_space(s))*(tau_ij

```

```

        ↪ + 2*tau_d + 2*tau_tx));
    reflection(s,:) = (SA_f*(reflection(s,:)).').'*s11;
    reflection_ant(s,:) = (SA_f*(reflection_ant(s,:)).').'*s11;
end;
a = a + reflection;

end;
a = a*s21/s11;
x = (a + c2)*weight;
x_ant = b_ant*weight;
ac_y = (x'*x)*W;
ac_y_ant = (x_ant'*x_ant)*W;
pwrSim(b) = (ac_y);
pwrSim_ant(b) = (ac_y_ant);

Tnumerical_narrow_num = 0;
Tnumerical_narrow_den = 0;

df = W/300;
powerClosedForm_S11zero_numerical_LNA(b) = 0;
powerClosedForm_S11zero_numerical_ANT(b) = 0;
df

for W_ = (fc-W/2):df:(fc+W/2)
    SA_f = SA_no_delay.*exp(-2*pi*j*(W_)*(tau_ij + 2*tau_d + 2*
        ↪ tau_tx));

```

```

G = inv(I - SR*SA_f);
auto_forward = c1Psd*(G*(SA_f*SA_f')*G')*abs(s21)^2;
forward_reverse = (rho)*sqrt(c2Psd*c1Psd)*(G*SA_f*s21);
auto_reverse = c2Psd*I;
auto_ant = kb*G*(I-SA_f*SA_f')*G'*abs(s21)^2;

% narrow band
[Tin, num, den] = simple_array_lna_model_Function_(Zopt, s2z(
    ↪ s11), Rn, Tmin, 1, s2z(SA_f), weight, SA_f);
Tnumerical_narrow_num = Tnumerical_narrow_num + num * df;
Tnumerical_narrow_den = Tnumerical_narrow_den + den * df;

powerClosedForm_S11zero_numerical_LNA(b) =
    ↪ powerClosedForm_S11zero_numerical_LNA(b) + weight'*(
    ↪ auto_forward + 2*real(forward_reverse) + auto_reverse)*
    ↪ weight*df;
powerClosedForm_S11zero_numerical_ANT(b) =
    ↪ powerClosedForm_S11zero_numerical_ANT(b) + weight'*(
    ↪ auto_ant)*weight*df;

end;

Tnumerical_narrow(b) = real(Tnumerical_narrow_num/
    ↪ Tnumerical_narrow_den);
TSim(b) = T0* pwrSim(b)/pwrSim_ant(b);
Tclosed_S11_zero_numerical(b) =
    ↪ powerClosedForm_S11zero_numerical_LNA(b)/

```

```

    ↪ powerClosedForm_S11zero_numerical_ANT(b);
    [T_standard(b), num, den] = simple_array_lna_model_Function_(Zopt,
    ↪ s2z(s11), Rn, Tmin, 1, s2z(SA), weight, SA);
    toc
end;

close all
fig = figure(1)
plot(BW_arr/1e6,abs(TSim), '-d')
hold on;
%plot((BW_arr)/1e6,abs(Tclosed_S11_zero_numerical),'-o')
plot((BW_arr)/1e6,abs(Tnumerical_narrow),'--x')
%title('Numerical simulation of a 19 element array with delays');
xlabel('Bandwidth (MHz)');
ylabel('Noise Temperature (K)');
plot((BW_arr)/1e6,abs(T_standard),'--')
ylim([min(TSim)-0.3 max(TSim)+0.3])
legend('Simulation','Theory', '1Hz Bandwidth')
yyaxis right
ylim(real([((min(TSim)-0.3) - T_standard(1))*100/T_standard(1) ((max(
    ↪ TSim)+0.3) - T_standard(1))*100/T_standard(1)]))
ylabel('T_r_e_c increase over minimum temperature (%)')
%saveas(fig,'../..//Figures/19-crayo-sim_no_tx.png');
saveas(fig,'../..//Figures/19-crayo-sim.png');

figure(2)

```

```
x = array_pos_vec(:,1)*1000; y = array_pos_vec(:,2)*1000; scatter(x,y
    ↪ , 'x');
a = [1:Nel]'; b_ = num2str(a); c_ = cellstr(b_);
dx = 0.001; dy = 0.001; % displacement so the text does not overlay
    ↪ the data points
%text(x+dx, y+dy, c);
xlabel('x(mm)');
ylabel('y(mm)');
title('Cryo PAF dipole array pattern');
ylim([-220 220]);
xlim([-220 220]);
axis equal;
```

Appendix B

Γ_{act} search simulation code

The following program listing is MATLAB code for simulating Γ_{act} as bandwidth is slowly increased. The code generates noise signals for both the array and the LNAs. The noise is then propagated through the array and beam equivalent receiver noise temperature is found. This is done for the entire Γ_{act} space. Γ_{act} is found to occur where the receiver noise is lowest for each bandwidth.

```
clear all;
close all;
beep off;

% create files and folders for sim
dirname = sprintf('C:/Users/Roshaan/SkyDrive/Grad School Work/Research
    ↪ /matlab sim/gamma_opt_sim_2_ant_%s/',datestr(now,'yyyy-mm-dd_HH
    ↪ -MM'));
mkdir(dirname);
filename = [dirname 'sim results.csv'];
FID = fopen(filename,'a+');

% save current script snapshot
snapshot_path = sprintf('%s/sim_script_snapshot.m',dirname);
copyfile(matlab.desktop.editor.getActiveFilename,snapshot_path);
tic

Nel = 2;
I = eye(Nel);
```

```

fc = 1e9;
Z0 = 50;
T0 = 290;
nSmp = 2000; % Number of noise samples to generate.
Ts = 1e-11; % Sampling period of this simulation (sec)
kb = 1.38064852e-23; % Boltzmann's constant (W/(Hz*K))
BW = 1e6;
c = 3e8; % speed of light in vacuum
Er = 2.4; % relative dielectric constant of PTFE for measurement cable
tau = (1/fc)/2;
tau_t = [0 tau*2; tau*2 0];

% generate gamma opt sweep parameters
numReflections = 5;
gammOpt_r_len = 5;
theta_len = 5
real_len = 20;
im_len = 20;
t_sweep_len = 10;
window = 0.015;
j = sqrt(-1);

% for weight [1 exp(1j*pi/4)]
%SA = [-0.2338 - 0.4204j 0.272+0.219j;0.272+0.219j -0.5438 - 0.0353j];
%SA = [0.5048-0.2436i -0.1516+0.2177i;
%-0.1516+0.2177i 0.5030+0.2338i]

```

```

SA = [0.5048-0.2436i -0.1516+0.2177i;
-0.1516+0.2177i 0.5030-0.2338i]
weight = [1;exp(1j*pi/4)];
w = weight;
% S Parameters of Measured LNA
s11 = 0.1;
s21 = 10;
s12 = 0;
s22 = 0;
%gain = abs(s21)^2; % Amplifier gain

% Noise Parameters of LNA
Tmin = 15;
N = 0.024;

%% generate uncorrelated random samples for LNAs
for ant = 1:Nel
    w1(:,ant) = (randn(nSmp,1)+j*randn(nSmp,1))/sqrt(2);
    w2(:,ant) = (randn(nSmp,1)+j*randn(nSmp,1))/sqrt(2);
end;

% generate correlated antenna noise
Cant = kb*T0*(I - SA*SA');
%mixingWeightsAnt = chol(Cant);
for ant = 1:Nel
    w_ant(:,ant) = fft((randn(nSmp,1)+j*randn(nSmp,1))/sqrt(2));
end;

```

```

%w_v_ant = w_ant * conj(mixingWeightsAnt);
%for ant = 1:Nel
% c_ant(ant,1,:) = fft(w_v_ant(:,ant));
%end;

% start with 1Hz gamma act
% gammaAct calculator

SR = I*s11;
% for ant = 1:Nel
% G = sqrt(Z0)*(I+I*s11)/(I - SA*s11);
% wf = G'*weight;
% gamma_sum = 0;
% for ant2 = 1:Nel
% gamma_sum = gamma_sum + wf(ant2)'*SA(ant2,ant);
% end;
% gammaAct(ant) = gamma_sum/wf(ant)';
% end;
% gammaAct calculator
for ant = 1:Nel
    S11arr = I*s11;
    S11arr(ant,ant) = 0;
    gammaSvec = (I-SA*S11arr)^-1*SA(:,ant);
    gammaS = gammaSvec(ant);
    selVec = [0 0]';
    selVec(ant) = 1;

```

```

    b = SA*(I-SA*s11)^-1*s1Vec;
    km = conj(b')*(weight)/(b(ant)*(weight(ant))) - 1;
    zetam = (1+km)/(1+gammaS*km*s11);
    gammActArr(ant) = zetam*gammaS;
end;

gammaActSim_init = gammActArr;
%algorithm:
gammaActSim = gammaActSim_init
[-0.2183 - 0.1186i -0.2073 + 0.0186i];

counter = 0;
n_b = 400;
for b = 1:1:n_b
    tic
    b
    Ts = 200e-9/b;
    BW(b) = (1/(Ts))/2;
    W = BW(b);
    BW(b)
    freq_space = fftshift(linspace(-BW(b),BW(b),nSmp));

    counter = counter + 1

    minTsim = inf;

```

```

r_1 = linspace(-1, 1, gammOpt_r_len)*window+real(gammaActSim(1));
theta_1 = linspace(-1, 1, theta_len)*window+imag(gammaActSim(1));
r_2 = linspace(-1, 1, gammOpt_r_len)*window+real(gammaActSim(2));
theta_2 = linspace(-1, 1, theta_len)*window+imag(gammaActSim(2));
for i_Gopt1 = 1:gammOpt_r_len
    for j_Gopt1 = 1:theta_len
        for i_Gopt2 = 1:gammOpt_r_len
            for j_Gopt2 = 1:theta_len
                %gamma_opt_var(i_Gopt,j_Gopt) = r_(i_Gopt)*exp(1j*
                    ↪ theta_(j_Gopt));
                gamma_opt_var1(i_Gopt1,j_Gopt1) = r_1(i_Gopt1)+1j*
                    ↪ theta_1(j_Gopt1);
                gamma_opt_var2(i_Gopt2,j_Gopt2) = r_2(i_Gopt2)+1j*
                    ↪ theta_2(j_Gopt2);
            end;
        end;
    end;
end;

for i_Gopt1 = 1:gammOpt_r_len
    %i_Gopt1
    for j_Gopt1 = 1:theta_len
        for i_Gopt2 = 1:gammOpt_r_len
            for j_Gopt2 = 1:theta_len

                gamma_arr = [gamma_opt_var1(i_Gopt1, j_Gopt1)
                    ↪ gamma_opt_var2(i_Gopt2, j_Gopt2)];
            end;
        end;
    end;
end;

```

```

Rn_arr = [N/real(1/s2z(gamma_arr(1))) N/real(1/s2z(
    ↪ gamma_arr(2)))]];

for ant = 1:Nel
    GammaOpt = gamma_arr(ant);
    Rn = Rn_arr(ant);
    % Noise wave power and correlation coefficient
    c1Psd(ant) = (kb*Tmin*(abs(s11)^2-1)+(4*kb*T0*Rn
    ↪ /Z0)*abs(1-s11*GammaOpt)^2/abs(1+GammaOpt)
    ↪ ^2); % Power spectral density of input
    ↪ noise (W/Hz)
    c2Psd(ant) = (abs(s21)^2*(kb*Tmin+(4*kb*T0*Rn/Z0
    ↪ )*abs(GammaOpt)^2/abs(1+GammaOpt)^2)); %
    ↪ Power spectral density of output noise (W/
    ↪ Hz)
    rho(ant) = (-conj(s21)*conj(GammaOpt)*(4*kb*T0*
    ↪ Rn/Z0)/abs(1+GammaOpt)^2+(s11/s21)*c2Psd(
    ↪ ant))/sqrt(c1Psd(ant)*c2Psd(ant)); % Cross
    ↪ correlation of the input and output noise
    ↪ .

    mixingWeights = chol(...
    [ c1Psd(ant) (rho(ant))*sqrt(c1Psd(ant)*c2Psd(
    ↪ ant)); ...
    conj(rho(ant))*sqrt(c1Psd(ant)*c2Psd(ant)) c2Psd
    ↪ (ant) ]);

```

```

        w_v = [ w1(:,ant) w2(:,ant) ] * conj(
            ↪ mixingWeights);
        c1(ant,1,:) = fft(w_v(:,1));
        c2(ant,1,:) = fft(w_v(:,2));
    end;
% G = inv(I - SR*SA);
% auto_forward = (G*(SA*diag(c1Psd)*SA')*G')*abs(s21)^2;
% forward_reverse = (G*SA*s21)*diag(rho).*(diag(c2Psd).*diag(c1Psd))
    ↪ .^0.5;
% auto_reverse = diag(c2Psd)*I;
% auto_ant = ko*G*(I-SA*SA')*G'*abs(s21)^2;
%
% Trec = (w'*(auto_forward + 2*real(forward_reverse) + auto_reverse)*w
    ↪ )/(w'*auto_ant*w);

% s_pi_ = SA*(exp(-j*2*pi*freq_space*(tau_t + 2*I*tau
    ↪ )));
for s = 1:nSmp
    SA_f(:,:,s) = (SA.*(exp(-j*2*pi*(freq_space(s))
        ↪ *(tau_t + tau))));
    Cant = kb*T0*(I - SA_f(:,:,s)*SA_f(:,:,s)');
    mixingWeightsAnt = chol(Cant);
    c_ant(:,1,s) = w_ant(s,:) * conj(
        ↪ mixingWeightsAnt);

```

```

end;

a = zeros(size(c1));
reflection = c1;
reflection_ant = (c_ant);
b_ant = reflection_ant*s21;

for r = 1:numReflections
    %for s = 1:nSmp
        %s_pi_ = SA.*(exp(-j*2*pi*(freq_space(s))*(
            ↪ tau_t + 2*I*tau)));
        %reflection(s,:) = (s_pi_*(reflection(s,:))
            ↪ .')'*s11;
        %reflection_ant(s,:) = (s_pi_*(reflection_ant
            ↪ (s,:))')'*s11;
    %end;

    reflection = pagentimes(SA_f*s11, reflection);
    reflection_ant = pagentimes(SA_f*s11,
        ↪ reflection_ant);
    a = a + reflection;
    b_ant = b_ant + reflection_ant*s21;
end;

a = a*s21/s11;
x = pagentimes(w.', a + c2);
x_ant = pagentimes(w.', b_ant);

```

```

        x = reshape(x,nSmp,1);
        x_ant = reshape(x_ant,nSmp,1);
        ac_y = (x'*x);
        ac_y_ant = (x_ant'*x_ant);
        pwrSim = (ac_y);
        pwrSim_ant = (ac_y_ant);

        TSim = T0*pwrSim/pwrSim_ant;

        if(minTsim > TSim)
            gamma_arr;
            TSim;
            gamma_opt_d(counter,:) = gamma_arr;
            minTsim = TSim;
        end;

    end;

end;

end;

end;

minTsim
% figure(5);
% hold on;
% surf(theta_*180/pi, r_, TSim);
% xlabel('theta');
% ylabel('r')

```

```

    %filename = sprintf('%s/%d.fig', dirname, tau*t_sweep);
    %savefig(filename)
    %close;

    gammaActSim = gamma_opt_d(counter,:);

    toc
end;

gamma_opt_d

clf;
figure(1);
smithplot(gamma_opt_d(:,1));
hold on;
smithplot(gamma_opt_d(:,2));
legend('GammaAct 1', 'GammaAct 2');
saveas(gcf, '../..//Figures/multi_gamma_sim_BW_sweep_5_1000.png');

figure(2)
plot(BW/1e6,abs(gamma_opt_d(:,1)))
hold on
plot(BW/1e6,abs(gamma_opt_d(:,2)))
%title('|\\Gamma_a_c_t| vs bandwidth with \\lambda/2 transmission line')
legend('|\\Gamma_a_c_t 1|', '|\\Gamma_a_c_t 2|')
xlabel('Bandwidth (MHz)')
ylabel('|\\Gamma_a_c_t|')

```

```

saveas(gcf, '..\..\Figures\milti_gamma_sim_abs_gamma_BW_sweep_5_1000.
    ↪ png');

fprintf(FID, 'sim start\n');
fprintf(FID, 'Dual Antenna weights [1 %g]\n', weight(2));
fprintf(FID, 'center frequency, %g num samples %d, Sampling period %g,
    ↪ bandwidth %g\n',fc, nSmp, BW);
fprintf(FID, 'LNA s11 %+g%+gi, s12 %+g%+gi, s21 %+g%+gi, s22 %+g%+gi\n
    ↪ ',real(s11), imag(s11), real(s12), imag(s12), real(s21), imag(
    ↪ s21), real(s22), imag(s22));
fprintf(FID, 'LNA Tmin %g, Rn %g, Z0 %g, T0 %g, GammaOpt %+g%+gi, BW %
    ↪ g\n', Tmin, Rn, Z0, T0, real(GammaOpt), imag(GammaOpt), BW);
fprintf(FID, 'LNA c2PSD %+g%+gi, c2PSD %+g%+gi, rho %+g%+gi\n',real(
    ↪ c1Psd), imag(c1Psd), real(c2Psd), imag(c2Psd), real(rho), imag(
    ↪ rho));
fprintf(FID, 'tau line delay : %g, tau inter element delay : not
    ↪ applied\n', tau);
fprintf(FID, 'num reflections %d\n', numReflections);
fprintf(FID, 'Sim time : %f hours\n\nStart of smith plot output\n',
    ↪ toc/3600);
fclose(FID);

outputM = [linspace(0,1,t_sweep_len)*tau gamma_opt_d(:,1) gamma_opt_d
    ↪ (:,2)];
dlmwrite(filename, outputM,'-append');

```

Appendix C

Optimal Γ_{act} derivation

Starting with Equation 4.55

$$T_{rec} = \frac{\int_{f_L}^{f_H} \mathbf{w}^H \mathbf{G} \left(\mathbf{T}_\alpha + \mathbf{S}_A \mathbf{T}_\beta \mathbf{S}_A^H - \mathbf{S}_A \mathbf{T}_\gamma - \mathbf{S}_A^H \mathbf{T}_\gamma^H \right) \mathbf{G}^H \mathbf{w} \cdot df}{\int_{f_L}^{f_H} \mathbf{w}^H \mathbf{G} \left(\mathbf{I} - \mathbf{S}_A \mathbf{S}_A^H \right) \mathbf{G}^H \mathbf{w} df}, \quad (\text{C.1})$$

and substituting Equations 4.49, 4.50, and 4.51

$$T_\alpha = \frac{N}{R_0 G_{opt}} T_0 + T_{min} - T_0 \frac{N}{G_{opt}} Y_{opt} - T_0 \frac{N}{G_{opt}} Y_{opt}^* + T_0 \frac{N}{G_{opt}} |Y_{opt}|^2 R_0 \quad (\text{C.2})$$

$$T_\beta = T_0 \frac{N}{G_{opt} R_0} - T_{min} + T_0 \frac{N}{G_{opt}} Y_{opt} + T_0 \frac{N}{G_{opt}} Y_{opt}^* + T_0 \frac{N}{G_{opt}} |Y_{opt}|^2 R_0 \quad (\text{C.3})$$

$$T_\gamma = T_0 \frac{N}{G_{opt} R_0} - T_0 \frac{N}{G_{opt}} Y_{opt} + T_0 \frac{N}{G_{opt}} Y_{opt}^* - T_0 \frac{N}{G_{opt}} |Y_{opt}|^2 R_0, \quad (\text{C.4})$$

into $\mathbf{T}_\alpha = T_\alpha \mathbf{I}$, $\mathbf{T}_\beta = T_\beta \mathbf{I}$, and $\mathbf{T}_\gamma = T_\gamma \mathbf{I}$, yields

$$\begin{aligned} \frac{dT_{rec}}{dB_{opt}} = & d \left[\frac{\int_{f_L}^{f_H} \mathbf{w}^H \mathbf{G} \left(\mathbf{T}_\alpha \right) \mathbf{G}^H \mathbf{w} df}{\int_{f_L}^{f_H} \mathbf{w}^H \mathbf{G} \left(\mathbf{I} - \mathbf{S}_A \mathbf{S}_A^H \right) \mathbf{G}^H \mathbf{w} df} \right] / dB_{opt} \\ & + d \left[\frac{\int_{f_L}^{f_H} \mathbf{w}^H \mathbf{G} \left(\mathbf{S}_A \mathbf{T}_\beta \mathbf{S}_A^H \right) \mathbf{G}^H \mathbf{w} df}{\int_{f_L}^{f_H} \mathbf{w}^H \mathbf{G} \left(\mathbf{I} - \mathbf{S}_A \mathbf{S}_A^H \right) \mathbf{G}^H \mathbf{w} df} \right] / dB_{opt} \\ & + d \left[\frac{\int_{f_L}^{f_H} \mathbf{w}^H \mathbf{G} \left(\mathbf{S}_A \mathbf{T}_\gamma + \mathbf{S}_A^H \mathbf{T}_\gamma^H \right) \mathbf{G}^H \mathbf{w} df}{\int_{f_L}^{f_H} \mathbf{w}^H \mathbf{G} \left(\mathbf{I} - \mathbf{S}_A \mathbf{S}_A^H \right) \mathbf{G}^H \mathbf{w} df} \right] / dB_{opt}. \end{aligned} \quad (\text{C.5})$$

Next expanding the above equation gives

$$\frac{dT_{rec}}{dB_{opt}} = d \left[\frac{N}{R_0 G_{opt}} T_0 + T_{min} - T_0 \frac{N}{G_{opt}} Y_{opt} - T_0 \frac{N}{G_{opt}} Y_{opt}^* + T_0 \frac{N}{G_{opt}} |Y_{opt}|^2 R_0 \right] / dB_{opt} \quad (C.6)$$

$$\begin{aligned} & \frac{\int_{f_L}^{f_H} \mathbf{w}^H \mathbf{G} \mathbf{I} \mathbf{G}^H \mathbf{w} df}{\int_{f_L}^{f_H} \mathbf{w}^H \mathbf{G} (\mathbf{I} - \mathbf{S}_A \mathbf{S}_A^H) \mathbf{G}^H \mathbf{w} df} \\ & + d \left[T_0 \frac{N}{G_{opt} R_0} - T_{min} + T_0 \frac{N}{G_{opt}} Y_{opt} + T_0 \frac{N}{G_{opt}} Y_{opt}^* + T_0 \frac{N}{G_{opt}} |Y_{opt}|^2 R_0 \right] / dB_{opt} \\ & \frac{\int_{f_L}^{f_H} \mathbf{w}^H \mathbf{G} (\mathbf{S}_A \mathbf{I} \mathbf{S}_A^H) \mathbf{G}^H \mathbf{w} df}{\int_{f_L}^{f_H} \mathbf{w}^H \mathbf{G} (\mathbf{I} - \mathbf{S}_A \mathbf{S}_A^H) \mathbf{G}^H \mathbf{w} df} \\ & - d \left[T_0 \frac{N}{G_{opt} R_0} - T_0 \frac{N}{G_{opt}} Y_{opt}^* + T_0 \frac{N}{G_{opt}} Y_{opt} - T_0 \frac{N}{G_{opt}} |Y_{opt}|^2 R_0 \right] / dB_{opt} \\ & \frac{\int_{f_L}^{f_H} \mathbf{w}^H \mathbf{G} (\mathbf{S}_A \mathbf{I}) \mathbf{G}^H \mathbf{w} df}{\int_{f_L}^{f_H} \mathbf{w}^H \mathbf{G} (\mathbf{I} - \mathbf{S}_A \mathbf{S}_A^H) \mathbf{G}^H \mathbf{w} df} \\ & - d \left[T_0 \frac{N}{G_{opt} R_0} - T_0 \frac{N}{G_{opt}} Y_{opt} + T_0 \frac{N}{G_{opt}} Y_{opt}^* - T_0 \frac{N}{G_{opt}} |Y_{opt}|^2 R_0 \right] / dB_{opt} \\ & \frac{\int_{f_L}^{f_H} \mathbf{w}^H \mathbf{G} (\mathbf{S}_A^H \mathbf{I}) \mathbf{G}^H \mathbf{w} df}{\int_{f_L}^{f_H} \mathbf{w}^H \mathbf{G} (\mathbf{I} - \mathbf{S}_A \mathbf{S}_A^H) \mathbf{G}^H \mathbf{w} df}. \end{aligned}$$

Next, find $\frac{\partial(T_{rec})}{\partial B_{opt}} = 0$ to find B_{opt} for minimum noise

$$\begin{aligned}
\frac{dT_{rec}}{dB_{opt}} = & \left[-jT_0 \frac{N}{G_{opt}} + jT_0 \frac{N}{G_{opt}} + T_0 \frac{N}{G_{opt}} (2B_{opt}) R_0 \right] \\
& \frac{\int_{f_L}^{f_H} \mathbf{w}^H \mathbf{G} \mathbf{I} \mathbf{G}^H \mathbf{w} df}{\int_{f_L}^{f_H} \mathbf{w}^H \mathbf{G} (\mathbf{I} - \mathbf{S}_A \mathbf{S}_A^H) \mathbf{G}^H \mathbf{w} df} \\
& + \left[jT_0 \frac{N}{G_{opt}} - jT_0 \frac{N}{G_{opt}} + T_0 \frac{N}{G_{opt}} (2B_{opt}) R_0 \right] \\
& \frac{\int_{f_L}^{f_H} \mathbf{w}^H \mathbf{G} (\mathbf{S}_A \mathbf{I} \mathbf{S}_A^H) \mathbf{G}^H \mathbf{w} df}{\int_{f_L}^{f_H} \mathbf{w}^H \mathbf{G} (\mathbf{I} - \mathbf{S}_A \mathbf{S}_A^H) \mathbf{G}^H \mathbf{w} df} \\
& - \left[jT_0 \frac{N}{G_{opt}} + jT_0 \frac{N}{G_{opt}} - T_0 \frac{N}{G_{opt}} (2B_{opt}) R_0 \right] \\
& \frac{\int_{f_L}^{f_H} \mathbf{w}^H \mathbf{G} (\mathbf{S}_A \mathbf{I}) \mathbf{G}^H \mathbf{w} df}{\int_{f_L}^{f_H} \mathbf{w}^H \mathbf{G} (\mathbf{I} - \mathbf{S}_A \mathbf{S}_A^H) \mathbf{G}^H \mathbf{w} df} \\
& - \left[-jT_0 \frac{N}{G_{opt}} - jT_0 \frac{N}{G_{opt}} - T_0 \frac{N}{G_{opt}} (2B_{opt}) R_0 \right] \\
& \frac{\int_{f_L}^{f_H} \mathbf{w}^H \mathbf{G} (\mathbf{S}_A^H \mathbf{I}) \mathbf{G}^H \mathbf{w} df}{\int_{f_L}^{f_H} \mathbf{w}^H \mathbf{G} (\mathbf{I} - \mathbf{S}_A \mathbf{S}_A^H) \mathbf{G}^H \mathbf{w} df} = 0.
\end{aligned} \tag{C.7}$$

The following steps simplify the above equation.

$$\begin{aligned}
& T_0 \frac{N}{G_{opt}} (2B_{opt}) R_0 \int_{f_L}^{f_H} \mathbf{w}^H \mathbf{G} \mathbf{I} \mathbf{G}^H \mathbf{w} df \\
& + T_0 \frac{N}{G_{opt}} (2B_{opt}) R_0 \int_{f_L}^{f_H} \mathbf{w}^H \mathbf{G} (\mathbf{S}_A \mathbf{I} \mathbf{S}_A^H) \mathbf{G}^H \mathbf{w} df \\
& - \left[2jT_0 \frac{N}{G_{opt}} - T_0 \frac{N}{G_{opt}} (2B_{opt}) R_0 \right] \int_{f_L}^{f_H} \mathbf{w}^H \mathbf{G} (\mathbf{S}_A \mathbf{I}) \mathbf{G}^H \mathbf{w} df \\
& - \left[-2jT_0 \frac{N}{G_{opt}} - T_0 \frac{N}{G_{opt}} (2B_{opt}) R_0 \right] \int_{f_L}^{f_H} \mathbf{w}^H \mathbf{G} (\mathbf{S}_A^H \mathbf{I}) \mathbf{G}^H \mathbf{w} df = 0
\end{aligned} \tag{C.8}$$

$$\begin{aligned}
& B_{opt}R_0 \sum_{f=f_0}^{f_n} \mathbf{w}^H \mathbf{G} \mathbf{I} \mathbf{G}^H \mathbf{w} + B_{opt}R_0 \int_{f_L}^{f_H} \mathbf{w}^H \mathbf{G} (\mathbf{S}_A \mathbf{I} \mathbf{S}_A^H) \mathbf{G}^H \mathbf{w} df \\
& - j \int_{f_L}^{f_H} \mathbf{w}^H \mathbf{G} (\mathbf{S}_A \mathbf{I}) \mathbf{G}^H \mathbf{w} df + B_{opt}R_0 \int_{f_L}^{f_H} \mathbf{w}^H \mathbf{G} (\mathbf{S}_A \mathbf{I}) \mathbf{G}^H \mathbf{w} df \\
& + j \int_{f_L}^{f_H} \mathbf{w}^H \mathbf{G} (\mathbf{S}_A^H \mathbf{I}) \mathbf{G}^H \mathbf{w} df + B_{opt}R_0 \int_{f_L}^{f_H} \mathbf{w}^H \mathbf{G} (\mathbf{S}_A^H \mathbf{I}) \mathbf{G}^H \mathbf{w} df = 0 \quad (\text{C.9})
\end{aligned}$$

$$\begin{aligned}
& B_{opt}R_0 \int_{f_L}^{f_H} \mathbf{w}^H \mathbf{G} \mathbf{I} \mathbf{G}^H \mathbf{w} df + B_{opt}R_0 \int_{f_L}^{f_H} \mathbf{w}^H \mathbf{G} (\mathbf{S}_A \mathbf{I} \mathbf{S}_A^H) \mathbf{G}^H \mathbf{w} df \\
& + B_{opt}R_0 \int_{f_L}^{f_H} \mathbf{w}^H \mathbf{G} (\mathbf{S}_A \mathbf{I}) \mathbf{G}^H \mathbf{w} df + B_{opt}R_0 \int_{f_L}^{f_H} \mathbf{w}^H \mathbf{G} (\mathbf{S}_A^H \mathbf{I}) \mathbf{G}^H \mathbf{w} df \quad (\text{C.10}) \\
& = j \int_{f_L}^{f_H} \mathbf{w}^H \mathbf{G} (\mathbf{S}_A \mathbf{I}) \mathbf{G}^H \mathbf{w} df - j \int_{f_L}^{f_H} \mathbf{w}^H \mathbf{G} (\mathbf{S}_A^H \mathbf{I}) \mathbf{G}^H \mathbf{w} df
\end{aligned}$$

$$\begin{aligned}
& B_{opt}R_0 \int_{f_L}^{f_H} \mathbf{w}^H \mathbf{G} \mathbf{I} \mathbf{G}^H \mathbf{w} df + B_{opt}R_0 \int_{f_L}^{f_H} \mathbf{w}^H \mathbf{G} (\mathbf{S}_A \mathbf{I} \mathbf{S}_A^H) \mathbf{G}^H \mathbf{w} df \\
& + B_{opt}R_0 \int_{f_L}^{f_H} \mathbf{w}^H \mathbf{G} (\mathbf{S}_A \mathbf{I}) \mathbf{G}^H \mathbf{w} df + B_{opt}R_0 \int_{f_L}^{f_H} \mathbf{w}^H \mathbf{G} (\mathbf{S}_A^H \mathbf{I}) \mathbf{G}^H \mathbf{w} df \quad (\text{C.11}) \\
& = j \int_{f_L}^{f_H} \mathbf{w}^H \mathbf{G} (\mathbf{S}_A - \mathbf{S}_A^H) \mathbf{G}^H \mathbf{w} df
\end{aligned}$$

$$\begin{aligned}
& B_{opt}R_0 \int_{f_L}^{f_H} \mathbf{w}^H \mathbf{G} \mathbf{I} \mathbf{G}^H \mathbf{w} df + B_{opt}R_0 \int_{f_L}^{f_H} \mathbf{w}^H \mathbf{G} (\mathbf{S}_A \mathbf{I} \mathbf{S}_A^H) \mathbf{G}^H \mathbf{w} df \\
& + B_{opt}R_0 \int_{f_L}^{f_H} \mathbf{w}^H \mathbf{G} (\mathbf{S}_A \mathbf{I}) \mathbf{G}^H \mathbf{w} df + B_{opt}R_0 \int_{f_L}^{f_H} \mathbf{w}^H \mathbf{G} (\mathbf{S}_A^H \mathbf{I}) \mathbf{G}^H \mathbf{w} df \quad (\text{C.12}) \\
& = j \int_{f_L}^{f_H} \mathbf{w}^H \mathbf{G} (\mathbf{S}_A - \mathbf{S}_A^H) \mathbf{G}^H \mathbf{w} df
\end{aligned}$$

$$\begin{aligned}
& B_{opt} R_0 \int_{f_L}^{f_H} \mathbf{w}^H \mathbf{G} \mathbf{I} \mathbf{G}^H \mathbf{w} df + B_{opt} R_0 \int_{f_L}^{f_H} \mathbf{w}^H \mathbf{G} (\mathbf{S}_A \mathbf{S}_A^H) \mathbf{G}^H \mathbf{w} df \\
& + B_{opt} R_0 \int_{f_L}^{f_H} \mathbf{w}^H \mathbf{G} (\mathbf{S}_A) \mathbf{G}^H \mathbf{w} df + B_{opt} R_0 \int_{f_L}^{f_H} \mathbf{w}^H \mathbf{G} (\mathbf{S}_A^H) \mathbf{G}^H \mathbf{w} df \\
& = j \int_{f_L}^{f_H} \mathbf{w}^H \mathbf{G} (\mathbf{S}_A - \mathbf{S}_A^H) \mathbf{G}^H \mathbf{w} df
\end{aligned} \tag{C.13}$$

Collecting the B_{opt} terms yields

$$B_{opt} R_0 \int_{f_L}^{f_H} \mathbf{w}^H \mathbf{G} [\mathbf{I} + \mathbf{S}_A \mathbf{S}_A^H + \mathbf{S}_A + \mathbf{S}_A^H] \mathbf{G}^H \mathbf{w} df = j \int_{f_L}^{f_H} \mathbf{w}^H \mathbf{G} (\mathbf{S}_A - \mathbf{S}_A^H) \mathbf{G}^H \mathbf{w} df. \tag{C.14}$$

Finally, solving for $B_{act} = B_{opt}$ gives Equation 4.62

$$B_{opt} = \frac{j \int_{f_L}^{f_H} \mathbf{w}^H \mathbf{G} (\mathbf{S}_A - \mathbf{S}_A^H) \mathbf{G}^H \mathbf{w} df}{R_0 \int_{f_L}^{f_H} \mathbf{w}^H \mathbf{G} [\mathbf{I} + \mathbf{S}_A \mathbf{S}_A^H + \mathbf{S}_A + \mathbf{S}_A^H] \mathbf{G}^H \mathbf{w} df} \tag{C.15}$$

$$\boxed{B_{act} = \frac{-2 \mathbf{w}^H \int_{f_L}^{f_H} \mathbf{G} (\Im \mathbf{S}_A) \mathbf{G}^H df \mathbf{w}}{R_0 \mathbf{w}^H \int_{f_L}^{f_H} \mathbf{G} [\mathbf{I} + \mathbf{S}_A \mathbf{S}_A^H + \mathbf{S}_A + \mathbf{S}_A^H] \mathbf{G}^H df \mathbf{w}}} \tag{C.16}$$

For G_{act} , find $\frac{\partial(T_{rec})}{\partial G_{opt}}$ much like B_{act} , but substitute B_{opt} with B_{act} from Equation 4.62.

$$\begin{aligned}
\frac{dT_{rec}}{dG_{opt}} &= d \left[\left[\frac{N}{R_0 G_{opt}} T_0 + T_{min} - T_0 \frac{N}{G_{opt}} Y_{opt} - T_0 \frac{N}{G_{opt}} Y_{opt}^* + T_0 \frac{N}{G_{opt}} |Y_{opt}|^2 R_0 \right] \right] / dG_{opt} \\
&\quad \frac{\int_{f_L}^{f_H} \mathbf{w}^H \mathbf{G} \mathbf{I} \mathbf{G}^H \mathbf{w} df}{\int_{f_L}^{f_H} \mathbf{w}^H \mathbf{G} (\mathbf{I} - \mathbf{S}_A \mathbf{S}_A^H) \mathbf{G}^H \mathbf{w} df} \\
&+ d \left[\left[T_0 \frac{N}{G_{opt} R_0} - T_{min} + T_0 \frac{N}{G_{opt}} Y_{opt} + T_0 \frac{N}{G_{opt}} Y_{opt}^* + T_0 \frac{N}{G_{opt}} |Y_{opt}|^2 R_0 \right] \right] / dG_{opt}
\end{aligned} \tag{C.17}$$

$$\begin{aligned}
&\quad \frac{\int_{f_L}^{f_H} \mathbf{w}^H \mathbf{G} (\mathbf{S}_A \mathbf{I} \mathbf{S}_A^H) \mathbf{G}^H \mathbf{w} df}{\int_{f_L}^{f_H} \mathbf{w}^H \mathbf{G} (\mathbf{I} - \mathbf{S}_A \mathbf{S}_A^H) \mathbf{G}^H \mathbf{w} df} \\
&- d \left[\left[T_0 \frac{N}{G_{opt} R_0} - T_0 \frac{N}{G_{opt}} Y_{opt}^* + T_0 \frac{N}{G_{opt}} Y_{opt} - T_0 \frac{N}{G_{opt}} |Y_{opt}|^2 R_0 \right] \right] / dG_{opt} \\
&\quad \frac{\int_{f_L}^{f_H} \mathbf{w}^H \mathbf{G} (\mathbf{S}_A \mathbf{I}) \mathbf{G}^H \mathbf{w} df}{\int_{f_L}^{f_H} \mathbf{w}^H \mathbf{G} (\mathbf{I} - \mathbf{S}_A \mathbf{S}_A^H) \mathbf{G}^H \mathbf{w} df} \\
&- d \left[\left[T_0 \frac{N}{G_{opt} R_0} - T_0 \frac{N}{G_{opt}} Y_{opt} + T_0 \frac{N}{G_{opt}} Y_{opt}^* - T_0 \frac{N}{G_{opt}} |Y_{opt}|^2 R_0 \right] \right] / dG_{opt} \\
&\quad \frac{\int_{f_L}^{f_H} \mathbf{w}^H \mathbf{G} (\mathbf{S}_A^H \mathbf{I}) \mathbf{G}^H \mathbf{w} df}{\int_{f_L}^{f_H} \mathbf{w}^H \mathbf{G} (\mathbf{I} - \mathbf{S}_A \mathbf{S}_A^H) \mathbf{G}^H \mathbf{w} df}
\end{aligned}$$

$$\begin{aligned}
& \frac{dT_{rec}}{dG_{opt}} \\
= & \left[-\frac{N}{R_0 G_{opt}^2} T_0 + T_0 N \frac{Y_{opt} - G_{opt}}{G_{opt}^2} + T_0 N \frac{Y_{opt}^* - G_{opt}}{G_{opt}^2} + T_0 N R_0 \frac{2G_{opt}^2 - (G_{opt}^2 + B_{opt}^2)}{G_{opt}^2} \right] \\
& \frac{\int_{f_L}^{f_H} \mathbf{w}^H \mathbf{G} \mathbf{I} \mathbf{G}^H \mathbf{w} df}{\int_{f_L}^{f_H} \mathbf{w}^H \mathbf{G} (\mathbf{I} - \mathbf{S}_A \mathbf{S}_A^H) \mathbf{G}^H \mathbf{w} df} \\
+ & \left[-\frac{N}{R_0 G_{opt}^2} T_0 - T_0 N \frac{Y_{opt} - G_{opt}}{G_{opt}^2} - T_0 N \frac{Y_{opt}^* - G_{opt}}{G_{opt}^2} + T_0 N R_0 \frac{2G_{opt}^2 - (G_{opt}^2 + B_{opt}^2)}{G_{opt}^2} \right] \\
& \frac{\int_{f_L}^{f_H} \mathbf{w}^H \mathbf{G} (\mathbf{S}_A \mathbf{I} \mathbf{S}_A^H) \mathbf{G}^H \mathbf{w} df}{\int_{f_L}^{f_H} \mathbf{w}^H \mathbf{G} (\mathbf{I} - \mathbf{S}_A \mathbf{S}_A^H) \mathbf{G}^H \mathbf{w} df} \\
& \tag{C.18} \\
- & \left[-\frac{N}{R_0 G_{opt}^2} T_0 + T_0 N \frac{Y_{opt}^* - G_{opt}}{G_{opt}^2} - T_0 N \frac{Y_{opt} - G_{opt}}{G_{opt}^2} - T_0 N R_0 \frac{2G_{opt}^2 - (G_{opt}^2 + B_{opt}^2)}{G_{opt}^2} \right] \\
& \frac{\int_{f_L}^{f_H} \mathbf{w}^H \mathbf{G} (\mathbf{S}_A \mathbf{I}) \mathbf{G}^H \mathbf{w} df}{\int_{f_L}^{f_H} \mathbf{w}^H \mathbf{G} (\mathbf{I} - \mathbf{S}_A \mathbf{S}_A^H) \mathbf{G}^H \mathbf{w} df} \\
- & \left[-\frac{N}{R_0 G_{opt}^2} T_0 + T_0 N \frac{Y_{opt} - G_{opt}}{G_{opt}^2} - T_0 N \frac{Y_{opt}^* - G_{opt}}{G_{opt}^2} - T_0 N R_0 \frac{2G_{opt}^2 - (G_{opt}^2 + B_{opt}^2)}{G_{opt}^2} \right] \\
& \frac{\int_{f_L}^{f_H} \mathbf{w}^H \mathbf{G} (\mathbf{S}_A^H \mathbf{I}) \mathbf{G}^H \mathbf{w} df}{\int_{f_L}^{f_H} \mathbf{w}^H \mathbf{G} (\mathbf{I} - \mathbf{S}_A \mathbf{S}_A^H) \mathbf{G}^H \mathbf{w} df}
\end{aligned}$$

Set $\frac{\partial(T_{rec})}{\partial G_{opt}}$ to 0, which cancels out the denominator terms,

$$\begin{aligned}
& [-1 + R_0 Y_{opt} - R_0 G_{opt} + R_0 Y_{opt}^* - R_0 G_{opt} + 2R_0^2 G_{opt}^2 - R_0^2 (G_{opt}^2 + B_{opt}^2)] \int_{f_L}^{f_H} \mathbf{w}^H \mathbf{G} \mathbf{G}^H \mathbf{w} df \\
& + [-1 - R_0 Y_{opt} + R_0 G_{opt} - R_0 Y_{opt}^* + R_0 G_{opt} + 2R_0^2 G_{opt}^2 - R_0^2 (G_{opt}^2 + B_{opt}^2)] \int_{f_L}^{f_H} \mathbf{w}^H \mathbf{G} \mathbf{S}_A \mathbf{S}_A^H \mathbf{G}^H \mathbf{w} df \\
& \hspace{15em} (C.19) \\
& - [-1 + R_0 Y_{opt}^* - R_0 G_{opt} - R_0 Y_{opt} + R_0 G_{opt} - 2R_0^2 G_{opt}^2 + R_0^2 (G_{opt}^2 + B_{opt}^2)] \int_{f_L}^{f_H} \mathbf{w}^H \mathbf{G} \mathbf{S}_A \mathbf{G}^H \mathbf{w} df \\
& - [-1 + R_0 Y_{opt} - R_0 G_{opt} - R_0 Y_{opt}^* + R_0 G_{opt} - 2R_0^2 G_{opt}^2 + R_0^2 (G_{opt}^2 + B_{opt}^2)] \int_{f_L}^{f_H} \mathbf{w}^H \mathbf{G} \mathbf{S}_A^H \mathbf{G}^H \mathbf{w} df = 0.
\end{aligned}$$

Collect the G_{opt} terms and simplify in the next few steps.

$$\begin{aligned}
& [-1 + R_0^2 G_{opt}^2 - R_0^2 B_{opt}^2] \int_{f_L}^{f_H} \mathbf{w}^H \mathbf{G} \mathbf{G}^H \mathbf{w} df \\
& + [-1 + R_0^2 G_{opt}^2 - R_0^2 B_{opt}^2] \int_{f_L}^{f_H} \mathbf{w}^H \mathbf{G} \mathbf{S}_A \mathbf{S}_A^H \mathbf{G}^H \mathbf{w} df \\
& - [-1 - j2R_0 B_{opt} - R_0^2 G_{opt}^2 + R_0^2 B_{opt}^2] \int_{f_L}^{f_H} \mathbf{w}^H \mathbf{G} \mathbf{S}_A \mathbf{G}^H \mathbf{w} df \hspace{5em} (C.20) \\
& - [-1 + 2jR_0 B_{opt} - R_0^2 G_{opt}^2 + R_0^2 B_{opt}^2] \int_{f_L}^{f_H} \mathbf{w}^H \mathbf{G} \mathbf{S}_A^H \mathbf{G}^H \mathbf{w} df = 0
\end{aligned}$$

$$\begin{aligned}
& R_0^2 G_{opt}^2 \int_{f_L}^{f_H} \mathbf{w}^H \mathbf{G} \mathbf{G}^H \mathbf{w} df + R_0^2 G_{opt}^2 \int_{f_L}^{f_H} \mathbf{w}^H \mathbf{G} \mathbf{S}_A \mathbf{S}_A^H \mathbf{G}^H \mathbf{w} df \\
& - [-R_0^2 G_{opt}^2] \int_{f_L}^{f_H} \mathbf{w}^H \mathbf{G} \mathbf{S}_A \mathbf{G}^H \mathbf{w} - [-R_0^2 G_{opt}^2] \int_{f_L}^{f_H} \mathbf{w}^H \mathbf{G} \mathbf{S}_A^H \mathbf{G}^H \mathbf{w} df \\
& + [-1 - R_0^2 B_{opt}^2] \int_{f_L}^{f_H} \mathbf{w}^H \mathbf{G} \mathbf{G}^H \mathbf{w} + [-1 - R_0^2 B_{opt}^2] \int_{f_L}^{f_H} \mathbf{w}^H \mathbf{G} \mathbf{S}_A \mathbf{S}_A^H \mathbf{G}^H \mathbf{w} df \hspace{5em} (C.21) \\
& - [-1 - j2R_0 B_{opt} + R_0^2 B_{opt}^2] \int_{f_L}^{f_H} \mathbf{w}^H \mathbf{G} \mathbf{S}_A \mathbf{G}^H \mathbf{w} df \\
& - [-1 + 2jR_0 B_{opt} + R_0^2 B_{opt}^2] \int_{f_L}^{f_H} \mathbf{w}^H \mathbf{G} \mathbf{S}_A^H \mathbf{G}^H \mathbf{w} df = 0
\end{aligned}$$

$$\begin{aligned}
& R_0^2 G_{opt}^2 \int_{f_L}^{f_H} \mathbf{w}^H \mathbf{G} [\mathbf{I} + \mathbf{S}_A \mathbf{S}_A^H + \mathbf{S}_A + \mathbf{S}_A^H] \mathbf{G}^H \mathbf{w} df \\
& + [-1 - R_0^2 B_{opt}^2] \int_{f_L}^{f_H} \mathbf{w}^H \mathbf{G} \mathbf{G}^H \mathbf{w} df \\
& + [-1 - R_0^2 B_{opt}^2] \int_{f_L}^{f_H} \mathbf{w}^H \mathbf{G} \mathbf{S}_A \mathbf{S}_A^H \mathbf{G}^H \mathbf{w} df \\
& - [-1 - j2R_0 B_{opt} + R_0^2 B_{opt}^2] \int_{f_L}^{f_H} \mathbf{w}^H \mathbf{G} \mathbf{S}_A \mathbf{G}^H \mathbf{w} df \\
& - [-1 + 2jR_0 B_{opt} + R_0^2 B_{opt}^2] \int_{f_L}^{f_H} \mathbf{w}^H \mathbf{G} \mathbf{S}_A^H \mathbf{G}^H \mathbf{w} df = 0
\end{aligned} \tag{C.22}$$

$$\begin{aligned}
& R_0^2 G_{opt}^2 \int_{f_L}^{f_H} \mathbf{w}^H \mathbf{G} [\mathbf{I} + \mathbf{S}_A \mathbf{S}_A^H + \mathbf{S}_A + \mathbf{S}_A^H] \mathbf{G}^H \mathbf{w} df = \\
& - [-1 - R_0^2 B_{opt}^2] \int_{f_L}^{f_H} \mathbf{w}^H \mathbf{G} \mathbf{G}^H \mathbf{w} df \\
& - [-1 - R_0^2 B_{opt}^2] \int_{f_L}^{f_H} \mathbf{w}^H \mathbf{G} \mathbf{S}_A \mathbf{S}_A^H \mathbf{G}^H \mathbf{w} df \\
& + [-1 - j2R_0 B_{opt} + R_0^2 B_{opt}^2] \int_{f_L}^{f_H} \mathbf{w}^H \mathbf{G} \mathbf{S}_A \mathbf{G}^H \mathbf{w} df \\
& + [-1 + 2jR_0 B_{opt} + R_0^2 B_{opt}^2] \int_{f_L}^{f_H} \mathbf{w}^H \mathbf{G} \mathbf{S}_A^H \mathbf{G}^H \mathbf{w} df = 0
\end{aligned} \tag{C.23}$$

$$\begin{aligned}
& R_0^2 G_{opt}^2 \int_{f_L}^{f_H} \mathbf{w}^H \mathbf{G} [\mathbf{I} + \mathbf{S}_A \mathbf{S}_A^H + \mathbf{S}_A + \mathbf{S}_A^H] \mathbf{G}^H \mathbf{w} df = \\
& \int_{f_L}^{f_H} -\mathbf{w}^H \mathbf{G} \\
& ([-1 - R_0^2 B_{opt}^2] - [-1 - R_0^2 B_{opt}^2] \mathbf{S}_A \mathbf{S}_A^H - [1 + j2R_0 B_{opt} - R_0^2 B_{opt}^2] \mathbf{S}_A - [1 - 2jR_0 B_{opt} - R_0^2 B_{opt}^2] \mathbf{S}_A^H) \\
& \mathbf{G}^H \mathbf{w} df
\end{aligned} \tag{C.24}$$

Next, collect all the G_{opt} terms to get

$$\begin{aligned}
R_0^2 G_{opt}^2 \int_{f_L}^{f_H} \mathbf{w}^H \mathbf{G} [\mathbf{I} + \mathbf{S}_A \mathbf{S}_A^H + \mathbf{S}_A + \mathbf{S}_A^H] \mathbf{G}^H \mathbf{w} df = \\
\int_{f_L}^{f_H} \mathbf{w}^H \mathbf{G} ([1 + R_0^2 B_{opt}^2] (\mathbf{I} + \mathbf{S}_A \mathbf{S}_A^H) - [1 + j2R_0 B_{opt} - R_0^2 B_{opt}^2] (\mathbf{S}_A + \mathbf{S}_A^H)) \mathbf{G}^H \mathbf{w} df.
\end{aligned} \tag{C.25}$$

$$\begin{aligned}
G_{act}^2 = \frac{-2\mathbf{w}^H \left[\int_{f_L}^{f_H} \mathbf{G} [(1 + R_0^2 B_{act}^2) (\mathbf{I} + \mathbf{S}_A \mathbf{S}_A^H) - (1 + 2jZ_0 B_{opt} - Z_0^2 B_{opt}^2) \mathbf{S}_A \right. \\
\left. R_0^2 \mathbf{w}^H \left[\int_{f_L}^{f_H} \mathbf{G} [\mathbf{I} + \mathbf{S}_A \mathbf{S}_A^H + 2\Re\{\mathbf{S}_A\}] \mathbf{G}^H df \right] \mathbf{w} \right. \\
\left. - (1 + 2jZ_0 B_{opt} - Z_0^2 B_{opt}^2)^* \mathbf{S}_A^H \right] \mathbf{G}^H df \mathbf{w} df}{R_0^2 \mathbf{w}^H \left[\int_{f_L}^{f_H} \mathbf{G} [\mathbf{I} + \mathbf{S}_A \mathbf{S}_A^H + 2\Re\{\mathbf{S}_A\}] \mathbf{G}^H df \right] \mathbf{w} df}
\end{aligned} \tag{C.26}$$

And simplify to arrive at Equation 4.63

$$\boxed{G_{act}^2 = \frac{-2\mathbf{w}^H \int_{f_L}^{f_H} \mathbf{G} (1 + R_0^2 B_{act}^2) (\mathbf{I} + \mathbf{S}_A \mathbf{S}_A^H) - 2\Re\{(1 + 2jZ_0 B_{opt} - Z_0^2 B_{opt}^2) \mathbf{S}_A\} \mathbf{G}^H df \mathbf{w}}{R_0^2 \mathbf{w}^H \left[\int_{f_L}^{f_H} \mathbf{G} [\mathbf{I} + \mathbf{S}_A \mathbf{S}_A^H + 2\Re\{\mathbf{S}_A\}] \mathbf{G}^H df \right] \mathbf{w}} \tag{C.27}}$$

Appendix D

71 element Vivaldi array simulation code

```
clear all
close all
% constants
Nel = 78;
I = eye(Nel);
Z0 = 50;
T0 = 290;
kb = 1.38064852e-23; % Boltzmann's constant (W/(Hz*K))
c = 3e8; % speed of light in vacuum
GHz = 1e9;
mm = 1e-3;
fc = 1.4*GHz;
lambda = c/fc;
nSmp = 100;

BW_arr = [1e-6 10 20 50 100 150 250 300:100:1000]*1e6;
%BW_arr = [1]*GHz;
TX_line_arr = [0 0.5 1 1.5 2 2.5]*lambda;
%TX_line_arr = [0];

% read array data
% Array S-parameters
[Data,freq,Coeff_array,Nant] = ReadInArrayData();
freq = freq * GHz;
```

```

idx = find(freq == 1.4*GHz);
SA = Data(idx).S; % original array data
Coeff = Coeff_array(idx,:).';

%LNA
Tmin = 15.1208;
GammaOpt = 0.2271 + 0.0881*1j;%0.2+1j*0.1; %0.1885 + 1j*0.1051;%-0.6-1
    ↪ j*0.5;
N = 0.0242;%Tmin/T0/2*0.9;
Zopt = Z0*(1+GammaOpt)/(1-GammaOpt);
Rn = N/real(1/Zopt);

% S Parameters of Measured LNA
s11 = 0.3827 - 0.2475*1j;%0.266*exp(1j*(pi/180)*75.87); % Reflection
    ↪ coefficient for LNA input.
s21 = 1+0*2.992*exp(1j*(pi/180)*(-166.12));
s12 = 0*0.016*exp(1j*(pi/180)*(160.89));
s22 = 0*0.361*exp(1j*(pi/180)*(-96.42));

%antenna feed length
ant_feed_length = 183*mm;

% create coordinates of each element in array
counter = 0
for m = 1:13
    for n = 1:6
        counter = counter + 1;

```

```

        ant_coord(counter).x = 100*mm * (m); % antennas are located on
            ↪ grid lines of 100mm
        ant_coord(counter).y = 100*mm * (n); % antennas are located on
            ↪ grid lines of 100mm
    end
end

% generate inter element delay
for k = 1:length(ant_coord)
    for l = 1:length(ant_coord)
        tau_ij(k,l) = sqrt((ant_coord(k).x - ant_coord(l).x)^2 + (
            ↪ ant_coord(k).y - ant_coord(l).y)^2)/c;
    end
end

%feed line delay
tau_d = ant_feed_length/c;

% total delay
tau = 2*tau_d + tau_ij;

% remove delay phase from antenna s parameter at 1.4GHz
for m = 1:Nel
    for n = 1:Nel
        delay_phase = exp(-j*2*pi*fc*tau(m,n));
        if(isnan(SA(m,n)))
            SA_wo_delay(m,n) = 0;
        end
    end
end

```

```

        SA(m,n) = 0;
    else
        SA_wo_delay(m,n) = SA(m,n) / delay_phase;
    end
end
end

end

% generate Gamma_opt space
counter = 0
for rho = 0:0.01:0.4
    for phi = 20:60
        counter = counter + 1;
        gamma_opt(counter) = rho*exp(j*phi/180*pi);
    end
end

% array constant matrices
% beamformer weights to remove vertically polarized elements
w = zeros(size(Coeff));
w(26:49) = 1;
w(66:71) = 1;
w(55:60) = 1;

SR = I*s11;

for t = 1:length(TX_line_arr)

```

```

TX_delay = TX_line_arr(t)/c;
for b = 1:length(BW_arr)
    BW = BW_arr(b)
    freq_space = linspace(-BW/2,BW/2,nSmp);
    Trec_arr = zeros(length(gamma_opt),1);

    tic
    parfor (g = 1:length(gamma_opt),16)
        %for g = 1:length(gamma_opt)
            Yopt = 1/s2z(gamma_opt(g));
            Gopt = real(Yopt);
            Bopt = imag(Yopt);
            R0 = real(Z0);
            Rn = N/Gopt;

            Tam = Tmin + T0*Rn/R0*abs(1-R0*Yopt)^2;
            Tbm = -Tmin + T0*Rn/R0*abs(1+R0*Yopt)^2;
            Tgm = T0*Rn/R0*(1+R0*Yopt)*(1-R0*Yopt');

            Trec_num = 0;
            Trec_den = 0;
            for s = 1:nSmp
                SA_f = SA_wo_delay.*exp(-2*j*pi*(fc+freq_space(s))*(tau
                    ↪ +2*TX_delay));
                SA_ = SA.*exp(-2*j*pi*(fc+freq_space(s))*(tau));
                G = sqrt(Z0)*(I+SR)/(I-SA_f*SR);
                wf = G'*w;

```

```

        Trec_num = Trec_num + wf'*(I*Tam + (SA_f*(I*Tbm)*SA_f'))
            ↪ - 2*real(Tgm*SA_f))*wf;
        Trec_den = Trec_den + wf'*(I - (SA_*SA_'))*wf;
    end
    Trec_arr(g) = Trec_num/Trec_den;
end

% find minimum Trec
[Trec(t,b) min_idx] = min(abs(Trec_arr));
Gamma_act(t,b) = gamma_opt(min_idx);
toc
end
end

% theory
for t = 1:length(TX_line_arr)
    TX_delay = TX_line_arr(t)/c;
    for b = 1:length(BW_arr)
        BW = BW_arr(b);
        freq_space = linspace(-BW/2,BW/2,nSmp);
        Gact_theory_num = 0;
        Gact_theory_den = 0;
        Bact_theory_num = 0;
        Bact_theory_den = 0;
        for s = 1:nSmp

```

```

SA_f = SA_wo_delay.*exp(-2*j*pi*(fc+freq_space(s))*(tau +
    ↪ 2*TX_delay));
G = sqrt(Z0)*(I+SR)/(I-SA_f*SR);
wf = G'*w;
Bact_theory_num = Bact_theory_num + (wf'*(j*SA_f - j*SA_f')
    ↪ *wf);
Bact_theory_den = Bact_theory_den + (Z0*wf'*(I+SA_f*SA_f' +
    ↪ SA_f + SA_f')*wf);
end

Bact_theory = Bact_theory_num/Bact_theory_den;

for s = 1:nSmp
    SA_f = SA_wo_delay.*exp(-2*j*pi*(fc+freq_space(s))*(tau+2*
        ↪ TX_delay));
    G = sqrt(Z0)*(I+SR)/(I-SA_f*SR);
    wf = G'*w;
    Gact_theory_num = Gact_theory_num + (wf'*((1+Z0^2*
        ↪ Bact_theory^2)*(I+SA_f*SA_f') - (1+2j*Z0*Bact_theory-
        ↪ Z0^2*Bact_theory^2)*SA_f - (1+2j*Z0*Bact_theory-Z0^2*
        ↪ Bact_theory^2)')*SA_f')*wf);
    Gact_theory_den = Gact_theory_den + (Z0^2*wf'*(I+SA_f*SA_f'
        ↪ + SA_f + SA_f')*wf);
end

Gact_theory = sqrt(Gact_theory_num) / sqrt(Gact_theory_den);

```

```

        Gamma_act_theory(t,b) = z2s(1 / (Gact_theory + j*Bact_theory));

    end

end

close all

figure(1);

smithplot(Gamma_act_theory(1,:), 'x');

hold on

smithplot(Gamma_act(1,:), 'o');

legend('\Gamma_a_c_t theory', '\Gamma_a_c_t simulated');

title('\Gamma_o_p_t simulation with no transmission line');

saveas(gcf, '../..//Figures/Vivaldi_no_TX_smith.png');

figure(2);

smithplot(Gamma_act_theory(6,:), 'x');

hold on

smithplot(Gamma_act(6,:), 'o');

legend('\Gamma_a_c_t theory', '\Gamma_a_c_t simulated');

title('\Gamma_o_p_t simulation with 2.5\lambda transmission line');

saveas(gcf, '../..//Figures/Vivaldi_2_5_lambda_TX_smith.png');

fig = figure(3)

plot(BW_arr/1e6, Trec(1,:), '-d')

hold on

plot(BW_arr/1e6, Trec(2,:), '-x')

plot(BW_arr/1e6, Trec(3,:), '-o')

plot(BW_arr/1e6, Trec(4,:), '-+')

```

```

plot(BW_arr/1e6,Trec(5,:), '-*')
plot(BW_arr/1e6,Trec(6,:), '-v')

title('T_r_e_c vs Bandwidth for different transmission lines');
xlabel('Bandwidth (MHz)');
ylabel('Noise Temperature (K)');
ylim([min(min(Trec))-0.3 max(max((Trec)))+0.3])

legend('No TX line', '0.5\lambda TX line', '1.0\lambda TX line', ...
'1.5\lambda TX line', '2.0\lambda TX line', '2.5\lambda TX line');

yyaxis right
ylim(real([((min(min(Trec))-0.3)-Tmin)*100/Tmin ((max(max(Trec)))
↪ +0.3)-Tmin)*100/Tmin]))
ylabel('T_r_e_c increase over T_m_i_n (%)')
saveas(gcf,'../..//Figures/Vivaldi_Trec.png');

figure(4)
plot(BW_arr/1e6,20*log10(abs(Gamma_act_theory(1,:))), '-d')
hold on
plot(BW_arr/1e6,20*log10(abs(Gamma_act_theory(2,:))), '-x')
plot(BW_arr/1e6,20*log10(abs(Gamma_act_theory(3,:))), '-o')
plot(BW_arr/1e6,20*log10(abs(Gamma_act_theory(4,:))), '-+')
plot(BW_arr/1e6,20*log10(abs(Gamma_act_theory(5,:))), '-*')
plot(BW_arr/1e6,20*log10(abs(Gamma_act_theory(6,:))), '-v')

title('| \Gamma_a_c_t | vs Bandwidth')
legend('No TX line', '0.5\lambda TX line', '1.0\lambda TX line', ...
'1.5\lambda TX line', '2.0\lambda TX line', '2.5\lambda TX line');
xlabel('Bandwidth (MHz)')
ylabel('| \Gamma_a_c_t | (dB)')

```

```
saveas(gcf,'../../Figures/Vivaldi__abs_Gamma_act.png');
```

Appendix E

Multi-beam average optimal Γ_{act} derivation

To find multi-beam optimal Γ_{act} , start with the average multi-beam receiver temperature

$$T_{av} = \frac{1}{P} \sum_{p=1}^P T_{rec}^p, \quad (\text{E.1})$$

and expand by substituting Equation 4.55 for each beam angle associated with the index p

$$T_{rec}^p = \frac{\int_{f_L}^{f_H} \left[\mathbf{w}_p^H \mathbf{G} \left[\mathbf{T}_\alpha + \mathbf{S}_A \mathbf{T}_\beta \mathbf{S}_A^H + \mathbf{T}_\gamma \mathbf{S}_A + \mathbf{T}_\gamma^H \mathbf{S}_A^H \right] \mathbf{G}^H \mathbf{w}_p \right] df}{\int_{f_L}^{f_H} \left[\mathbf{w}_p^H \mathbf{G} \left(\mathbf{I} - \mathbf{S}_A \mathbf{S}_A^H \right) \mathbf{G}^H \mathbf{w}_p \right] df}. \quad (\text{E.2})$$

Next, substitute in $\mathbf{T}_\alpha = T_\alpha \mathbf{I}$, $\mathbf{T}_\beta = T_\beta \mathbf{I}$, and $\mathbf{T}_\gamma = T_\gamma \mathbf{I}$

$$T_\alpha = \frac{N}{R_0 G_{opt}} T_0 + T_{min} - T_0 \frac{N}{G_{opt}} Y_{opt} - T_0 \frac{N}{G_{opt}} Y_{opt}^* + T_0 \frac{N}{G_{opt}} |Y_{opt}|^2 R_0 \quad (\text{E.3})$$

$$T_\beta = T_0 \frac{N}{G_{opt} R_0} - T_{min} + T_0 \frac{N}{G_{opt}} Y_{opt} + T_0 \frac{N}{G_{opt}} Y_{opt}^* + T_0 \frac{N}{G_{opt}} |Y_{opt}|^2 R_0 \quad (\text{E.4})$$

$$T_\gamma = T_0 \frac{N}{G_{opt} R_0} - T_0 \frac{N}{G_{opt}} Y_{opt} + T_0 \frac{N}{G_{opt}} Y_{opt}^* - T_0 \frac{N}{G_{opt}} |Y_{opt}|^2 R_0 \quad (\text{E.5})$$

from Equations 4.49, 4.50, and 4.51

Then, find $\frac{dT_{av}}{dB_{opt}} = 0$ to find a B_{opt} that minimizes T_{av}

$$\frac{dT_{av}}{dB_{opt}} = \left[\frac{1}{P} \sum_{p=1}^P T_{rec}^p \right] / dB_{opt}. \quad (\text{E.6})$$

Since the derivative operator is distributive,

$$\frac{dT_{av}}{dB_{opt}} = \frac{1}{P} \sum_{p=1}^P [dT_{rec}^p / dB_{opt}]. \quad (\text{E.7})$$

Next, expand the equation in the next few steps.

$$\begin{aligned} \frac{dT_{av}}{dB_{opt}} &= \frac{1}{P} \sum_{p=1}^P d \left[\frac{\int_{f_L}^{f_H} \mathbf{w}_p^H \mathbf{G} (\mathbf{T}_\alpha) \mathbf{G}^H \mathbf{w}_p df}{\int_{f_L}^{f_H} \mathbf{w}_p^H \mathbf{G} (\mathbf{I} - \mathbf{S}_A \mathbf{S}_A^H) \mathbf{G}^H \mathbf{w}_p df} \right] / dB_{opt} \\ &+ \frac{1}{P} \sum_{p=1}^P d \left[\frac{\int_{f_L}^{f_H} \mathbf{w}_p^H \mathbf{G} (\mathbf{S}_A \mathbf{T}_\beta \mathbf{S}_A^H) \mathbf{G}^H \mathbf{w}_p df}{\int_{f_L}^{f_H} \mathbf{w}_p^H \mathbf{G} (\mathbf{I} - \mathbf{S}_A \mathbf{S}_A^H) \mathbf{G}^H \mathbf{w}_p df} \right] / dB_{opt} \\ &- \frac{1}{P} \sum_{p=1}^P d \left[\frac{\int_{f_L}^{f_H} \mathbf{w}_p^H \mathbf{G} (\mathbf{S}_A \mathbf{T}_\gamma + \mathbf{S}_A^* \mathbf{T}_\gamma^*) \mathbf{G}^H \mathbf{w}_p df}{\int_{f_L}^{f_H} \mathbf{w}_p^H \mathbf{G} (\mathbf{I} - \mathbf{S}_A \mathbf{S}_A^H) \mathbf{G}^H \mathbf{w}_p df} \right] / dB_{opt} \end{aligned} \quad (\text{E.8})$$

$$\begin{aligned} \frac{dT_{av}}{dB_{opt}} &= \frac{1}{P} \sum_{p=1}^P d \left[T_\alpha \frac{\int_{f_L}^{f_H} \mathbf{w}_p^H \mathbf{G} \mathbf{I} \mathbf{G}^H \mathbf{w}_p df}{\int_{f_L}^{f_H} \mathbf{w}_p^H \mathbf{G} (\mathbf{I} - \mathbf{S}_A \mathbf{S}_A^H) \mathbf{G}^H \mathbf{w}_p df} \right] / dB_{opt} \\ &+ \frac{1}{P} \sum_{p=1}^P d \left[T_\beta \frac{\int_{f_L}^{f_H} \mathbf{w}_p^H \mathbf{G} (\mathbf{S}_A \mathbf{I} \mathbf{S}_A^H) \mathbf{G}^H \mathbf{w}_p df}{\int_{f_L}^{f_H} \mathbf{w}_p^H \mathbf{G} (\mathbf{I} - \mathbf{S}_A \mathbf{S}_A^H) \mathbf{G}^H \mathbf{w}_p df} \right] / dB_{opt} \\ &- \frac{1}{P} \sum_{p=1}^P d \left[T_\gamma \frac{\int_{f_L}^{f_H} \mathbf{w}_p^H \mathbf{G} (\mathbf{S}_A \mathbf{I}) \mathbf{G}^H \mathbf{w}_p df}{\int_{f_L}^{f_H} \mathbf{w}_p^H \mathbf{G} (\mathbf{I} - \mathbf{S}_A \mathbf{S}_A^H) \mathbf{G}^H \mathbf{w}_p df} \right] / dB_{opt} \\ &- \frac{1}{P} \sum_{p=1}^P d \left[T_\gamma^* \frac{\int_{f_L}^{f_H} \mathbf{w}_p^H \mathbf{G} (\mathbf{S}_A^* \mathbf{I}) \mathbf{G}^H \mathbf{w}_p df}{\int_{f_L}^{f_H} \mathbf{w}_p^H \mathbf{G} (\mathbf{I} - \mathbf{S}_A \mathbf{S}_A^H) \mathbf{G}^H \mathbf{w}_p df} \right] / dB_{opt} \end{aligned} \quad (\text{E.9})$$

$$\begin{aligned}
\frac{dT_{av}}{dB_{opt}} &= \frac{1}{P} \sum_{p=1}^P d \left[\frac{N}{R_0 G_{opt}} T_0 + T_{min} - T_0 \frac{N}{G_{opt}} Y_{opt} - T_0 \frac{N}{G_{opt}} Y_{opt}^* + T_0 \frac{N}{G_{opt}} |Y_{opt}|^2 R_0 \right] / dB_{opt} \\
&\quad \frac{\int_{f_L}^{f_H} \mathbf{w}_p^H \mathbf{G} \mathbf{I} \mathbf{G}^H \mathbf{w}_p df}{\int_{f_L}^{f_H} \mathbf{w}_p^H \mathbf{G} (\mathbf{I} - \mathbf{S}_A \mathbf{S}_A^H) \mathbf{G}^H \mathbf{w}_p df} \\
&+ \frac{1}{P} \sum_{p=1}^P d \left[T_0 \frac{N}{G_{opt} R_0} - T_{min} + T_0 \frac{N}{G_{opt}} Y_{opt} + T_0 \frac{N}{G_{opt}} Y_{opt}^* + T_0 \frac{N}{G_{opt}} |Y_{opt}|^2 R_0 \right] / dB_{opt} \\
&\quad \frac{\int_{f_L}^{f_H} \mathbf{w}_p^H \mathbf{G} (\mathbf{S}_A \mathbf{I} \mathbf{S}_A^H) \mathbf{G}^H \mathbf{w}_p df}{\int_{f_L}^{f_H} \mathbf{w}_p^H \mathbf{G} (\mathbf{I} - \mathbf{S}_A \mathbf{S}_A^H) \mathbf{G}^H \mathbf{w}_p df} \\
&- \frac{1}{P} \sum_{p=1}^P d \left[T_0 \frac{N}{G_{opt} R_0} - T_0 \frac{N}{G_{opt}} Y_{opt}^* + T_0 \frac{N}{G_{opt}} Y_{opt} - T_0 \frac{N}{G_{opt}} |Y_{opt}|^2 R_0 \right] / dB_{opt}
\end{aligned} \tag{E.10}$$

$$\begin{aligned}
&\quad \frac{\int_{f_L}^{f_H} \mathbf{w}_p^H \mathbf{G} (\mathbf{S}_A \mathbf{I}) \mathbf{G}^H \mathbf{w}_p df}{\int_{f_L}^{f_H} \mathbf{w}_p^H \mathbf{G} (\mathbf{I} - \mathbf{S}_A \mathbf{S}_A^H) \mathbf{G}^H \mathbf{w}_p df} \\
&- \frac{1}{P} \sum_{p=1}^P d \left[T_0 \frac{N}{G_{opt} R_0} - T_0 \frac{N}{G_{opt}} Y_{opt} + T_0 \frac{N}{G_{opt}} Y_{opt}^* - T_0 \frac{N}{G_{opt}} |Y_{opt}|^2 R_0 \right] / dB_{opt} \\
&\quad \frac{\int_{f_L}^{f_H} \mathbf{w}_p^H \mathbf{G} (\mathbf{S}_A^* \mathbf{I}) \mathbf{G}^H \mathbf{w}_p df}{\int_{f_L}^{f_H} \mathbf{w}_p^H \mathbf{G} (\mathbf{I} - \mathbf{S}_A \mathbf{S}_A^H) \mathbf{G}^H \mathbf{w}_p df}
\end{aligned}$$

$$\begin{aligned}
\frac{dT_{av}}{dB_{opt}} &= \frac{1}{P} \sum_{p=1}^P \left[-jT_0 \frac{N}{G_{opt}} + jT_0 \frac{N}{G_{opt}} + T_0 \frac{N}{G_{opt}} (2B_{opt}) R_0 \right] \frac{\int_{f_L}^{f_H} \mathbf{w}_p^H \mathbf{G} \mathbf{I} \mathbf{G}^H \mathbf{w}_p df}{\int_{f_L}^{f_H} \mathbf{w}_p^H \mathbf{G} (\mathbf{I} - \mathbf{S}_A \mathbf{S}_A^H) \mathbf{G}^H \mathbf{w}_p df} \\
&+ \left[jT_0 \frac{N}{G_{opt}} - jT_0 \frac{N}{G_{opt}} + T_0 \frac{N}{G_{opt}} (2B_{opt}) R_0 \right] \frac{\int_{f_L}^{f_H} \mathbf{w}_p^H \mathbf{G} (\mathbf{S}_A \mathbf{I} \mathbf{S}_A^H) \mathbf{G}^H \mathbf{w}_p df}{\int_{f_L}^{f_H} \mathbf{w}_p^H \mathbf{G} (\mathbf{I} - \mathbf{S}_A \mathbf{S}_A^H) \mathbf{G}^H \mathbf{w}_p df}
\end{aligned} \tag{E.11}$$

$$\begin{aligned}
&- \left[jT_0 \frac{N}{G_{opt}} + jT_0 \frac{N}{G_{opt}} - T_0 \frac{N}{G_{opt}} (2B_{opt}) R_0 \right] \frac{\int_{f_L}^{f_H} \mathbf{w}_p^H \mathbf{G} (\mathbf{S}_A \mathbf{I}) \mathbf{G}^H \mathbf{w}_p df}{\int_{f_L}^{f_H} \mathbf{w}_p^H \mathbf{G} (\mathbf{I} - \mathbf{S}_A \mathbf{S}_A^H) \mathbf{G}^H \mathbf{w}_p df} \\
&- \left[-jT_0 \frac{N}{G_{opt}} - jT_0 \frac{N}{G_{opt}} - T_0 \frac{N}{G_{opt}} (2B_{opt}) R_0 \right] \frac{\int_{f_L}^{f_H} \mathbf{w}_p^H \mathbf{G} (\mathbf{S}_A^* \mathbf{I}) \mathbf{G}^H \mathbf{w}_p df}{\int_{f_L}^{f_H} \mathbf{w}_p^H \mathbf{G} (\mathbf{I} - \mathbf{S}_A \mathbf{S}_A^H) \mathbf{G}^H \mathbf{w}_p df} = 0
\end{aligned}$$

Next, set $\frac{dT_{av}}{dB_{opt}} = 0$ to minimize T_{av}

$$\begin{aligned}
0 = & \sum_{p=1}^P \left[-jT_0 \frac{N}{G_{opt}} + jT_0 \frac{N}{G_{opt}} + T_0 \frac{N}{G_{opt}} (2B_{opt}) R_0 \right] \frac{\int_{f_L}^{f_H} \mathbf{w}_p^H \mathbf{G} \mathbf{I} \mathbf{G}^H \mathbf{w}_p df}{\int_{f_L}^{f_H} \mathbf{w}_p^H \mathbf{G} (\mathbf{I} - \mathbf{S}_A \mathbf{S}_A^H) \mathbf{G}^H \mathbf{w}_p df} \\
& + \sum_{p=1}^P \left[jT_0 \frac{N}{G_{opt}} - jT_0 \frac{N}{G_{opt}} + T_0 \frac{N}{G_{opt}} (2B_{opt}) R_0 \right] \frac{\int_{f_L}^{f_H} \mathbf{w}_p^H \mathbf{G} (\mathbf{S}_A \mathbf{I} \mathbf{S}_A^H) \mathbf{G}^H \mathbf{w}_p df}{\int_{f_L}^{f_H} \mathbf{w}_p^H \mathbf{G} (\mathbf{I} - \mathbf{S}_A \mathbf{S}_A^H) \mathbf{G}^H \mathbf{w}_p df} \\
& - \sum_{p=1}^P \left[jT_0 \frac{N}{G_{opt}} + jT_0 \frac{N}{G_{opt}} - T_0 \frac{N}{G_{opt}} (2B_{opt}) R_0 \right] \frac{\int_{f_L}^{f_H} \mathbf{w}_p^H \mathbf{G} (\mathbf{S}_A \mathbf{I}) \mathbf{G}^H \mathbf{w}_p df}{\int_{f_L}^{f_H} \mathbf{w}_p^H \mathbf{G} (\mathbf{I} - \mathbf{S}_A \mathbf{S}_A^H) \mathbf{G}^H \mathbf{w}_p df} \\
& - \sum_{p=1}^P \left[-jT_0 \frac{N}{G_{opt}} - jT_0 \frac{N}{G_{opt}} - T_0 \frac{N}{G_{opt}} (2B_{opt}) R_0 \right] \frac{\int_{f_L}^{f_H} \mathbf{w}_p^H \mathbf{G} (\mathbf{S}_A^* \mathbf{I}) \mathbf{G}^H \mathbf{w}_p df}{\int_{f_L}^{f_H} \mathbf{w}_p^H \mathbf{G} (\mathbf{I} - \mathbf{S}_A \mathbf{S}_A^H) \mathbf{G}^H \mathbf{w}_p df} = 0,
\end{aligned} \tag{E.12}$$

And simplify in the next few steps.

$$\begin{aligned}
& B_{opt} R_0 \sum_{p=1}^P \frac{\int_{f_L}^{f_H} \mathbf{w}_p^H \mathbf{G} \mathbf{I} \mathbf{G}^H \mathbf{w}_p df}{\int_{f_L}^{f_H} \mathbf{w}_p^H \mathbf{G} (\mathbf{I} - \mathbf{S}_A \mathbf{S}_A^H) \mathbf{G}^H \mathbf{w}_p df} \\
& + B_{opt} R_0 \sum_{p=1}^P \frac{\int_{f_L}^{f_H} \mathbf{w}_p^H \mathbf{G} (\mathbf{S}_A \mathbf{I} \mathbf{S}_A^H) \mathbf{G}^H \mathbf{w}_p df}{\int_{f_L}^{f_H} \mathbf{w}_p^H \mathbf{G} (\mathbf{I} - \mathbf{S}_A \mathbf{S}_A^H) \mathbf{G}^H \mathbf{w}_p df} \\
& - [j - B_{opt} R_0] \sum_{p=1}^P \frac{\int_{f_L}^{f_H} \mathbf{w}_p^H \mathbf{G} (\mathbf{S}_A \mathbf{I}) \mathbf{G}^H \mathbf{w}_p df}{\int_{f_L}^{f_H} \mathbf{w}_p^H \mathbf{G} (\mathbf{I} - \mathbf{S}_A \mathbf{S}_A^H) \mathbf{G}^H \mathbf{w}_p df} \\
& - [-j - B_{opt} R_0] \sum_{p=1}^P \frac{\int_{f_L}^{f_H} \mathbf{w}_p^H \mathbf{G} (\mathbf{S}_A^* \mathbf{I}) \mathbf{G}^H \mathbf{w}_p df}{\int_{f_L}^{f_H} \mathbf{w}_p^H \mathbf{G} (\mathbf{I} - \mathbf{S}_A \mathbf{S}_A^H) \mathbf{G}^H \mathbf{w}_p df} = 0
\end{aligned} \tag{E.13}$$

$$\begin{aligned}
& B_{opt}R_0 \sum_{p=1}^P \frac{\int_{f_L}^{f_H} \mathbf{w}_p^H \mathbf{G} \mathbf{I} \mathbf{G}^H \mathbf{w}_p df}{\int_{f_L}^{f_H} \mathbf{w}_p^H \mathbf{G} (\mathbf{I} - \mathbf{S}_A \mathbf{S}_A^H) \mathbf{G}^H \mathbf{w}_p df} \\
& + B_{opt}R_0 \sum_{p=1}^P \frac{\int_{f_L}^{f_H} \mathbf{w}_p^H \mathbf{G} (\mathbf{S}_A \mathbf{I} \mathbf{S}_A^H) \mathbf{G}^H \mathbf{w}_p df}{\int_{f_L}^{f_H} \mathbf{w}_p^H \mathbf{G} (\mathbf{I} - \mathbf{S}_A \mathbf{S}_A^H) \mathbf{G}^H \mathbf{w}_p df} \\
& + B_{opt}R_0 \sum_{p=1}^P \frac{\int_{f_L}^{f_H} \mathbf{w}_p^H \mathbf{G} (\mathbf{S}_A \mathbf{I}) \mathbf{G}^H \mathbf{w}_p df}{\int_{f_L}^{f_H} \mathbf{w}_p^H \mathbf{G} (\mathbf{I} - \mathbf{S}_A \mathbf{S}_A^H) \mathbf{G}^H \mathbf{w}_p df} \\
& + B_{opt}R_0 \sum_{p=1}^P \frac{\int_{f_L}^{f_H} \mathbf{w}_p^H \mathbf{G} (\mathbf{S}_A^* \mathbf{I}) \mathbf{G}^H \mathbf{w}_p df}{\int_{f_L}^{f_H} \mathbf{w}_p^H \mathbf{G} (\mathbf{I} - \mathbf{S}_A \mathbf{S}_A^H) \mathbf{G}^H \mathbf{w}_p df} \\
& = -2 \sum_{p=1}^P \frac{\int_{f_L}^{f_H} \mathbf{w}_p^H \mathbf{G} \mathfrak{S} \{ \mathbf{S}_A \} \mathbf{G}^H \mathbf{w}_p df}{\int_{f_L}^{f_H} \mathbf{w}_p^H \mathbf{G} (\mathbf{I} - \mathbf{S}_A \mathbf{S}_A^H) \mathbf{G}^H \mathbf{w}_p df}
\end{aligned} \tag{E.17}$$

$$\begin{aligned}
& B_{opt}R_0 \sum_{p=1}^P \frac{\int_{f_L}^{f_H} \mathbf{w}_p^H \mathbf{G} \mathbf{I} \mathbf{G}^H \mathbf{w}_p df}{\int_{f_L}^{f_H} \mathbf{w}_p^H \mathbf{G} (\mathbf{I} - \mathbf{S}_A \mathbf{S}_A^H) \mathbf{G}^H \mathbf{w}_p df} \\
& + B_{opt}R_0 \sum_{p=1}^P \frac{\int_{f_L}^{f_H} \mathbf{w}_p^H \mathbf{G} (\mathbf{S}_A \mathbf{I} \mathbf{S}_A^H) \mathbf{G}^H \mathbf{w}_p df}{\int_{f_L}^{f_H} \mathbf{w}_p^H \mathbf{G} (\mathbf{I} - \mathbf{S}_A \mathbf{S}_A^H) \mathbf{G}^H \mathbf{w}_p df} \\
& + B_{opt}R_0 \sum_{p=1}^P \frac{\int_{f_L}^{f_H} \mathbf{w}_p^H \mathbf{G} (\mathbf{S}_A \mathbf{I}) \mathbf{G}^H \mathbf{w}_p df}{\int_{f_L}^{f_H} \mathbf{w}_p^H \mathbf{G} (\mathbf{I} - \mathbf{S}_A \mathbf{S}_A^H) \mathbf{G}^H \mathbf{w}_p df} \\
& + B_{opt}R_0 \sum_{p=1}^P \frac{\int_{f_L}^{f_H} \mathbf{w}_p^H \mathbf{G} (\mathbf{S}_A^* \mathbf{I}) \mathbf{G}^H \mathbf{w}_p df}{\int_{f_L}^{f_H} \mathbf{w}_p^H \mathbf{G} (\mathbf{I} - \mathbf{S}_A \mathbf{S}_A^H) \mathbf{G}^H \mathbf{w}_p df} \\
& = -2 \sum_{p=1}^P \frac{\int_{f_L}^{f_H} \mathbf{w}_p^H \mathbf{G} \mathfrak{S} \{ \mathbf{S}_A \} \mathbf{G}^H \mathbf{w}_p df}{\int_{f_L}^{f_H} \mathbf{w}_p^H \mathbf{G} (\mathbf{I} - \mathbf{S}_A \mathbf{S}_A^H) \mathbf{G}^H \mathbf{w}_p df}
\end{aligned} \tag{E.18}$$

Collect all the B_{opt} terms on the left hand side, and set $B_{act} = B_{opt}$

$$\begin{aligned}
B_{opt} R_0 \sum_{p=1}^P \frac{\int_{f_L}^{f_H} \mathbf{w}_p^H \mathbf{G} [\mathbf{I} + \mathbf{S}_A \mathbf{S}_A^H + 2\Re\{\mathbf{S}_A\}] \mathbf{G}^H \mathbf{w}_p df}{\int_{f_L}^{f_H} \mathbf{w}_p^H \mathbf{G} (\mathbf{I} - \mathbf{S}_A \mathbf{S}_A^H) \mathbf{G}^H \mathbf{w}_p df} \\
= -2 \sum_{p=1}^P \frac{\int_{f_L}^{f_H} \mathbf{w}_p^H \mathbf{G} \Im\{\mathbf{S}_A\} \mathbf{G}^H \mathbf{w}_p df}{\int_{f_L}^{f_H} \mathbf{w}_p^H \mathbf{G} (\mathbf{I} - \mathbf{S}_A \mathbf{S}_A^H) \mathbf{G}^H \mathbf{w}_p df}, \tag{E.19}
\end{aligned}$$

and arrive at Equation 4.72

$$B_{act} = \frac{-2 \sum_{p=1}^P \frac{\int_{f_L}^{f_H} \mathbf{w}_p^H \mathbf{G} \Im\{\mathbf{S}_A\} \mathbf{G}^H \mathbf{w}_p df}{\int_{f_L}^{f_H} \mathbf{w}_p^H \mathbf{G} (\mathbf{I} - \mathbf{S}_A \mathbf{S}_A^H) \mathbf{G}^H \mathbf{w}_p df}}{R_0 \sum_{p=1}^P \frac{\int_{f_L}^{f_H} \mathbf{w}_p^H \mathbf{G} [\mathbf{I} + \mathbf{S}_A \mathbf{S}_A^H + 2\Re\{\mathbf{S}_A\}] \mathbf{G}^H \mathbf{w}_p df}{\int_{f_L}^{f_H} \mathbf{w}_p^H \mathbf{G} (\mathbf{I} - \mathbf{S}_A \mathbf{S}_A^H) \mathbf{G}^H \mathbf{w}_p df}} \tag{E.20}$$

For G_{act} , find $\frac{\partial(T_{av})}{\partial G_{opt}}$ much like B_{act} , but substitute B_{opt} with B_{act} from Equation 4.72.

Starting with

$$\frac{dT_{av}}{dG} = \left[\frac{1}{P} \sum_{p=1}^P T_{rec}^p \right] / dG_{opt}, \tag{E.21}$$

and bringing the derivative inside the sum

$$\frac{dT_{av}}{dG_{opt}} = \frac{1}{P} \sum_{p=1}^P [T_{rec}^p / dG_{opt}], \tag{E.22}$$

and expanding gives

$$\begin{aligned}
\frac{dT_{av}}{dG_{opt}} &= d \left[\frac{N}{R_0 G_{opt}} T_0 + T_{min} - T_0 \frac{N}{G_{opt}} Y_{opt} - T_0 \frac{N}{G_{opt}} Y_{opt}^* + T_0 \frac{N}{G_{opt}} |Y_{opt}|^2 R_0 \right] / dG_{opt} \\
&\quad \sum_{p=1}^P \frac{\int_{f_L}^{f_H} \mathbf{w}_p^H \mathbf{G} \mathbf{I} \mathbf{G}^H \mathbf{w}_p df}{\int_{f_L}^{f_H} \mathbf{w}_p^H \mathbf{G} (\mathbf{I} - \mathbf{S}_A \mathbf{S}_A^H) \mathbf{G}^H \mathbf{w}_p df} \\
&\quad + d \left[T_0 \frac{N}{G_{opt} R_0} - T_{min} + T_0 \frac{N}{G_{opt}} Y_{opt} + T_0 \frac{N}{G_{opt}} Y_{opt}^* + T_0 \frac{N}{G_{opt}} |Y_{opt}|^2 R_0 \right] / dG_{opt}
\end{aligned} \tag{E.23}$$

$$\begin{aligned}
&\quad \sum_{p=1}^P \frac{\int_{f_L}^{f_H} \mathbf{w}_p^H \mathbf{G} (\mathbf{S}_A \mathbf{I} \mathbf{S}_A^H) \mathbf{G}^H \mathbf{w}_p df}{\int_{f_L}^{f_H} \mathbf{w}_p^H \mathbf{G} (\mathbf{I} - \mathbf{S}_A \mathbf{S}_A^H) \mathbf{G}^H \mathbf{w}_p df} \\
&\quad - d \left[T_0 \frac{N}{G_{opt} R_0} - T_0 \frac{N}{G_{opt}} Y_{opt}^* + T_0 \frac{N}{G_{opt}} Y_{opt} - T_0 \frac{N}{G_{opt}} |Y_{opt}|^2 R_0 \right] / dG_{opt} \\
&\quad \sum_{p=1}^P \frac{\int_{f_L}^{f_H} \mathbf{w}_p^H \mathbf{G} (\mathbf{S}_A \mathbf{I}) \mathbf{G}^H \mathbf{w}_p df}{\int_{f_L}^{f_H} \mathbf{w}_p^H \mathbf{G} (\mathbf{I} - \mathbf{S}_A \mathbf{S}_A^H) \mathbf{G}^H \mathbf{w}_p df} \\
&\quad - d \left[T_0 \frac{N}{G_{opt} R_0} - T_0 \frac{N}{G_{opt}} Y_{opt} + T_0 \frac{N}{G_{opt}} Y_{opt}^* - T_0 \frac{N}{G_{opt}} |Y_{opt}|^2 R_0 \right] / dG_{opt} \\
&\quad \sum_{p=1}^P \frac{\int_{f_L}^{f_H} \mathbf{w}_p^H \mathbf{G} (\mathbf{S}_A^* \mathbf{I}) \mathbf{G}^H \mathbf{w}_p df}{\int_{f_L}^{f_H} \mathbf{w}_p^H \mathbf{G} (\mathbf{I} - \mathbf{S}_A \mathbf{S}_A^H) \mathbf{G}^H \mathbf{w}_p df}.
\end{aligned}$$

Next, expand the terms to get

$$\begin{aligned}
\frac{dT_{av}}{dG_{opt}} = & d \left[-\frac{N}{R_0 G_{opt}^2} T_0 + T_0 N \frac{Y_{opt} - G_{opt}}{G_{opt}^2} + T_0 N \frac{Y_{opt}^* - G_{opt}}{G_{opt}^2} + T_0 N R_0 \frac{2G_{opt}^2 - (G_{opt}^2 + B_{opt}^2)}{G_{opt}^2} \right] / dG_{opt} \\
& \sum_{p=1}^P \frac{\int_{f_L}^{f_H} \mathbf{w}_p^H \mathbf{G} \mathbf{I} \mathbf{G}^H \mathbf{w}_p df}{\int_{f_L}^{f_H} \mathbf{w}_p^H \mathbf{G} (\mathbf{I} - \mathbf{S}_A \mathbf{S}_A^H) \mathbf{G}^H \mathbf{w}_p df} \\
& + d \left[-\frac{N}{R_0 G_{opt}^2} T_0 - T_0 N \frac{Y_{opt} - G_{opt}}{G_{opt}^2} - T_0 N \frac{Y_{opt}^* - G_{opt}}{G_{opt}^2} + T_0 N R_0 \frac{2G_{opt}^2 - (G_{opt}^2 + B_{opt}^2)}{G_{opt}^2} \right] / dG_{opt} \\
& \sum_{p=1}^P \frac{\int_{f_L}^{f_H} \mathbf{w}_p^H \mathbf{G} (\mathbf{S}_A \mathbf{I} \mathbf{S}_A^H) \mathbf{G}^H \mathbf{w}_p df}{\int_{f_L}^{f_H} \mathbf{w}_p^H \mathbf{G} (\mathbf{I} - \mathbf{S}_A \mathbf{S}_A^H) \mathbf{G}^H \mathbf{w}_p df} \\
& - d \left[-\frac{N}{R_0 G_{opt}^2} T_0 + T_0 N \frac{Y_{opt}^* - G_{opt}}{G_{opt}^2} - T_0 N \frac{Y_{opt} - G_{opt}}{G_{opt}^2} - T_0 N R_0 \frac{2G_{opt}^2 - (G_{opt}^2 + B_{opt}^2)}{G_{opt}^2} \right] / dG_{opt}
\end{aligned} \tag{E.24}$$

$$\begin{aligned}
& \sum_{p=1}^P \frac{\int_{f_L}^{f_H} \mathbf{w}_p^H \mathbf{G} (\mathbf{S}_A \mathbf{I}) \mathbf{G}^H \mathbf{w}_p df}{\int_{f_L}^{f_H} \mathbf{w}_p^H \mathbf{G} (\mathbf{I} - \mathbf{S}_A \mathbf{S}_A^H) \mathbf{G}^H \mathbf{w}_p df} \\
& - d \left[-\frac{N}{R_0 G_{opt}^2} T_0 + T_0 N \frac{Y_{opt} - G_{opt}}{G_{opt}^2} - T_0 N \frac{Y_{opt}^* - G_{opt}}{G_{opt}^2} - T_0 N R_0 \frac{2G_{opt}^2 - (G_{opt}^2 + B_{opt}^2)}{G_{opt}^2} \right] / dG_{opt} \\
& \sum_{p=1}^P \frac{\int_{f_L}^{f_H} \mathbf{w}_p^H \mathbf{G} (\mathbf{S}_A^* \mathbf{I}) \mathbf{G}^H \mathbf{w}_p df}{\int_{f_L}^{f_H} \mathbf{w}_p^H \mathbf{G} (\mathbf{I} - \mathbf{S}_A \mathbf{S}_A^H) \mathbf{G}^H \mathbf{w}_p df}.
\end{aligned}$$

Next, set $\frac{dT_{av}}{dG_{opt}} = 0$ to minimize T_{av}

$$\begin{aligned}
& \left[-1 + R_0 Y_{opt} - R_0 G_{opt} + R_0 Y_{opt}^* - R_0 G_{opt} + 2R_0^2 G_{opt}^2 - R_0^2 (G_{opt}^2 + B_{opt}^2) \right] \\
& \sum_{p=1}^P \frac{\int_{f_L}^{f_H} \mathbf{w}_p^H \mathbf{G} \mathbf{I} \mathbf{G}^H \mathbf{w}_p df}{\int_{f_L}^{f_H} \mathbf{w}_p^H \mathbf{G} (\mathbf{I} - \mathbf{S}_A \mathbf{S}_A^H) \mathbf{G}^H \mathbf{w}_p df} \\
& + \left[-1 - R_0 Y_{opt} + R_0 G_{opt} - R_0 Y_{opt}^* + R_0 G_{opt} + 2R_0^2 G_{opt}^2 - R_0^2 (G_{opt}^2 + B_{opt}^2) \right] \\
& \sum_{p=1}^P \frac{\int_{f_L}^{f_H} \mathbf{w}_p^H \mathbf{G} (\mathbf{S}_A \mathbf{I} \mathbf{S}_A^H) \mathbf{G}^H \mathbf{w}_p df}{\int_{f_L}^{f_H} \mathbf{w}_p^H \mathbf{G} (\mathbf{I} - \mathbf{S}_A \mathbf{S}_A^H) \mathbf{G}^H \mathbf{w}_p df} \\
& - \left[-1 + R_0 Y_{opt} - R_0 G_{opt} - R_0 Y_{opt} + R_0 G_{opt} - 2R_0^2 G_{opt}^2 + R_0^2 (G_{opt}^2 + B_{opt}^2) \right] \quad (E.25) \\
& \sum_{p=1}^P \frac{\int_{f_L}^{f_H} \mathbf{w}_p^H \mathbf{G} (\mathbf{S}_A \mathbf{I}) \mathbf{G}^H \mathbf{w}_p df}{\int_{f_L}^{f_H} \mathbf{w}_p^H \mathbf{G} (\mathbf{I} - \mathbf{S}_A \mathbf{S}_A^H) \mathbf{G}^H \mathbf{w}_p df} \\
& - \left[-1 + R_0 Y_{opt} - R_0 G_{opt} - R_0 Y_{opt}^* + R_0 G_{opt} - 2R_0^2 G_{opt}^2 + R_0^2 (G_{opt}^2 + B_{opt}^2) \right] \\
& \sum_{p=1}^P \frac{\int_{f_L}^{f_H} \mathbf{w}_p^H \mathbf{G} (\mathbf{S}_A^* \mathbf{I}) \mathbf{G}^H \mathbf{w}_p df}{\int_{f_L}^{f_H} \mathbf{w}_p^H \mathbf{G} (\mathbf{I} - \mathbf{S}_A \mathbf{S}_A^H) \mathbf{G}^H \mathbf{w}_p df} = 0.
\end{aligned}$$

Simplify the equation in the next few steps.

$$\begin{aligned}
& \left[-1 + R_0^2 G_{opt}^2 - R_0^2 B_{opt}^2 \right] \sum_{p=1}^P \frac{\int_{f_L}^{f_H} \mathbf{w}_p^H \mathbf{G} \mathbf{I} \mathbf{G}^H \mathbf{w}_p df}{\int_{f_L}^{f_H} \mathbf{w}_p^H \mathbf{G} (\mathbf{I} - \mathbf{S}_A \mathbf{S}_A^H) \mathbf{G}^H \mathbf{w}_p df} \\
& + \left[-1 + R_0^2 G_{opt}^2 - R_0^2 B_{opt}^2 \right] \sum_{p=1}^P \frac{\int_{f_L}^{f_H} \mathbf{w}_p^H \mathbf{G} (\mathbf{S}_A \mathbf{I} \mathbf{S}_A^H) \mathbf{G}^H \mathbf{w}_p df}{\int_{f_L}^{f_H} \mathbf{w}_p^H \mathbf{G} (\mathbf{I} - \mathbf{S}_A \mathbf{S}_A^H) \mathbf{G}^H \mathbf{w}_p df} \\
& - \left[-1 - j2R_0 B_{opt} - R_0^2 G_{opt}^2 + R_0^2 B_{opt}^2 \right] \sum_{p=1}^P \frac{\int_{f_L}^{f_H} \mathbf{w}_p^H \mathbf{G} (\mathbf{S}_A \mathbf{I}) \mathbf{G}^H \mathbf{w}_p df}{\int_{f_L}^{f_H} \mathbf{w}_p^H \mathbf{G} (\mathbf{I} - \mathbf{S}_A \mathbf{S}_A^H) \mathbf{G}^H \mathbf{w}_p df} \quad (E.26) \\
& - \left[-1 + 2jR_0 B_{opt} - R_0^2 G_{opt}^2 + R_0^2 B_{opt}^2 \right] \sum_{p=1}^P \frac{\int_{f_L}^{f_H} \mathbf{w}_p^H \mathbf{G} (\mathbf{S}_A^* \mathbf{I}) \mathbf{G}^H \mathbf{w}_p df}{\int_{f_L}^{f_H} \mathbf{w}_p^H \mathbf{G} (\mathbf{I} - \mathbf{S}_A \mathbf{S}_A^H) \mathbf{G}^H \mathbf{w}_p df} = 0
\end{aligned}$$

Collect the G_{act} terms on the left hand side to get

$$R_0^2 G_{opt}^2 \sum_{p=1}^P \frac{\int_{f_L}^{f_H} \mathbf{w}_p^H \mathbf{G} [\mathbf{I} + \mathbf{S}_A \mathbf{S}_A^H + \mathbf{S}_A + \mathbf{S}_A^*] \mathbf{G}^H \mathbf{w}_p df}{\int_{f_L}^{f_H} \mathbf{w}_p^H \mathbf{G} (\mathbf{I} - \mathbf{S}_A \mathbf{S}_A^H) \mathbf{G}^H \mathbf{w}_p df} =$$

$$\sum_{p=1}^P \frac{\int_{f_L}^{f_H} \mathbf{w}_p^H \mathbf{G} ([1 + R_0^2 B_{opt}^2] (\mathbf{I} + \mathbf{S}_A \mathbf{S}_A^H) - 2\Re\{[1 + j2R_0 B_{opt} - R_0^2 B_{opt}^2] \mathbf{S}_A\}) \mathbf{G}^H \mathbf{w}_p df}{\int_{f_L}^{f_H} \mathbf{w}_p^H \mathbf{G} (\mathbf{I} - \mathbf{S}_A \mathbf{S}_A^H) \mathbf{G}^H \mathbf{w}_p df},$$

(E.29)

and simplify to arrive at Equation 4.73

$$G_{opt}^2 = \frac{\sum_{p=1}^P \frac{\int_{f_L}^{f_H} \mathbf{w}_p^H \mathbf{G} [\mathbf{I} + \mathbf{S}_A \mathbf{S}_A^H + \mathbf{S}_A + \mathbf{S}_A^*] \mathbf{G}^H \mathbf{w}_p df}{\int_{f_L}^{f_H} \mathbf{w}_p^H \mathbf{G} (\mathbf{I} - \mathbf{S}_A \mathbf{S}_A^H) \mathbf{G}^H \mathbf{w}_p df}}{\sum_{p=1}^P \frac{\int_{f_L}^{f_H} \mathbf{w}_p^H \mathbf{G} ([1 + R_0^2 B_{opt}^2] (\mathbf{I} + \mathbf{S}_A \mathbf{S}_A^H) - 2\Re\{[1 + j2R_0 B_{opt} - R_0^2 B_{opt}^2] \mathbf{S}_A\}) \mathbf{G}^H \mathbf{w}_p df}{\int_{f_L}^{f_H} \mathbf{w}_p^H \mathbf{G} (\mathbf{I} - \mathbf{S}_A \mathbf{S}_A^H) \mathbf{G}^H \mathbf{w}_p df}}$$

(E.30)